ENGINEERING ANTI-HER2 ANTIBODIES FOR ENHANCED THERAPEUTIC POTENCY

A Dissertation

by

JEFFREY CHE-WEI KANG

Submitted to the Office of Graduate and Professional Studies of
Texas A&M University
in partial fulfillment of the requirements for the degree of

DOCTOR OF PHILOSOPHY

Chair of Committee,	E. Sally Ward
Co-Chair of Committee,	Raimund J. Ober
Committee Members,	Siegfried Musser
	Vytas Bankaitis
Head of Program,	Warren E. Zimmer

December 2018

Major Subject: Medical Sciences

ABSTRACT

HER2-postive breast cancer constitutes approximately 25% of breast cancer patients and leads to a worse prognosis. Antibody therapy, such as the anti-HER2 antibody trastuzumab, is used in the clinical setting to treat these cancers. Unfortunately, these cancers can resist trastuzumab treatment through ligand-mediated HER2/HER3 signaling. The first study addresses this issue by engineering a bispecific antibody targeting HER2 and HER3. A combination of immunoblots and proliferation assays were used to characterize the interaction between HER2, HER3, and the bispecific antibody. Another treatment for HER2-expressing cancers is the antibody-drug conjugate (ADC), trastuzumab emtansine (T-DM1). ADCs, however, suffer from a small therapeutic window due to a low maximum tolerated dose. The second study addresses this issue by engineering variants of the anti-HER2 antibody pertuzumab to bind HER2 tightly at neutral pH and weakly at acidic pH—termed acid-switched—using phage display and histidine scanning. Acid-switched antibodies were then used to generate ADCs that were characterized *in vitro* by flow cytometry, mass spectrometry, and cytotoxicity assays. Mice bearing tumor xenografts were treated with acid-switched ADCs to test their potency *in vivo*.

Ligand-induced HER2/HER3 dimers activate the PI3K/Akt signaling axis and individual treatments such as trastuzumab or the small molecule inhibitor lapatinib which targets HER2 phosphorylation are unable to prevent this signaling cascade. The bispecific antibody was constructed from trastuzumab and an anti-HER3 antibody with

the goal of preventing HER2/HER3 dimer signaling. A combination treatment of the bispecific antibody and lapatinib significantly inhibited cancer cell proliferation *in vitro*.

Acid-switched ADCs were engineered to bind tightly to HER2 on the target cell surface and to dissociate after internalization into acidic endosomes. These acid-switched antibodies were observed to have at least an ~100-fold reduced binding affinity at pH 5.8 relative to pH 7.4. The difference in binding affinity led to enhanced accumulation of acid-switched ADCs and greater release of cytotoxic drug in HER2-expressing cancer cells in comparison to treatments with ADCs derived from the parent antibody. Mice implanted with the HER2-expressing cancer cell lines MDA-MB-453 and JIMT-1 showed tumor regression or slowed growth when treated with acid-switched ADCs in comparison to the parental ADC, respectively.

ACKNOWLEDGEMENTS

I would like to thank my mentors Prof. Sally Ward and Prof. Raimund Ober who have been vital in directing me through my graduate studies. Their interdisciplinary lab allowed me to discover aspects of research from multiple angles which greatly developed what interests in research I had. I would also like to thank my other committee members Prof. Vytas Bankaitis and Prof. Siegfried Musser for giving valuable input during the various crossroads I encountered.

I would also like to acknowledge the Cancer Prevention Research Institute of Texas (CPRIT) which has funded much of my research.

Lastly, I would like to acknowledge my family and friends who have given me much support during my Ph.D.

CONTRIBUTORS AND FUNDING SOURCES

This work was supported by Professor Sally Ward [advisor] of the Department of Molecular and Cellular Medicine and the Department of Microbial Pathogenesis and Immunology, Professor Raimund J. Ober [co-advisor] of the Department of Biomedical Engineering and the Department of Molecular and Cellular Medicine, Professor Siegfried Musser of the Department of Molecular and Cellular Medicine, and Professor Vytas A. Bankaitis of the Department of Molecular and Cellular Medicine.

Dr. Jayakumar Poovassery formerly of the Department of Immunology at the University of Texas Southwestern Medical Center contributed significantly towards the direction and experiments in Section 2. Sungyong You of the Department of Biomedical Engineering was responsible for the imaging experiments shown in Figure 2-6 and Figure 2-7. Dr. Isabel Manjarres formerly of the Department of Immunology at the University of Texas Southwestern Medical Center was responsible for Figure 2-15. Dr. Wei Sun of Department of Molecular and Cellular Medicine discovered the phage display mutant used in Section 3 and aided in the ELISA experiments shown in Figure 3-3 and 3-4. Dr. Xiaoli Wang of the Department of Molecular and Cellular Medicine imaged and processed data for Figure 3-7. Mass spectrometry in Figure 3-8 was run by Smriti Shankar and Dr. Cory Klemashevich of the Integrated Metabolomics Analysis Core. The *in vivo* mouse experiments shown in Figures 3-9, 3-10, and 3-11 were conducted by Dr. Priyanka Khare of the Department of Molecular and Cellular Medicine. Modeling data (Figure 3-12) were done by Mostafa Karimi of the

Department of Electrical and Computer Engineering. The rest of the experiments were conducted by myself.

The studies presented were supported by the Cancer Prevention and Research Institute of Texas (CPRIT; RP110069, RP110070, and RP140141).

NOMENCLATURE

Ab6tet – Ab6 antibody with Ab6 scFv

ADCC – Antibody-dependent cellular cytotoxicity

ADCP – Antibody-dependent cellular phagocytosis

ADC – Antibody-drug conjugate

Akt – Protein kinase B

ALT – Alanine transaminase

ATCC – American Type Culture Collection

AUC – Area under the curve

BsAb – Bispecific antibody

CDC – Complement-dependent cytotoxicity

CL – Constant light

CH – Constant heavy

CHO – Chinese hamster ovary

DAR – Drug-antibody-ratio

DMSO – dimethyl sulfoxide

EGFR – Human epidermal growth factor receptor 1

ELISA – Enzyme-linked immunosorbent assay

ERK – Extracellular signal-regulated kinases

Fab – fragment antigen binding

Fc – fragment crystallizable

FcγR – Fc gamma receptor

FcRn – neonatal Fc receptor

Fv – variable fragment

HER2 – Human epidermal growth factor receptor 2

HER3 – Human epidermal growth factor receptor 3

HPLC – High-performance liquid chromatography

HIC – Hydrophobic interaction column

HRG – Heregulin beta 1

IgG – Immunoglobulin G

Lap – Lapatinib

LC-MS/MS – Liquid chromatography with tandem mass spectrometry

MMAE – Monomethyl auristatin E

MTS – 3-(4,5-DimethylThiazol-2-yl)-5-(3-carboxymethoxyphenyl)-2-(4-sulfophenyl)-2H-tetrazolium, inner salt

MTX - Methotrexate

VH – Variable heavy

VHH – Single-domain antibody

VL – Variable light

PAb6 – Pertuzumab with Ab6 scFv

PI3K – Phosphatidylinositol 3-kinase

PBS – Phosphate buffered saline

PBST – Phosphate buffered saline with Tween-20

PVDF – Polyvinylidene difluoride

ScFv – Single-chain variable fragment

TAb6 – Trastuzumab IgG with Ab6 scFv

TBS – Tris-buffered saline

TBST – Tris-buffered saline with Tween-20

T-DM1 – Trastuzumab emtansine

TKI – Tyrosine kinase inhibitor

TABLE OF CONTENTS

Page

LIST OF FIGURES

1. INTRODUCTION AND LITERATURE REVIEW

1.1 Antibody therapeutics

1.1.1 Antibody structure and function

Antibodies are proteins created during the process of the adaptive immune response to specifically target foreign antigens. Overall, there are 5 different classes of antibodies (IgG, IgE, IgM, IgD, and IgA) that are distinguished by their constant domains. IgGs are further subdivided into four separate subclasses: IgG1, IgG2, IgG3, and IgG4[1]. Therapeutic antibodies are typically based on IgG1 because this subclass displays potent effector functions and is highly prevalent in the body[2]. Examples of IgG1-based therapeutic antibodies include the anti-HER2 antibodies trastuzumab[3] and pertuzumab[4], both of which are used in the studies presented in this thesis.

IgG1 is a Y-shaped molecule that consists of separate polypeptide chains—two identical heavy chains (HCs) and two identical light chains (LCs). The HC is an ~50 kDa polypeptide chain consisting of a variable domain (VH) and three constant domains (CH1, CH2, and CH3), while the LC is an ~25 kDa polypeptide and is composed of a variable domain (VL) and a constant domain (CL). Furthermore, the CL domain is subdivided into two classes, kappa (κ) and lambda (λ). The hinge region, a flexible amino acid stretch, connects the CH1 domain to the CH2 domain. Two disulfide bonds located in the hinge region links two HCs together. A third disulfide bond in the hinge region connects to the CL, connecting the HC with the LC. The IgG can be further divided into two components—the Fab fragments (fragment antigen-binding) and the Fc

fragment (fragment crystallizable region). Each of the two Fab fragments is composed of the VH, CH1, VL, and CL domains, whereas the Fc fragment consists of the two CH2 and CH3 domains. Additionally, the combination of a single VH and VL domain is known as an Fv fragment. (Figure 1-1).

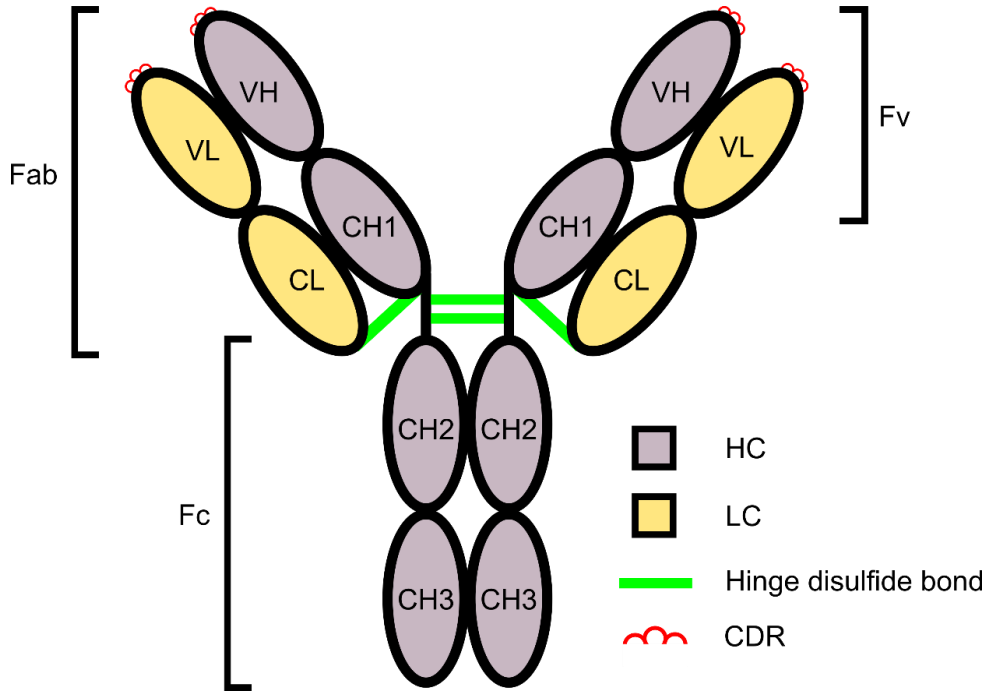

Figure 1-1. Illustration of IgG1 antibody structure. The heavy chain (HC) and light chain (LC) are shown in purple and yellow, respectively. Domains of both HC and LC are indicated. The three red circles on top of the VH and VL domains represent the three complementarity-determining regions (CDRs) on each respective gene. Hinge disulfide bonds are represented by green lines.

The Fab fragments of the antibody are responsible for binding to antigen. The VH and VL domains each have three complementarity-determining regions (CDRs) that together, are responsible for binding to a specific antigen. Through V(D)J

recombination[5], a unique mechanism by which a wide array of Ig gene segments are spliced to create a highly diverse antibody repertoire, B cells are able to generate antibodies to target a wide range of antigens. The affinity for these antigens can be further enhanced through affinity maturation, an iterative process that involves the rapid introduction of mutations into the CDRs and the clonal selection of high affinity binders. Unlike the variable domains, the constant domains, HC and LC, are relatively well conserved. The Fc portion of the antibody has multiple binding sites located on the CH2 and CH3 domains and is important for many antibody effector functions along with antibody homeostasis within the body. Effector functions such as antibody-dependent cell-mediated cytotoxicity (ADCC) and complement-dependent cytotoxicity (CDC), are initiated through the binding of the CH2 domain to Fcγ receptors and complement proteins, respectively[6-8].

1.1.2 Antibodies as therapeutics

The first major hurdle for the use of antibodies as a therapy was the ability to produce large amounts of monoclonal antibodies—antibodies that bind the same epitope. This issue was first addressed in 1975 by Köhler and Milstein through hybridoma technology[9]. An antibody-producing B cell is fused with an immortal myeloma cell to create a hybrid cell that is not only able to secrete the desired monoclonal antibody, but can also be propagated indefinitely. The creation of hybridoma cells was essential in providing the machinery necessary for producing large quantities of select homogenous antibody. Shortly after the introduction of hybridoma technology, muromonab-CD3 was

clinically approved for the treatment of acute allograft rejection in renal transplants[10]. However, the use of muronmonab-CD3 was limited due to the immunogenic response that was mounted against the murine antibody[10, 11], and to the antibody's short half-life which results from the low affinity of human neonatal Fc receptor (FcRn) to rodent antibodies[12]. Various strategies have been implemented that either produce chimeric or humanized antibodies to prevent the host's immune system from targeting and removing the rodent antibodies. Examples of chimeric or humanized therapeutic antibodies are as follows:

1. Rituximab, a clinically approved chimeric antibody against CD20, was created by grafting murine VH and VL domains onto human IgG1 constant domains[13].
2. Alemtuzumab, an anti-CD52 antibody, was the first therapeutic humanized antibody[14]. The CDRs of a rodent anti-CD52 antibody was cloned into human IgG1, replacing the original IgG's CDRs. Overall, this antibody would be a human IgG1 with rodent CDR sequences which is a significant reduction in comparison to rituximab in exposed rodent protein sequences, an entire Fv in comparison to the CDRs, for the body to generate an immune response to[15, 16].
3. Trastuzumab, an antibody clinically approved for the treatment of HER2-overexpressing breast cancers, was designed by further humanizing a chimeric anti-HER2 antibody (mumAb4D5)[3]. The chimeric anti-HER2

antibody was humanized by gene conversion mutagenesis[3] where the rodent sequences of the antibody were mutated to resemble human sequences. Fully human antibodies against target antigen can also be created. Humira, the first clinically approved fully human monoclonal antibody, was discovered by phage display against tumor necrosis factor alpha (TNFα) using a process known as chain shuffling[17]. In summary, the use of antibody-based therapies has become prominent for treating multiple diseases including cancer.

1.1.3 Mechanism of action of therapeutic antibodies against cancer

Therapeutic antibodies for cancer treatment target antigens that are usually over-expressed on the surface of tumor cells, whereas expression levels on normal cells are substantially lower. HER2, for instance, can be found on breast cancer cells but has limited expression on normal cell types[18]. Antibodies can be engineered to target surface-expressing tumor antigens to treat cancer through multiple mechanisms:

1. Antibodies can inhibit signaling by binding key epitopes on either ligand or receptor and preventing them from binding to one another. MM-121[19], for instance, binds to domain I of HER3, preventing the HER3 receptor from binding its ligand heregulin and undergoing a conformational change to interact with other receptors. Pertuzumab, an anti-HER2 antibody, binds to the dimerization arm of HER2 (domain II) and prevents ligand-dependent signaling in HER2-overexpressing cancers. Trastuzumab, an anti-HER2

antibody, binds to domain IV of HER2, preventing ligand-independent signaling of HER2[20].

2. Cancer cells opsonized by antibodies can activate CDC. Opsonized cells can recruit complement proteins, such as the C1 proteins, which recruit macrophages and neutrophils to phagocytose cancer cells and cause inflammation[21]. The formation of a membrane attack complexes (MAC) can also be activated through CDC, however membrane-bound regulators often prevent MAC formation[22]. Rituximab, for instance, is known to function through CDC in treating leukemia[21].
3. Opsonized cancer cells can recruit immune cells such as natural killer (NK) cells, macrophages, and monocytes to actively lyse the cell in a process known as ADCC[23, 24]. Bound antibodies interact with FcγRIIIa on the NK cell surface and activates the NK cells[25]. The activated NK cells release proteases, perforin, granzymes, and cytotoxic factors to kill the opsonized cell. ADCC has been shown to contribute to trastuzumab's efficacy against HER2-positive breast cancer[26].
4. Opsonized cancer cells can also recruit macrophages and other phagocytes to fully engulf whole cells and degrade them in a process known as antibody-dependent cellular phagocytosis (ADCP). Antibody-coated cells are detected by Fc gamma receptors on macrophages or phagocytes, where cross-linking of the Fc gamma receptors initiates ADCP[27]. *In vivo* studies have shown that ADCP is important in the clearance of certain tumors[28].

5. Trogocytosis, or “nibbling” of cell membrane can occur on opsonized cancer cells. Similar to phagocytosis, the macrophages detect and initiate trogocytosis of opsonized cells through their Fc gamma receptors[29, 30]. In contrast to phagocytosis where the macrophage engulfs the opsonized cell, in trogocytosis the macrophage only removes small portions of the opsonized cell, and internalizes it, which can lead to cell death[31, 32].

1.2 Bispecific antibodies

1.2.1 Bispecific antibodies as a therapeutic treatment

Monoclonal antibodies, by design, are only able to bind to a single epitope of an antigen. However, cancer cells can overcome antibody therapy by downregulating the expression of the target antigen, mutation of the target epitope, or dimerization with other surface receptors. Bispecific antibodies (bsAbs) address some of these issues by simultaneously targeting multiple epitopes or antigens. While the application of two or more separate monoclonal antibodies is possible, the use of a bsAb has certain advantages[33, 34]. Targeting two different antigens enhances specificity for the target cell[35]. Furthermore, targeting two separate receptors on cancer cells can promote anti-proliferative effects and prevent the development of resistance[36]. In some cases, bsAbs are used to recruit immune cells to the target cell by targeting an antigen on the target cell and a receptor on the immune cell[37-39]. Moreover, the combination of two separate antibodies into a bsAb reduces the cost of development and clinical trials[40].

1.2.2 Format of bispecific antibodies

In contrast to a traditional antibody, bsAbs can come in multiple structural formats. bsAbs can be as simple as two separate single-domain antibodies (VHH)[41] or two separate single-chain variable fragments (scFv; composed of a VH and VL domain)[42] attached to one another with a short peptide linker. Other small bsAbs include two separate Fabs attached to one another[43] or a number of combinations of the above mentioned fragments. Traditional antibodies can be engineered to become bsAbs

through cloning techniques. While early bsAbs were produced by hybrid hybridomas or chemical conjugation of two antibodies[44-47], current bsAbs can be generated using molecular biology techniques such that additional VHHs, scFvs, or Fabs are cloned as part of an antibody and produced from cultures of mammalian cells [e.g. Chinese hamster ovary (CHO) cells and human embryonic kidney (HEK293) cells][48]. Technologies such as knobs-into-holes mutations in the Fc region[49, 50], Fab domain swap (CrossMAb)[51], and electrostatic steering mutations in the Fc region[52, 53] allow a single antibody to have Fabs that target different antigens or epitopes. (Figure 1-2)

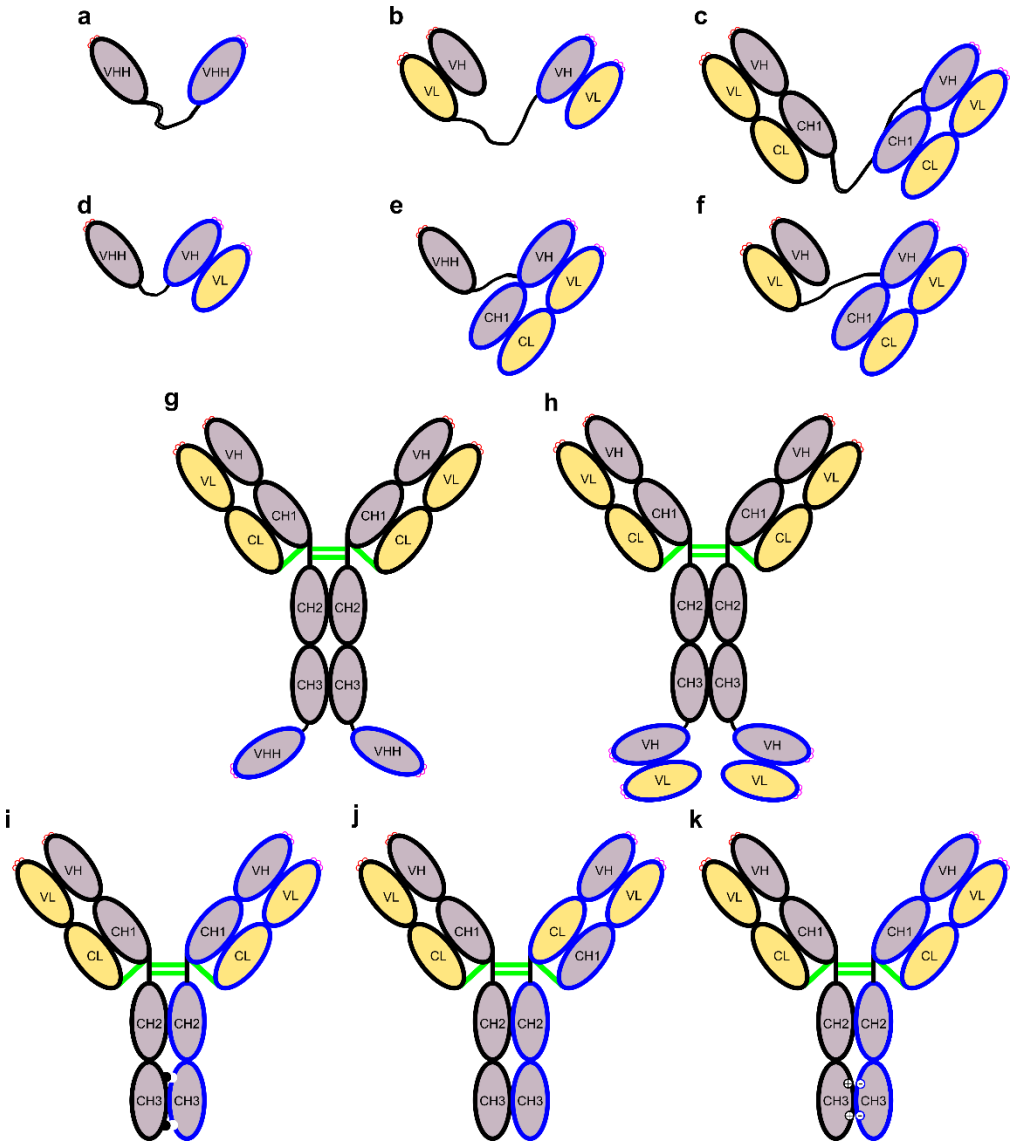

Figure 1-2. Possible bispecific antibody (bsAb) formats. Two single-domain antibodies (VHH, a) single-chain variable fragments (scFv, b) and Fabs (c) can be combined by a linker to form bsAbs. Combinations of (a), (b), and (c) can be combined with a linker to create a VHH-scFv bsAb (d), VHH-Fab bsAb (e), or a scFv-Fab bsAb (f). IgGs can also be engineered to have an additional VHH or scFv domain to create IgG-VHH (g) and IgG-scFv (h) bsAbs, respectively. Introduction of knobs-into-holes mutations (i), swapping of domains (CrossMAb, j), or eletrosteering mutations (k) can allow IgG to bind two separate antigens.

1.2.3 Bispecific antibodies as a therapeutic agent

As mentioned above, bsAbs differ from monoclonal antibodies in their ability to target two separate antigens. bsAbs can be divided into two separate groups based on the antigens they target. One type of bsAb is designed to bind disease/cancer antigens as one target and immune cell receptors as the other target. Such bsAbs have the ability to recruit immune cells to the diseased/cancer cell and enhance immune responses such as ADCC. Examples of this design are MDX-H210 (targeting HER2 and CD64)[54], catumaxomab (anti-EpCAM and CD3)[55], and blinatumomab (anti-CD3 and anti-CD19)[42]. The other type of bsAbs target two antigens, or two different epitopes on the same antigen (e.g. trastuzumab and pertuzumab)[56], on the target cell, which can lead to cross-linking and downregulation of the targeted antigen[57]. A common tumor escape mechanism for cancer cells in antibody therapeutics is signaling through a separate receptor complex[58-62]. Targeting both the primary and secondary receptor can prevent downstream survival signaling, causing the cancer cells to die. Examples of such bsAbs are the anti-HER2/anti-HER3 dual scFv linked human serum albumin MM-111[63], a two-in-one antibody against HER3 and HER1, and istiratumab (an anti-IGF1R and anti-HER3 bsAb)[64].

1.2.4 Bispecific antibodies and HER2/HER3 tumorgenesis

The importance of bsAbs is demonstrated in HER2-expressing cancers. While the monoclonal antibody trastuzumab can effectively treat patients with HER2-expressing cancers, a portion of tumors escape trastuzumab treatment through

dimerization of the HER2 receptor with the HER3 receptor. Trastuzumab binds to domain IV of the HER2 extracellular domain and does not inhibit ligand-mediated heterodimerization of HER2 and HER3[65]. The HER2/HER3 complex is known to actively signal through the PI3K/Akt pathway, allowing the tumor to escape HER2 signaling inhibition. bsAbs targeting both HER2 and HER3[34, 63, 66-68] were created to overcome ligand-mediated signaling of HER2/HER3 dimers. This topic is further addressed in Section 2 of this study.

1.3 Antibody-drug conjugates

1.3.1 Overview of antibody-drug conjugates

Cancer therapeutics have changed rapidly over the last two decades, particularly in the area of antibody therapy. While antibodies, such as trastuzumab, have shown initial therapeutic efficacy, many tumors acquire trastuzumab resistance[69, 70]. Monoclonal antibodies are often paired with chemotherapy or small molecule inhibitors to enhance their efficacy and to prevent tumor escape. Cytotoxic drugs, such as those used in chemotherapy, while potent, are not cancer cell-specific and therefore leave a narrow therapeutic window where a physician can safely administer the cytotoxic drug while achieving clinical efficacy. Antibody-drug conjugates (ADCs), however, combine the target specificity of an antibody with the potency of cytotoxic drugs to enhance the therapeutic window. Ideally, the ADC would cause much higher on-target toxicity in comparison to off-target toxicity (target-dependent and target independent toxicity, respectively)[71]. Much can still be done to enhance the therapeutic window, as evidenced by the low maximum tolerated dose of ADCs in clinical trials[72, 73].

ADCs are composed of a targeting antibody, a cytotoxic drug, and a linker that attaches the cytotoxic drug to the antibody (Figure 1-3). While an ADC appears simplistic in structure, the attachment of hydrophobic cytotoxic drugs to the antibody is challenging and has resulted in many failed ADCs in pre-clinical trials[74]. Both T-DM1 and Adcetris have demonstrated the efficacy of ADCs in the clinic, and with more than 50 other ADCs in different phases of clinical testing[73], the future for ADCs seems bright. However, both current and upcoming ADCs suffer from short-comings in which antigens can be targeted,

linker technology used, and cytotoxic drugs used, which ultimately limits the therapeutic window. Issues such as hydrophobicity of conjugated cytotoxic drug can lead to off-target toxicity and limits how many cytotoxic drug molecules can be conjugated to an antibody[75]. Current methods to enlarge the therapeutic window are focused on improving the cytotoxic drug and linker of an ADC. These methods include using more potent cytotoxic drugs, masking the hydrophobic cytotoxic drug, and engineering both linker and cytotoxic drug to be less hydrophobic[76-81]. Methods involving engineering the antibody of ADCs, however, are in the minority[82]. A method of engineering acid-switched ADCs for enhancing the therapeutic window of ADCs will be outlined in Section 3.

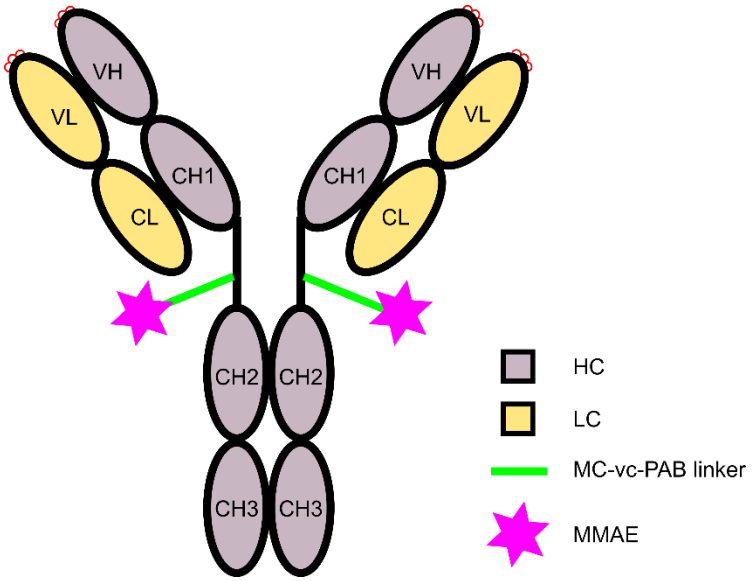

Figure 1-3. ADC schematic depicting the cytotoxic drug monomethyl auristatin E (MMAE) conjugated to the hinge region of an antibody with a maleimidocaproyl-valine-citrulline-para-aminobenzyloxycarbonyl linker. Schematic shows a 2:1 drug-to-antibody ratio.

1.3.2 Antibody and antigen requirements for ADCs

Although ADCs would appear to be easily implemented to treat several diseases and cancers, this is not the case due to the stringent requirements that need to be met in order to attain ADC efficacy[83]. Early ADCs such as KS1/4[84] and BR96[85], which comprise antibodies conjugated with methotrexate and doxorubicin, respectively, did not show any therapeutic activity despite significant tumor localization. The failures of these ADCs were attributed to all three components of the ADC. Both KS1/4 and BR96 targeted antigens with limited surface expression, the linkers used (a cleavable amide linker and an acid-labile hydrazone linker for KS1/4 and BR96, respectively) were either prone to cleavage prior to entering the target cell or inefficient release of the drug inside the target cell, and lastly the cytotoxic drugs used were only moderately cytotoxic. Due to the lessons learned from these early ADCs, requirements for a successful ADC were outlined.

1. The target antigen should be highly expressed on the target cell. The target antigen should have limited to no expression on normal cells to prevent non-specific targeting and uptake. Furthermore, the target antigen should be readily accessible on the surface of the target cells.
2. The antibody should be rapidly internalized through receptor-mediated endocytosis and the receptor should not recycle back to the cell surface otherwise the ADC cannot be delivered into the cell. This is critical in the delivery of cytotoxic drugs as some ADCs must be degraded in lysosomal compartments of target cells to release their cytotoxic payloads. Recently, some groups have constructed non-internalizing ADCs[86-89]. While they show efficacy

in *in vitro* and *in vivo* rodent studies, these non-internalizing ADCs need to be delivered repeatedly in relatively large doses in order to obtain a therapeutic effect.

1.3.3 Linker technology

The linker in ADCs is responsible for the attachment of the cytotoxic drug to the antibody combined with the efficient release of the cytotoxic drug within the target cell. As the goal of ADCs is to enhance the therapeutic window of the cytotoxic drug, the linker is vital in determining the on-target and off-target toxicity of an ADC. A linker must be stable in circulation in order to prevent off-target toxicity. Release of the cytotoxic drug due to linker failure increases off-target toxicity and can decreases on-target toxicity. Decreased off-target toxicity can lead to a loss in efficacy of the ADC in treating the target tumor and result in tumor escape.

As mentioned above, how rapidly the target antigen is internalized is important in determining if an ADC specific for the target antigen should be made. Furthermore, as the pH drops when the antigen/ADC complex is internalized from the cell surface into early endosomes and trafficked into the lysosome[18, 90, 91], the linker that is used critically determines to where and how the cytotoxic drug is delivered. Linkers used in ADCs are divided into two categories—cleavable and non-cleavable.

1. Cleavable linkers are chemically or enzymatically cleaved within or near the target cells. These linkers include hydrazones, disulfides, and peptides.

a. Hydrazone linkers are hydrolyzed in the acidic environment of endosomes to release the cytotoxic drug. However, this type of linker is known to have a short half-life[92] . Mylotarg, the first clinically approved ADC, used the hydrazone linker technology but was withdrawn from the clinic due to lethal liver toxicity which was attributed to the instability of the linker. Furthermore, the tumor microenvironment can have an acidic pH which can lead to the release of the cytotoxic drug prior to ADC internalization[93].
b. Disulfide linkers are designed to be released in the reducing conditions of endosomes after ADC internalization. These linkers rely on the higher concentrations of reduced glutathione within cells (1-10 mM) in comparison to its extracellular concentrations in the blood[94] to specifically cleave disulfide bonds and release the cytotoxic drug within the target cell. ADCs with disulfide linkers are usually internalized and undergo degradation before glutathione can release the cytotoxic drug from the linker[95, 96].
c. Peptide linkers, such as Val-Ala and Val-Cit, rely on the enzyme cathepsin β for cleavage within endosomes after internalization. As cathepsins are enzymatically active in acidic environments, such as in late endosomes and lysosomes, enzymatic cleavage of the peptide linkers in the extracellular environment is rare. Peptide linkers have therefore become one of the most prevalent designs for cleavable

linkers due to their plasma stability and specific release mechanism. Notably, Brentuximab Vendotin uses this technology for delivery of monomethyl auristatin E (MMAE).

2. Non-cleavable linkers fully rely on ADC degradation by lysosomal proteases to release their cytotoxic drug into the target cell. While non-cleavable linkers have superior plasma stability, the cytotoxic payload is sometimes derivatized to a less potent form in order to be conjugated to a non-cleavable linker[97]. T-DM1 uses a non-cleavable linker as prior iterations of T-DM1 using cleavable linkers showed lower efficacy[98].

1.3.4 Cytotoxic drugs

Initially, ADCs used cytotoxic drugs that were commonly used in chemotherapy (e.g. methotrexate and doxorubicin) which had moderate potency. As a small fraction of antibody/ADC reaches the tumor site (as little as 0.003-0.08% injected dose per gram of tumor)[99], significantly more potent cytotoxic drugs were needed to generate effective ADCs. Current cytotoxic drugs, such as monomethyl auristatin E (MMAE) and auristatins, have toxicity at nanomolar concentrations[100, 101]. One method to increase delivery of ADC to the tumor site is to increase the ADC dose given to a patient, however, this can be problematic as increases in ADC delivery to normal cells can lead to dose-limiting toxicities. An alternative approach for enhancing drug delivery is to increase the drug-to-antibody ratio (DAR) of an ADC. ADCs with high DAR (DAR ≥ 8), however, are rapidly cleared in the liver, resulting in shorter times of tumor

exposure[75, 102]. To overcome this, engineered linkers with reduced hydrophobicity are currently being investigated for ADCs with high DARs. [75, 103, 104].

Cytotoxic drugs can be used to separate ADCs into two main groups. The first group is comprised of drugs that disrupt microtubule assembly, disassembly, and formation. Such anti-mitotics include dolastatin 10 analogs[105], maytansinoids[106], and tubulysins[107]. As microtubules play an essential role in many cellular processes, including cell division, drugs targeting microtubules prove to be highly cytotoxic in rapidly dividing cells, such as cancer cells. The second group of cytotoxic drugs comprises DNA targeting drugs such as duocarmycin[81], calicheamicins[108], and pyrrolobenzodiazepine dimers[79]. DNA-targeting drugs cause DNA strand scission, alkylation or cross-linking. Unlike the anti-mitotics, the DNA-targeting drugs do not necessarily depend on the rapid proliferation of cancer cells and may therefore be used to target cancer cells with lower proliferation rates.

1.4 Thesis overview

Antibody and ADC therapy targeting HER2-expressing cancers is expanding with the prevalence of HER2 found in multiple cancers. However, resistance to antibody treatment such as ligand-mediated tumor escape and a small therapeutic window for ADCs suggest there are still many issues to address for better therapeutic efficacy. This thesis presents studies that use antibody engineering to address the issues of tumor escape by HER2 family receptor dimerization and the inefficient delivery of cytotoxic drug by ADCs. The first aim focuses on the generation of a bsAb that targets both HER2 and its favored dimerization partner, HER3, which is known to trigger potent PI3K/Akt signaling after binding to its ligand heregulin and undergoing receptor dimerization with HER2. The second aim focuses on the generation of acid-switched antibodies that bind tightly to HER2 at neutral pH and dissociate from HER2 under acidic conditions to take advantage of the acidic environment of the endosomal lumen for better trafficking of antibodies towards the degradative pathway in cells. The third aim characterizes the acid-switched antibodies before and after conjugation with the cytotoxic drug MMAE. Furthermore, the acid-switched ADC is assessed *in vitro* for the accumulation of the ADC and the delivery of MMAE and *in vivo* for tumor inhibition in contrast to the wild-type ADC.

Aim 1: Analyze the efficacy of a bsAb in preventing ligand-induced resistance in HER2-overexpressing breast cancer cells.

A bsAb was engineered in the format of an IgG-scFv to target both HER2 and HER3 receptors on HER2-overexpressing breast cancer cells. This bsAb was designed to stop ligand-mediated HER2/HER3 dimers from causing cell-proliferative downstream signaling through the PI3K/Akt pathway. Immunoblots of signaling pathways and receptor expression were analyzed to interpret cell proliferation results after treatment with the bsAb. Proliferation was assayed to determine the efficacy of the bsAb in inhibiting cancer cell proliferation in the presence and absence of the HER3 ligand heregulin and the small molecule tyrosine kinase inhibitor lapatinib.

Aim 2: Generation and characterization of acid-switched antibodies.

An antibody that binds tightly to HER2 at neutral conditions but only weakly at acidic conditions is considered to be an acid-switched antibody. Antibody engineering techniques such as histidine scanning and phage display were used to isolate acid-switched mutants. The acid-switched antibody was analyzed by flow cytometry, surface plasmon resonance, and enzyme-linked immunosorbent assay (ELISA) to characterize its binding behavior to HER2 at both neutral and acidic pHs.

Aim 3: Analysis of acid-switched antibodies as ADCs for enhanced delivery of cytotoxic drug to target cells.

Stability and therapeutic efficacy are crucial determinants of the promise of acid-switched ADCs. Acid-switched antibodies and their respective ADCs were assayed for stability in human serum. The ADCs were analyzed for accumulation by flow cytometry and for localization by fluorescence microscopy. MTS assays and mass spectrometry were used to analyze the dose response and release of cytotoxic drug *in vitro*. Mouse experiments were conducted to test the efficacy of the acid-switched ADC in comparison to T-DM1 and the wild-type ADC.

2. ENGINEERING MULTIVALENT ANTIBODIES TO TARGET HEREGULIN-INDUCED HER3 SIGNALING IN BREAST CANCER CELLS[*]

2.1 Introduction

Multiple cancers are driven by aberrant signaling through the human epidermal growth factor receptor (HER), also known as ErbB, family members. Recent studies have indicated that HER2-HER3 heterodimers can play a central role in tumorigenesis[19, 20, 109-111]. HER3 is a preferred dimerization partner for HER2, which has no known ligand and is constitutively active[20, 112, 113]. Although HER3 has very low intrinsic kinase activity, there are six phosphorylation-dependent binding sites for PI3K on the cytosolic tail of this receptor[114]. Consequently, HER2-HER3 heterodimers are the most effective activators identified to date of the PI3K/Akt pathway through both ligand-independent and ligand-dependent signaling[20, 65]. Ligand-dependent activation of HER3 involves the binding of heregulin or other ligands to induce a conformational switch in the dimerization arm, driving heterodimer formation with kinase competent partners such as HER2 or EGFR[20, 113].

[*] This study has been published in the journal *MAbs* [Kang JC, Poovassery JS, Bansal P, You S, Manjarres, IM, Ober RJ, Ward ES. (2014) Engineering multivalent antibodies to target heregulin-induced HER3 signaling in breast cancer cells. MAbs 6(2): 340-353] It is reprinted here with permission from the Taylor & Francis Group.

Consistent with HER3 as a driver of tumorigenesis, loss of HER3 expression in breast cancer cells results in reductions in both PI3K/Akt signaling and proliferation[109, 110]. Further, modeling studies demonstrate that HER3 represents a central node in PI3K/Akt signaling[111]. In conjunction with the limited efficacy of solely targeting HER2 with monotherapies such as trastuzumab[115-117], these observations have motivated the development of therapeutics targeting HER3 or HER2-HER3 heterodimers[19, 63, 68, 118]. Recent data indicate that the targeting of this axis with antibodies is less effective in the presence of heregulin[63], which is expressed in either autocrine or paracrine fashion in many tumor types[119-121]. Thus, there is a need for the generation of improved therapeutics directed toward ligand-dependent activation of HER3. The current study involves a comparison of two distinct approaches using bispecific HER2/HER3 specific antibodies or multivalent HER3-specific antibodies to target HER3 in the presence of the HER3 ligand, heregulin.

As an alternative to targeting HER family members with antibodies, the use of small molecule inhibitors of the tyrosine kinase activity of EGFR or HER2, or of the downstream kinase, PI3K, has attracted much interest[122-128]. However, these inhibitors can lead to tumor escape due to upregulation of compensatory signaling pathways and complex cross-regulatory networks involving negative feedback loops. For example, the delivery of lapatinib, a tyrosine kinase inhibitor (TKI) that targets both EGFR and HER2, results in upregulation of HER2 and HER3 expression and PI3K/Akt signaling[129-132]. Lapatinib resistance pathways can also include activating mutations of PI3K[133], and the inhibitory effects of lapatinib can be dampened by the presence of the

HER3 ligand, heregulin[63, 134-136]. This suggests that lapatinib in combination with antibodies or bispecifics that bind to HER3 might provide an effective route for therapy, particularly for tumors involving autocrine or paracrine heregulin loops that can result in limited efficacy of monotherapies.

Related to the limited therapeutic efficacy of TKIs such as lapatinib that inhibit EGFR and HER2 activation, HER3 can associate with other activating receptors such as cMET and insulin-like growth factor type I receptor I/insulin receptor substrate-1[20, 112, 137, 138]. A possible strategy to extinguish HER3-PI3K signaling would therefore be to inhibit multiple potential HER3 partners. This provides the impetus for directly targeting HER3, which would avoid the complexity of identifying and globally inhibiting all HER3 partners. Here, we have taken the approach of investigating the ability of a bispecific anti-HER2/HER3 antibody to drive HER3 into HER2-HER3 heterodimers that, through combination treatment with lapatinib, are "kinase-dead". Locking HER3 into such inactive complexes is expected to sequester this receptor from interactions with other signaling competent partners and, as such, have anti-tumor effects.

A second route toward extinguishing HER3 signaling is to develop strategies to induce the efficient internalization and degradation of this receptor. In support of this approach, several studies have demonstrated that reduction of HER3 expression has anti-proliferative effects[109, 110]. HER3 is constitutively internalized into the endolysosomal pathway[139] and it is well documented that receptor crosslinking leads to downregulation in multiple different cellular systems. We therefore reasoned that a multivalent (tetrameric) anti-HER3 antibody would induce more efficient HER3 internalization or

degradation relative to its bivalent counterpart, thereby enhancing clearance from the cell surface. The efficacy of this approach has been compared with that of recruiting HER3 into kinase-inactivated HER2-HER3 heterodimers. These comparative studies have also been extended to microscopy analyses of the trafficking behavior of the different antibodies within cells, which relates to both drug delivery for antibody-drug conjugates and Fc-mediated cytotoxicity[140, 141].

Our study has led to several observations that are of relevance to targeting HER3. First, we show that in the presence of heregulin, combination treatment with antibodies and lapatinib is necessary to achieve inhibition of signaling and growth. Under these conditions, a tetravalent HER3-specific antibody induces increased degradation of HER3 and has more potent anti-tumor effects relative to its bivalent counterpart. Importantly, when used in combination with lapatinib, the bispecific anti-HER2/ HER3 antibody is a more effective inhibitor of heregulin-driven signaling and growth compared with anti-HER3 antibodies, tetravalent anti-HER3 antibodies or mixtures of individual antibodies specific for HER2 and HER3. Our observations are consistent with a model in which the bispecific antibody recruits HER3 into HER2-HER3 heterodimers that are inactive in the presence of lapatinib. Collectively, these studies provide support for the combined use of multimeric anti-growth factor receptor antibodies with small molecule TKIs for the therapy of cancer.

2.2 Results

2.2.1 Antibodies specific for HER2 and HER3 have differential effects on signaling and proliferation

The anti-HER3 antibody, Ab6 (MM-121[19]), which competes with heregulin for binding to HER3, was generated in our laboratory as a biosimilar and used throughout these studies. To investigate whether a tetravalent anti-HER3 antibody is more effective than its bivalent counterpart in inhibiting cell growth and proliferation, we fused the Ab6 single chain variable fragment (scFv) to the CH3 domains of Ab6 via a Gly-Ser-Ser linker (Ab6tet). In addition, a bispecific trastuzumab (anti-HER2)-Ab6 antibody (TAb6) and a bispecific pertuzumab (anti-HER2)-Ab6 antibody (PAb6) were generated by fusing scFv fragments corresponding to Ab6 to the CH3 domains of trastuzumab and pertuzumab, respectively, using an analogous design (Fig. 2-1). All antibodies were expressed in transfected Chinese hamster ovary (CHO) cells. The expression yields of the bispecific antibodies were 4.5 mg/L, 2.5 mg/L, and 8 mg/L for Ab6tet, PAb6 and TAb6, respectively. Size exclusion and serum stability analyses of the bispecific proteins are presented in the Supplementary Materials (Fig. 2-2 and 2-3). For comparative purposes, size exclusion studies of Ab6, trastuzumab and pertuzumab are shown (Fig. 2-2). Ab6 and the bispecific antibodies also bound to immobilized, recombinant Fc-HER2 (TAb6, PAb6) or HER3 (Ab6, Ab6tet, TAb6, PAb6) in surface plasmon resonance experiments (BIAcore; data not shown). The *in vivo* half-lives (β-phase) of Ab6tet and

TAb6 were also determined in BALB/c SCID mice and were 228 ± 14 (n = 4 mice) and 215 ± 11 (n = 5 mice) hours, respectively.

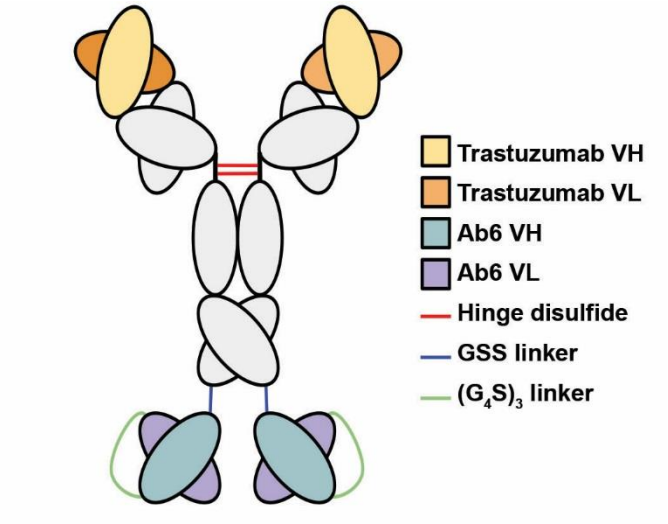

Figure 2-1. Schematic representation of the bispecific antibody (TAb6) comprising trastuzumab and a scFv derived from the anti-HER3 antibody, Ab6, used in the current study.

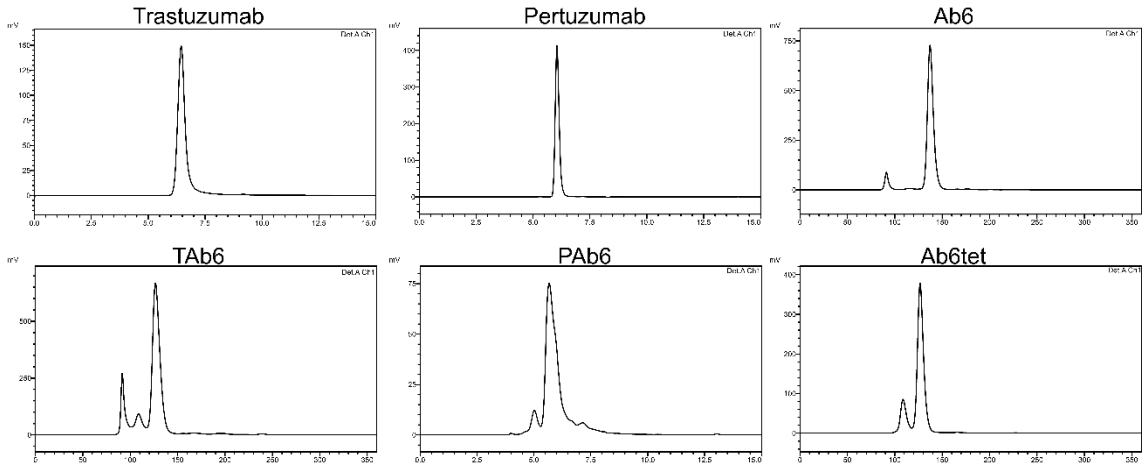

Figure 2-2. Analysis of trastuzumab, pertuzumab, Ab6, bispecific trastuzumab with anti-HER3 Ab6 scFv (TAb6), bispecific pertuzumab with anti-HER3 Ab6 scFv (PAb6), and tetrameric anti-HER3 (Ab6tet) using HPLC and size exclusion chromatography. Trastuzumab, pertuzumab, TAb6, and PAb6 were analyzed using a Yarra 3U SEC-3000 column, whereas a Hiload 16/600 Superdex 200pg column was used for Ab6 and Ab6tet. The major peak runs at the expected size for either an antibody homodimer (150 kDa) or bispecific homodimer (200 kDa).

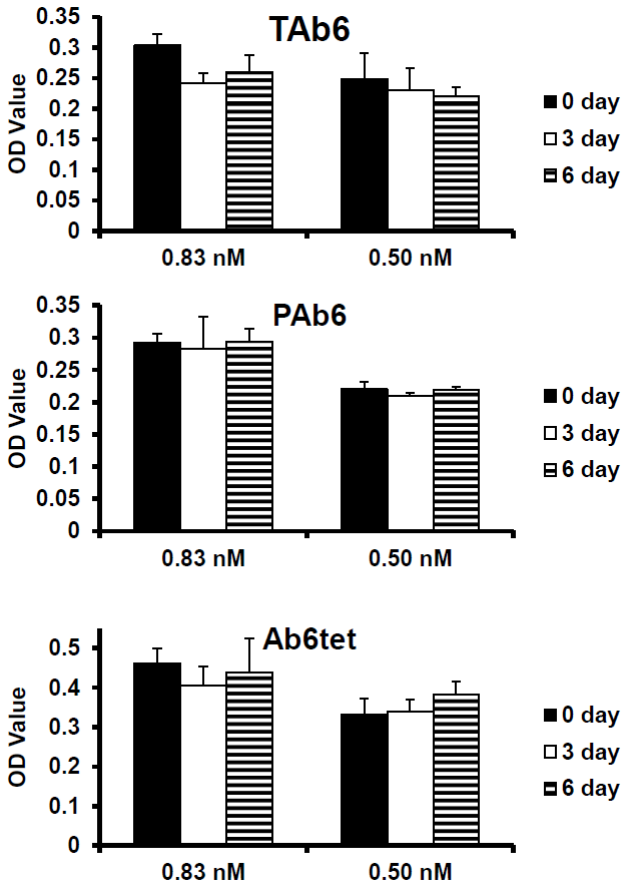

Figure 2-3. Serum stability analyses of the bispecific trastuzumab with anti-HER3 Ab6 scFv (TAb6), bispecific pertuzumab with anti-HER3 scFv (PAb6), and tetrameric anti-HER3 (Ab6tet). Antibodies were incubated in mouse serum for 0, 3, or 6 days at 37ºC, diluted into PBS to concentrations of 0.83 or 0.50 nM, and analyzed by sandwich ELISA. Differences were not significant for comparisons of 0 and 6 day samples (*P* value > 0.05; Student's *t*-test).

We initially assessed the effect of targeting HER3 and HER2/HER3 with several different antibody formats in the absence of the HER3 ligand, heregulin. For comparative purposes we also included the anti-HER2 antibodies, trastuzumab and pertuzumab, which bind to domain IV and the dimerization arm (domain II), respectively, of HER2[142, 143]. The anti-HER3 antibody, Ab6, and its tetrameric form, Ab6tet, reduced proliferation in the HER2-overexpressing cancer cell lines, SK-BR-3

and HCC1419 (Fig. 2-4A). Although Ab6 and Ab6tet treatment resulted in a trend toward reduced proliferation in BT-474 cells, the effects were not significant. By contrast with SK-BR-3 and HCC1419 cells, BT-474 cells express a gain of function variant of PI3K[144, 145] which could account for the reduced efficacy of anti-HER3 antibodies. Consistent with the observations of others[146], trastuzumab has higher anti-proliferative activity on ligand-independent growth of SK-BR-3 and BT-474 cells relative to pertuzumab (Fig. 2-4A). A mixture of pertuzumab and Ab6 is also less effective than trastuzumab and Ab6.

Although combinations of anti-HER2 and anti-HER3 antibodies (Ab6 combined with trastuzumab or pertuzumab) had anti-proliferative activities, exposure of cells to the bispecific, TAb6, comprising trastuzumab plus Ab6, resulted in increased proliferation (Fig. 2-4A). Further, the bispecific antibody comprising Ab6 and pertuzumab (PAb6) induced proliferation (Fig. 2-4A). The effects of both PAb6 and TAb6, which bind to different sites of HER2[142, 143], indicate that proximity of HER2 and HER3 is sufficient for proliferative signaling, rather than a need for the receptors to dimerize in a specific configuration. This proximity model is also consistent with the observation that exposure of cells to a mixture of trastuzumab or pertuzumab and Ab6, which would not be expected to drive formation of HER2-HER3 heterodimers, results in reduced proliferation (Fig. 2-4A).

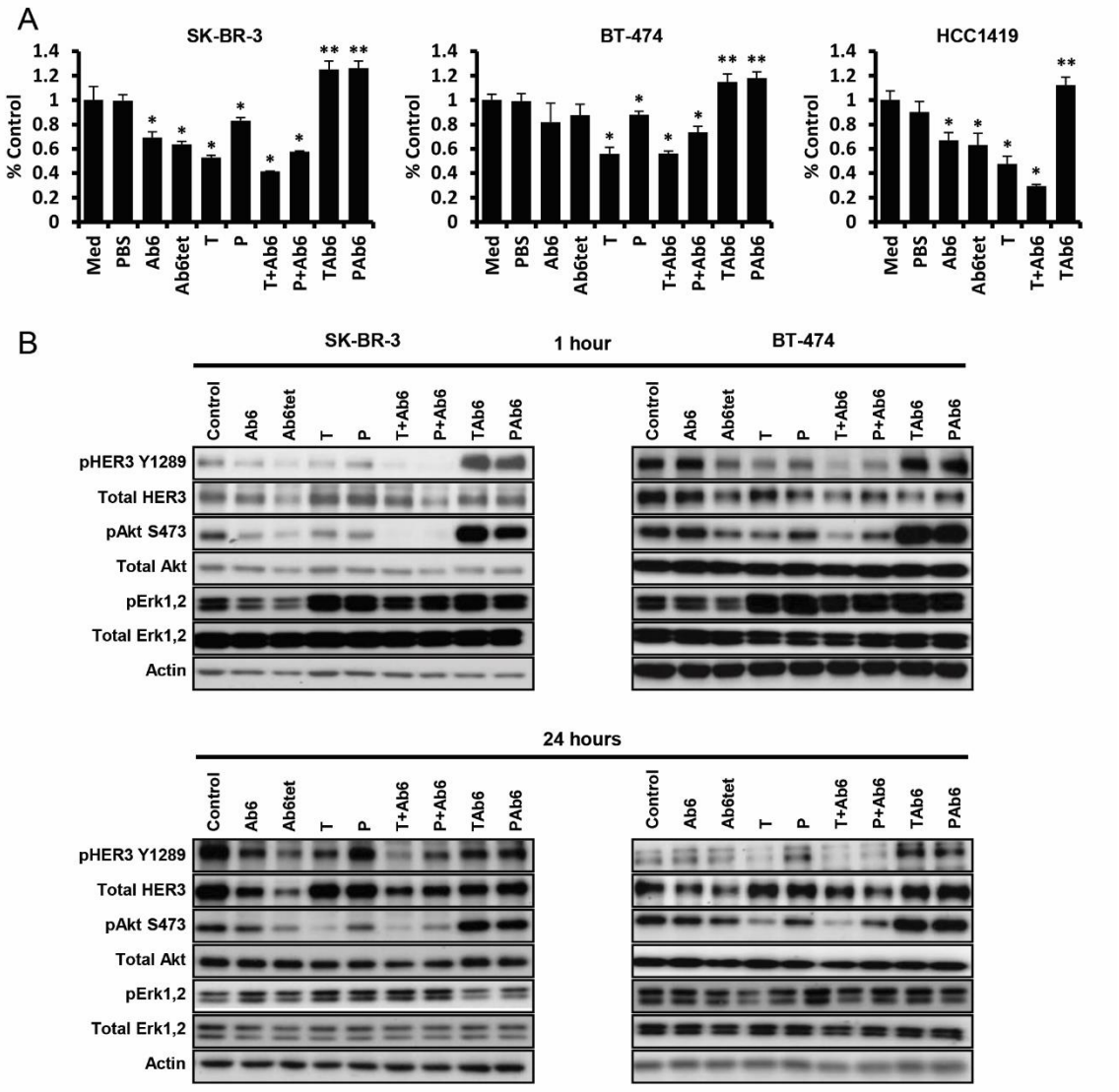

Figure 2-4. Effects of antibodies specific for HER2 and/or HER3 on HER2-overexpressing breast cancer cells. (A) Cells were incubated with 50 nM anti-HER3 (Ab6), tetrameric anti-HER3 (Ab6tet), trastuzumab (T), pertuzumab (P), trastuzumab or pertuzumab and Ab6 (T + Ab6 or P + Ab6), bispecific trastuzumab with anti-HER3 Ab6 scFv (TAb6), or bispecific pertuzumab with anti-HER3 Ab6 scFv (PAb6) for 5 d. Proliferative responses were assessed using the MTS reagent and were normalized against the proliferation of cells incubated in medium (Med) only. Data shown are means of triplicates ± standard deviation. The symbols * and ** indicate significantly lower or higher proliferative responses, respectively, between cells treated with antibody and PBS vehicle (Student t-test; $P < 0.05$). (B) SK-BR-3 or BT-474 cells were treated with anti-HER2/HER3 antibodies (50 nM) for 1 or 24 h, and cell lysates analyzed by immunoblotting. Data shown are representative of at least two independent experiments.

Analyses of the effects of the antibodies on the phosphorylation of HER3, Akt and Erk demonstrated that the anti-proliferative effects are associated with decreased pAkt levels in SK-BR-3 and BT-474 cells (Fig. 2-4B). Although pErk levels were lower following treatment of cells for one hour with Ab6, Ab6tet, or Ab6 combined with anti-HER2 antibodies than for cells treated with trastuzumab, pertuzumab, TAb6 or PAb6, these differences were not sustained at the 24 h time point (Fig. 2-4B). Exposure of SK-BR-3 or BT-474 cells to TAb6 or PAb6 resulted in increased pAkt (S473) levels that persisted for at least 24 h, consistent with the pro-proliferative effects of these bispecific antibodies. By contrast, the levels of pAkt at 24 h were decreased in cells treated with any of the other antibodies or antibody combinations (Fig. 2-4B). Pertuzumab as a single agent, or in combination with Ab6, was less effective than trastuzumab (with or without Ab6) in reducing pAkt (S473) phosphorylation, which is congruent with the lower anti-proliferative activity of this antibody (Fig. 2-4A).

Earlier studies have shown that relief of feedback inhibition of the FoxO1/3a transcription factors can lead to upregulation of multiple receptor tyrosine kinases such as HER3 and insulin-like growth factor-1 receptor (IGF-1R) and subsequent reactivation of Akt[130, 147, 148]. However, the possibility of pAkt reactivation occurring in the current study following treatment of cells with the bispecific antibodies, TAb6 or PAb6, can be excluded by the relatively rapid kinetics of pAkt induction observed (1 h, Fig. 2-4B). To further support this, we observed phosphorylation of Akt following 15 min of exposure of SK-BR-3 and BT-474 cells to the bispecific antibodies (Fig. 2-5).

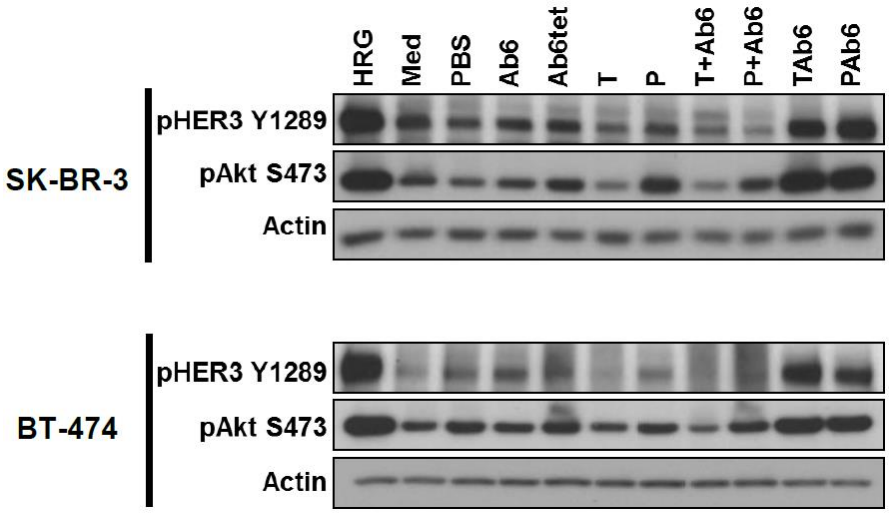

Figure 2-5. The bispecific anti-HER2/HER3 antibodies, TAb6 and PAb6, induce phosphorylation of Akt and HER3 within 15 minutes. SK-BR-3 and BT-474 cells were treated with 50 nM anti-HER3 (Ab6), tetrameric anti-HER3 (Ab6tet), trastuzumab (T), pertuzumab (P), trastuzumab and Ab6 (T + Ab6), pertuzumab and Ab6 (P + Ab6), bispecific trastuzumab with anti-HER3 Ab6 scFv (TAb6) or bispecific pertuzumab with anti-HER3 scFv (PAb6) for 15 minutes. Cell lysates were analyzed by immunoblotting.

Total HER3 levels in the cells following treatment with anti-HER3 antibodies were also analyzed. In general, HER3 levels were reduced by treatment with anti-HER3 antibodies, Ab6 and Ab6tet, whereas exposure of cells to the bispecific antibodies, TAb6 and PAb6, resulted in less HER3 degradation ($P < 0.05$; Fig. 2-4B; Fig. 2-6). Reduced HER3 degradation following TAb6 or PAb6 treatment is consistent with the inhibitory effects of HER2 expression on the internalization of ligand-activated EGFR or HER3[149, 150]. The increased HER3 degradation induced by Ab6tet relative to Ab6 was more marked for SK-BR-3 than BT-474 cells, although in both cases the differences were statistically significant ($P < 0.05$; Fig. 2-4B).

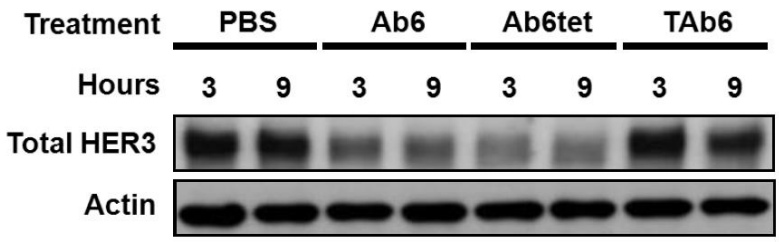

Figure 2-6. The multivalent anti-HER3 antibody, Ab6tet, induces higher levels of HER3 degradation compared with the bivalent counterpart, Ab6, and bispecific TAb6. SK-BR-3 cells were treated with 50 nM anti-HER3 antibody (Ab6), Ab6tet, bispecific trastuzumab with anti-HER3 Ab6 scFv (TAb6), or PBS vehicle for 3 or 9 hours. Cell lysates were analyzed for total HER3 using immunoblotting.

Microscopy analyses were used to further investigate the intracellular trafficking pathways taken by Ab6, Ab6tet and TAb6 (Fig. 2-7). These studies demonstrate that Ab6tet is internalized into EEA-1 positive early endosomes more rapidly than Ab6, and enters these compartments within 5 min of treatment. Following 15 min of treatment, both Ab6 and Ab6tet are internalized into early endosomes, although the levels of Ab6 remaining on the plasma membrane are greater than for Ab6tet (Fig. 2-7). By contrast, the majority of TAb6 is present on the plasma membrane following 5–60 min of treatment (Fig. 2-7; Fig. 2-8). Within 60 min of treatment, Ab6 and Ab6tet are present in LAMP-1+ lysosomes (Fig. 2-8). Multivalent antibody binding to HER3 therefore enhances the rate of HER3 internalization into the endolysosomal pathway, consistent with the increased degradation of HER3 in the presence of Ab6tet relative to Ab6.

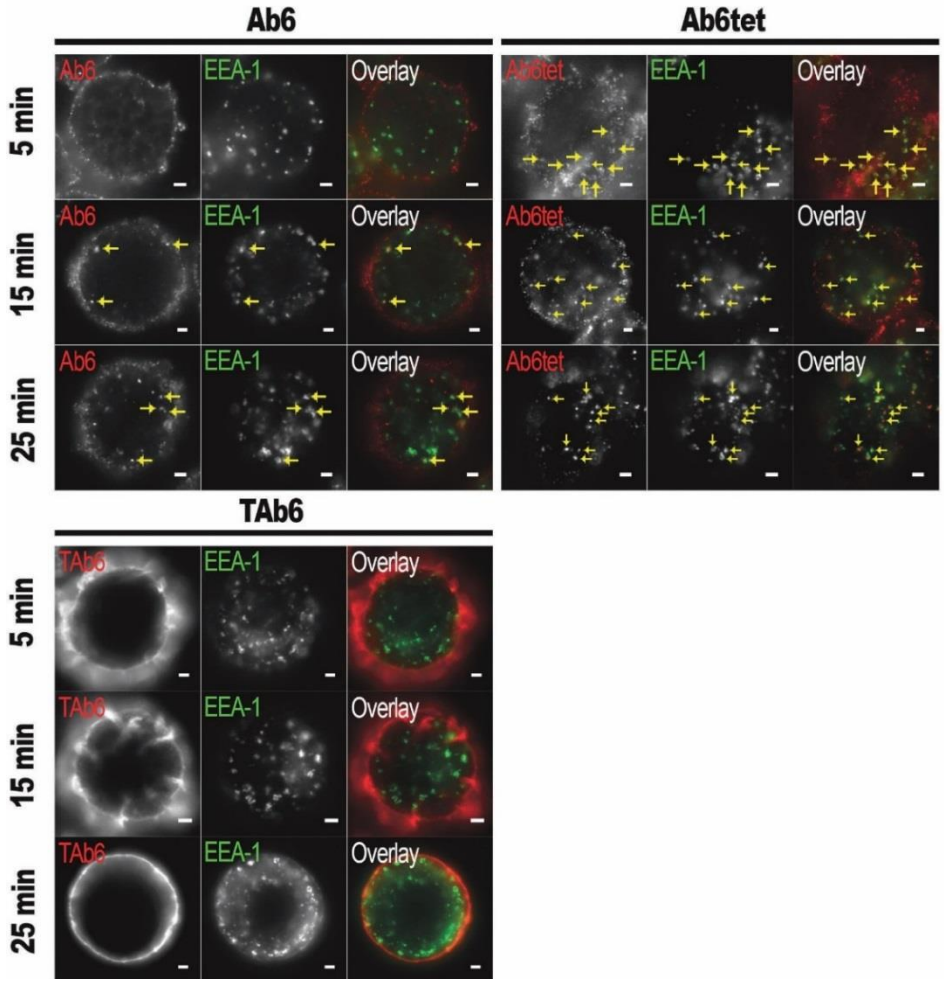

Figure 2-7. Ab6tet internalizes into SK-BR-3 cells more rapidly than Ab6. Cells were pulsed with 50 nM anti-HER3 (Ab6), tetrameric anti-HER3 (Ab6tet) or bispecific trastuzumab with anti-HER3 Ab6 scFv (TAb6) for 5 minutes at 37°C, chased for 0, 10 or 20 minutes, fixed, permeabilized and stained with anti-EEA-1 antibody. The combined pulse plus chase times are indicated on the left margin. Anti-HER3 or HER2/HER3 antibodies were detected with Alexa 555-labeled secondary antibody (pseudocolored red in overlay) and anti-EEA-1 antibody with Alexa 647-labeled secondary antibody (pseudocolored green in overlay). Yellow arrows in the images for Ab6tet-treated cells indicate examples of internalized Ab6tet that is associated with EEA-1 positive endosomes. Scale bars = 2 μm.

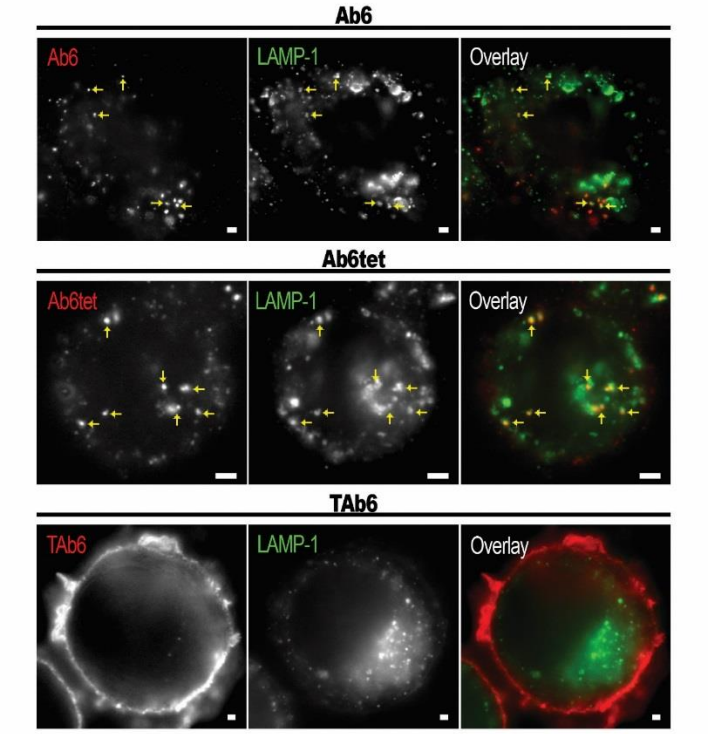

Figure 2-8. The bivalent anti-HER3 antibody, Ab6, and its multivalent counterpart, Ab6tet, traffic into LAMP-1 positive endosomal structures within one hour of treatment. SK-BR-3 cells were treated with 50 nM Ab6, Ab6tet, or bispecific trastuzumab with anti-HER3 scFv Ab6 (TAb6) for 15 minutes at 37 °C and chased in medium for 45 minutes at 37 °C. Cells were fixed, permeabilized and stained for LAMP-1. Anti-HER3 or HER2/HER3 antibodies were detected with Alexa 555-labeled secondary antibody (pseudocolored red in overlay) and anti-LAMP-1 antibody with Alexa 488-labeled secondary antibody (pseudocolored green in overlay). Examples of co-localization of antibody and LAMP-1+ compartments are indicated by yellow arrows. Scale bars = 2 µm.

2.2.2 Targeting HER2/HER3 with antibodies is ineffective in the presence of heregulin

Heregulin is frequently present in tumors due to autocrine or paracrine production[119-121], motivating an investigation of the effects of the antibodies on tumor cell growth in the presence of this HER3 ligand. HCC1419 cells showed increased proliferation in the presence of heregulin, whereas reduced proliferation was observed for SK-BR-3 cells (Fig. 2-9A). Although BT-474 cells showed a trend toward heregulin-stimulated proliferation, differences between vehicle- and heregulin-treated cells were not always significant. Reduced proliferation of SK-BR-3 cells in response to heregulin has been described previously[151]. Heregulin exposure ablated the inhibitory effects of Ab6, Ab6tet, trastuzumab or trastuzumab plus Ab6 on ligand-independent proliferation of BT-474 or HCC1419 cells (Fig. 2-4A and 2-9A). Slightly higher proliferation of HCC1419 cells was observed following TAb6 relative to trastuzumab plus Ab6 treatment, but differences for these two treatments were not significant for SK-BR-3 and BT-474 cells.

The reduced efficacy of the antibodies in the presence of heregulin was accompanied by either no change (SK-BR-3 cells with trastuzumab and TAb6 24 h following treatment and BT-474 cells with all treatments), or a reduction (SK-BR-3 cells with Ab6, Ab6tet, or a mixture of trastuzumab plus Ab6 at 24 h) in pAkt levels (Fig. 2-9B). Collectively, the data indicate that antibody targeting of HER2 and HER3 has limited efficacy in the presence of intratumoral HER3 ligands.

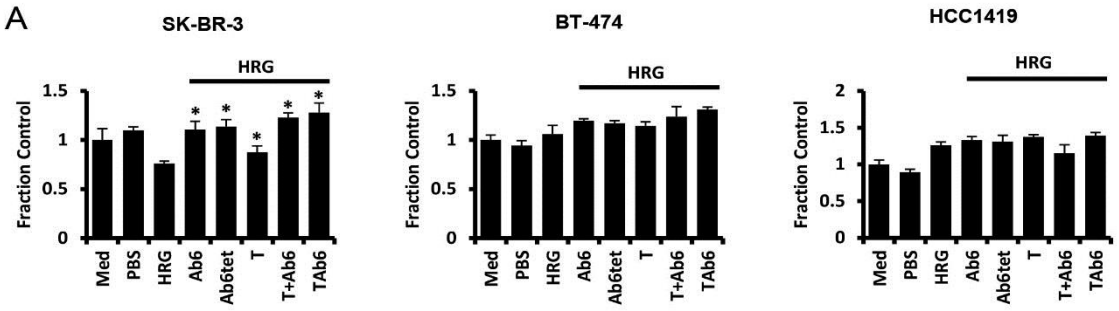

Figure 2-9. Antibodies specific for HER2 and/or HER3 have reduced efficacy in inhibiting proliferation and PI3K/Akt signaling in the presence of heregulin. A, Cells were incubated with heregulin (HRG, 6.25 nM) and 50 nM anti-HER3 (Ab6), tetrameric anti-HER3 (Ab6tet), trastuzumab (T), trastuzumab and Ab6 (T + Ab6) or bispecific trastuzumab with anti-HER3 Ab6 scFv (TAb6) for 5 days. Proliferative responses were assessed using the MTS reagent and were normalized against the proliferation of cells incubated in medium (Med) only. Data shown are means of triplicates ± standard deviation. * indicates statistically significant differences between proliferative responses for cells treated with antibody in the presence of heregulin and cells treated with heregulin only (Student's *t*-test; $P < 0.05$). B, SK-BR-3 or BT-474 cells were treated with anti-HER2/HER3 antibodies (50 nM) in the presence of 6.25 nM heregulin for 1 or 24 hours, and cell lysates analyzed by immunoblotting. Data shown are representative of at least two independent experiments.

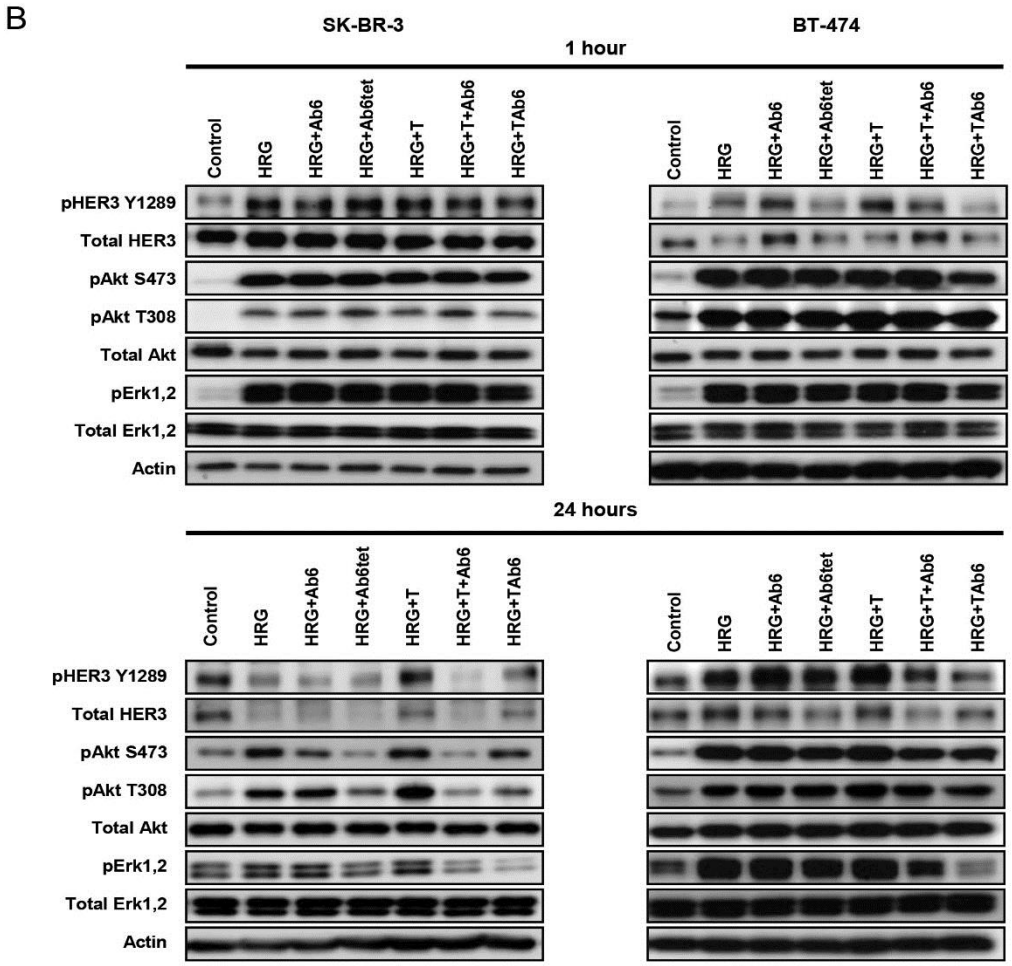

Figure 2-9. Continued

2.2.3 Lapatinib combined with antibodies specific for HER2/HER3 overcomes heregulin-mediated resistance

The induction of proliferative signaling by HER2-HER3 dimerization "forced" by TAb6 treatment suggested that the combination of this bispecific antibody with the small molecule inhibitor of HER2 (and EGFR) kinase activity, lapatinib, might stabilize HER2-HER3 heterodimers in an inactive state. Further, we hypothesized that such

complexes would preclude the interaction of HER3 with signaling competent partners. Lapatinib treatment is known to result in upregulation of HER2 and HER3 levels on the plasma membrane[129, 132], and we confirmed these observations under the conditions of our assay (except that HER2 was not upregulated on BT-474 cells; Fig. 2-10). Treatment of SK-BR-3 and BT-474 cells with lapatinib at doses ranging from 50 nM–1 μM resulted in inhibition of proliferation (Fig. 2-11A). However, this growth inhibition was ablated by exposure of cells to heregulin (Fig. 2-11A). Although lapatinib treatment alone resulted in potent inhibition of HER3, Akt and Erk phosphorylation, this was partially reversed by incubation of cells with lapatinib plus heregulin (Fig. 2-11B).

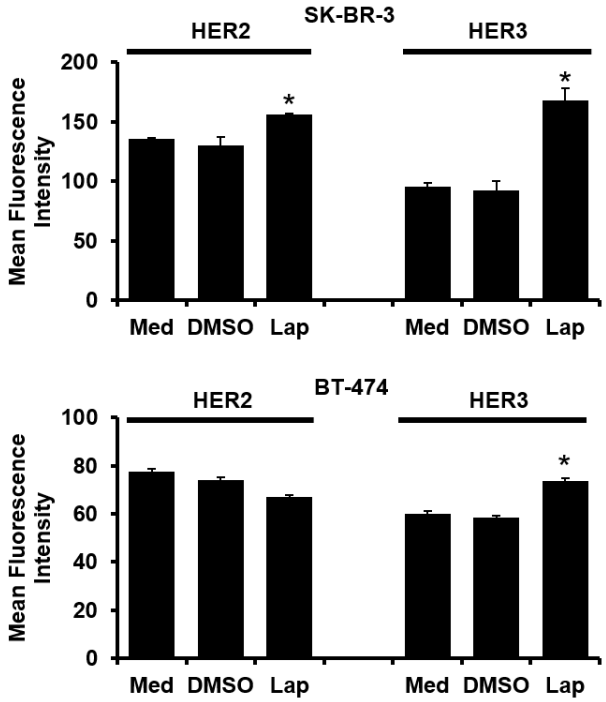

Figure 2-10. Lapatinib treatment induces upregulation of HER2 and HER3 (SK-BR-3) or HER3 (BT-474) levels on the plasma membrane of breast cancer cells. Cells were treated with 1 μM lapatinib (Lap), medium (Med) or vehicle control (DMSO) for 24 hours. Cell surface HER2 or HER3 was detected by incubation with 50 nM Alexa 488-labeled trastuzumab or Alexa 647-labeled Ab6 followed by flow cytometric analyses. Data shown represent means of mean fluorescence intensities ± standard deviation of triplicate samples following subtraction of background fluorescence intensities. * indicates statistically significant differences between lapatinib and DMSO (vehicle) treated cells ($P < 0.005$; Student's *t*-test). Data shown are representative of at least two independent experiments.

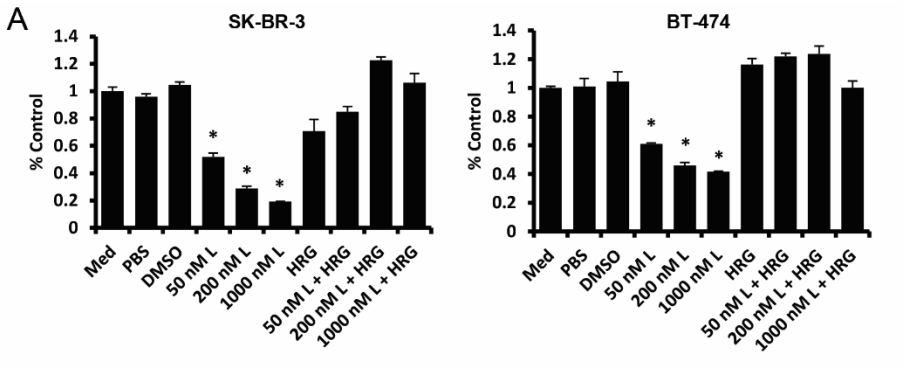

Figure 2-11. Heregulin treatment reverses the anti-proliferative effects of lapatinib in HER2 overexpressing cell lines. A, cells were incubated with different concentrations of lapatinib (L) in the presence and absence of heregulin (HRG; 6.25 nM) for 5 days. Proliferative responses were assessed using the MTS reagent and were normalized against the proliferation of cells incubated in medium (Med) only. Data shown are means of triplicates ± standard deviation. * indicates statistically significant differences between proliferative responses for cells treated with lapatinib and DMSO vehicle (Student's *t*-test; $P < 0.001$). B, SK-BR-3 or BT-474 cells were treated with 1 μM lapatinib (Lap) in the presence and absence of heregulin (6.25 nM) for 1 or 24 hours, and cell lysates analyzed by immunoblotting. Data shown are representative of at least two independent experiments.

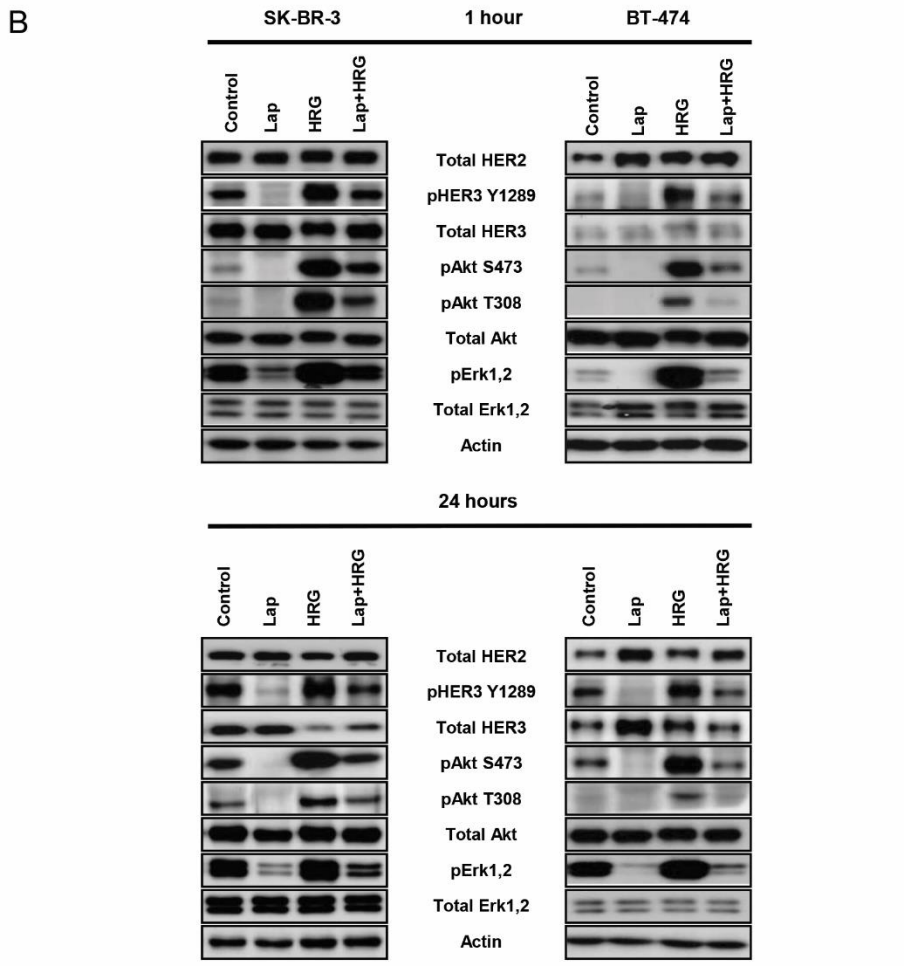

Figure 2-11. Continued.

The observation that lapatinib alone has limited efficacy in blocking cell proliferation in the presence of heregulin prompted us to investigate the effect of combination treatment of heregulin-exposed SK-BR-3, BT-474 and HCC1419 cells with lapatinib and HER3-targeting antibodies. Addition of Ab6 or Ab6tet to lapatinib resulted in anti-proliferative effects compared with the effects of lapatinib alone (Fig. 2-12A). In addition, for SK-BR-3 and HCC1419 cells, Ab6tet was more effective than Ab6 (Fig. 2-

12A). Consistent with the inability of trastuzumab to inhibit ligand-dependent HER2-HER3 signaling[146], this HER2-specific antibody did not reduce proliferation in the presence of heregulin and lapatinib. By contrast, of the antibodies/bispecifics tested, the anti-HER2/HER3 bispecific, TAb6, was the most potent of the antibodies tested in combination with lapatinib in reducing proliferation of heregulin-treated cells (Fig. 2-12A). Importantly, this bispecific also had increased anti-proliferative effects relative to a mixture of trastuzumab and Ab6 (Fig. 2-12A). Trastuzumab has superior activity over pertuzumab in inhibiting ligand-independent activity[146] (Fig. 2-4), suggesting that TAb6 would more effectively target both ligand-dependent (heregulin) and ligand-independent signaling than PAb6. In combination with the lower expression yield of PAb6 relative to that of TAb6 (2.5 mg/L vs. 8 mg/L), we therefore focused on the use of TAb6 in the lapatinib/bispecific combination studies. In the absence of heregulin, none of the antibodies further reduced the anti-proliferative activity of lapatinib (Fig. 2-13).

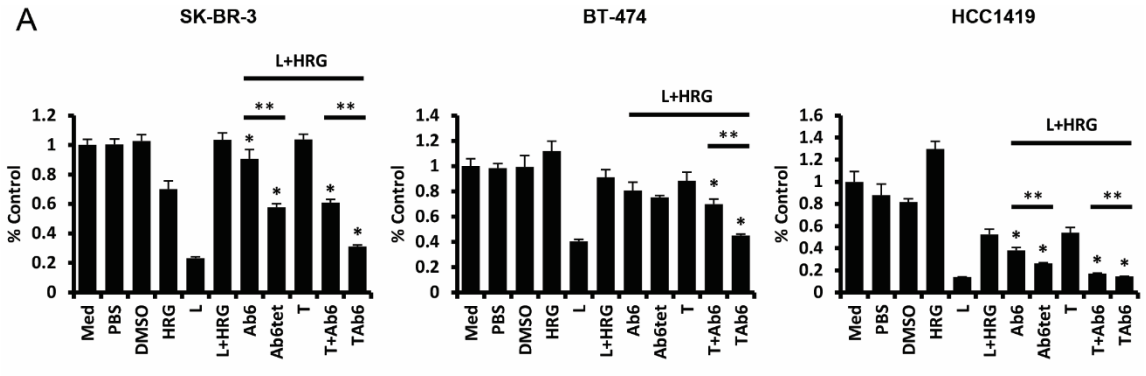

Figure 2-12. The bispecific anti-HER2/HER3 antibody, TAb6, has the highest activity in reducing cell proliferation and PI3K/Akt signaling in the presence of heregulin and lapatinib. A, cells were incubated with 1 μM lapatinib (L) in the presence of heregulin (HRG; 6.25 nM) and treated with 50 nM anti-HER3 (Ab6), tetrameric anti-HER3 (Ab6tet), trastuzumab (T), trastuzumab and Ab6 (T + Ab6) or bispecific trastuzumab with anti-HER3 Ab6 scFv (TAb6) for 5 days. Proliferative responses were assessed using the MTS reagent and were normalized against the proliferation of cells incubated in medium (Med) only. Data shown are means of triplicates ± standard deviation. * indicates statistically significant differences between proliferative responses for cells treated with antibodies vs. vehicle in the presence of lapatinib and heregulin (Student's *t*-test; $P < 0.05$). ** indicates statistically significant differences between proliferative responses for the pairwise comparison of the two indicated treatments (horizontal bars). B, SK-BR-3 or BT-474 cells were treated with lapatinib (Lap), heregulin (6.25 nM) and anti-HER2/HER3 antibodies (50 nM) as indicated for 1 or 24 hours, and cell lysates analyzed by immunoblotting. Data shown are representative of at least two independent experiments.

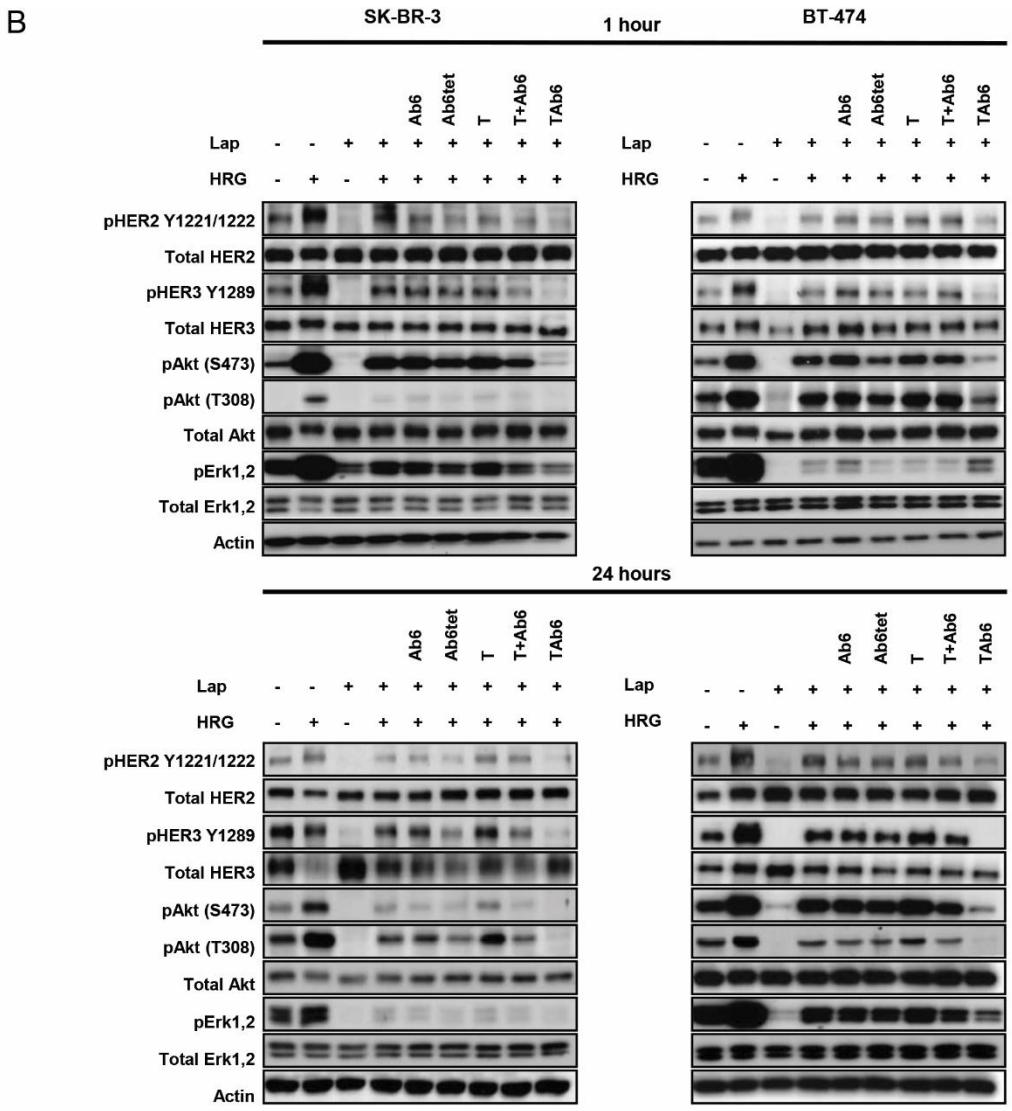

Figure 2-12. Continued.

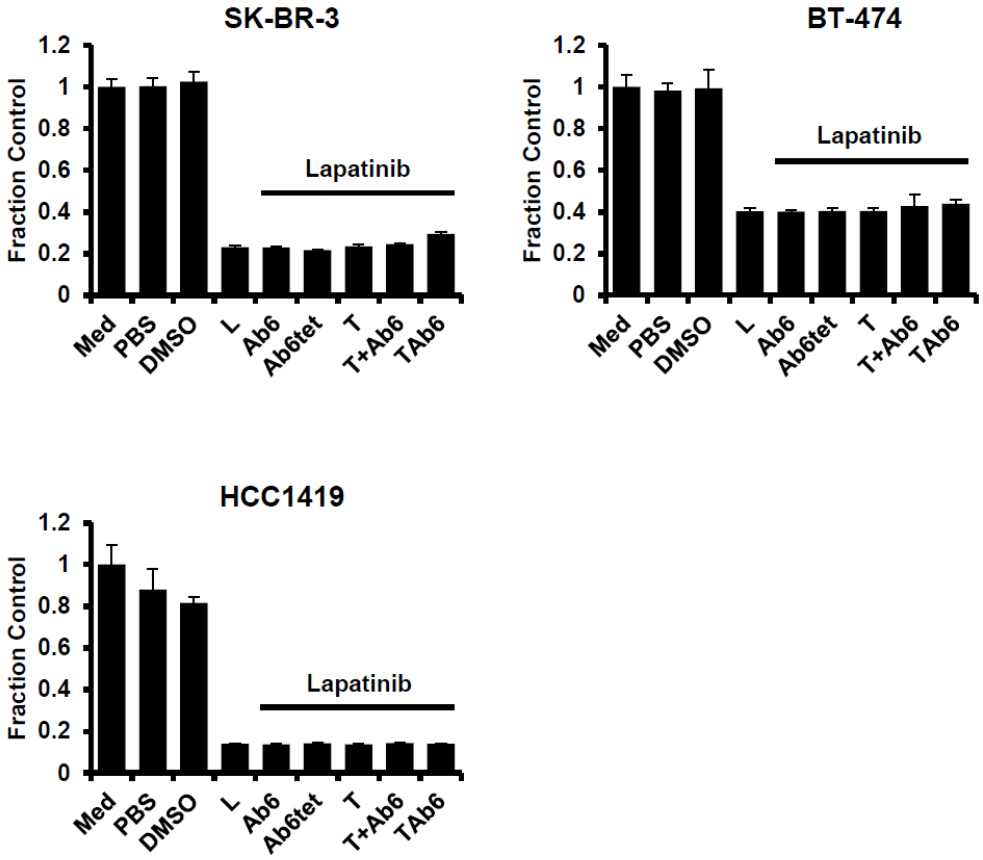

Figure 2-13. Antibodies specific for HER2 and/or HER3 do not increase the anti-proliferative effect of lapatinib. SK-BR-3, BT-474, and HCC1419 cells were treated 1 μM lapatinib (L) alone or lapatinib in combination with 50 nM anti-HER3 (Ab6), tetrameric anti-HER3 (Ab6tet), trastuzumab (T), trastuzumab and Ab6 (T + Ab6) or bispecific trastuzumab with anti-HER3 Ab6 scFv (TAb6) for 5 days. Proliferative responses were assessed using the MTS reagent and were normalized against the proliferation of cells incubated in medium (Med) only. Data shown are means of triplicates ± standard deviation and are representative of at least two independent experiments.

In the presence of lapatinib and heregulin, Ab6tet, trastuzumab plus Ab6 or TAb6 treatment resulted in lower levels of pHER3, pErk and pAkt (S473, T308) for SK-BR-3 and HCC1419 cells (Fig. 2-12B; Fig. 2-14). The improved activity of Ab6tet compared with Ab6 in SK-BR-3 and HCC1419 cells is consistent with the increased

degradation of HER3 in the presence of the tetrameric antibody ($P < 0.05$; Fig. 2-14 and 2-15). TAb6 was the most potent antibody in reducing downstream signaling in SK-BR-3, BT-474 and HCC1419 cells, and was more inhibitory than mixtures of trastuzumab and Ab6 (Fig. 2-12B; Fig. 2-14). Further, TAb6 was the only antibody in combination with lapatinib that reduced heregulin-induced pAkt and pErk in BT-474 cells. Collectively, the data indicate that in the presence of lapatinib the bispecific antibody, TAb6, is the most potent inhibitor of ligand-induced activation.

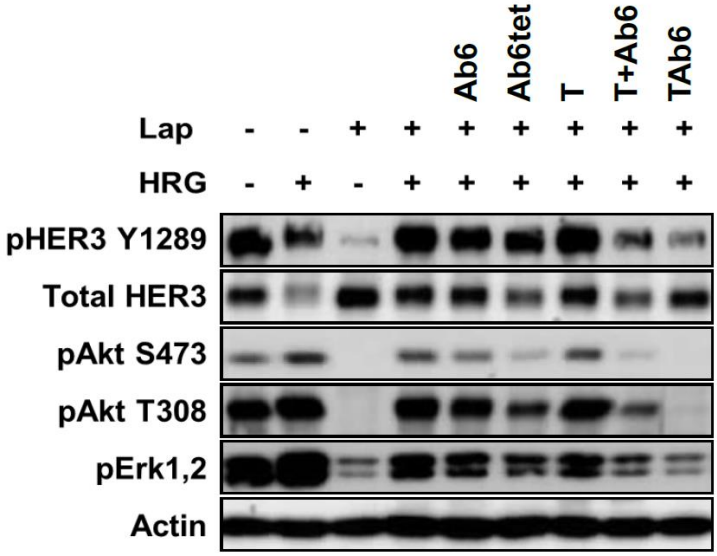

Figure 2-14. The bispecific anti-HER2/HER3 antibody, TAb6, has the highest activity in reducing PI3K/Akt signaling in HCC1419 cells in the presence of heregulin and lapatinib. Cells were treated for 24 hours with 1 μM lapatinib (Lap), 6.25 nM heregulin (HRG) and 50 nM anti-HER3 (Ab6), tetrameric anti-HER3 (Ab6tet), trastuzumab (T), trastuzumab and Ab6 (T + Ab6) or bispecific trastuzumab with anti-HER3 Ab6 scFv (TAb6) as indicated. Cell lysates were analyzed by immunoblotting.

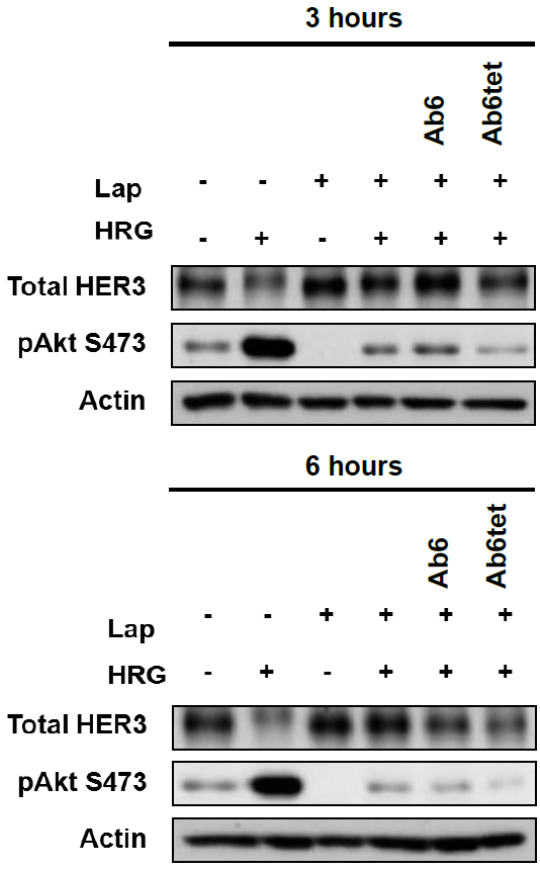

Figure 2-15. The multivalent anti-HER3 antibody, Ab6tet, induces higher levels of HER3 degradation compared with the bivalent counterpart, Ab6, in the presence of heregulin (HRG) and lapatinib (Lap). SK-BR-3 cells were treated as indicated with combinations of 1 µM lapatinib, 6.25 nM heregulin, 50 nM anti-HER3 (Ab6) or tetrameric anti-HER3 (Ab6tet) for 3 or 6 hours. Cell lysates were analyzed for total HER3 and pAkt (S473) by immunoblotting.

2.3 Discussion

The limitations of targeting individual components of the HER3/PI3K/Akt signaling axis, including the activity of the preferred dimerization partner HER2, is well documented. Several factors contribute to the poor efficacy of this approach: first, antibodies specific for HER2 and HER3 have reduced activity in inhibiting proliferation and signaling in the presence of the HER3 ligand heregulin[63, 134, 135] (this study), which is expressed in multiple tumor types[119-121]. Second, the use of small molecule TKIs such as lapatinib or gefitinib results in compensatory HER2 and HER3 upregulation and signaling through either incomplete blockade of HER2 kinase activity or HER3 association with other signaling competent partners[20, 112, 129-132, 137, 138]. Third, these compensatory effects are exacerbated by the presence of heregulin[63, 134-136]. Consequently, TKIs such as lapatinib are ineffective as single agents in inhibiting breast tumor cell proliferation, indicating a need for the development of combination therapies[63, 129-132].

In the current study, we analyzed the efficacy of two HER3-focused strategies directed toward reducing breast cancer cell signaling and proliferation. These approaches also have broader relevance to the targeting of other cell surface receptors, and involve the use of distinct antibody designs to recruit HER3 into kinase-inhibited HER2-HER3 complexes or induce HER3 degradation. We demonstrate that the recruitment of HER3 into lapatinib-inactivated HER2-HER3 complexes by a bispecific anti-HER2/HER3 antibody (TAb6, comprising trastuzumab and an anti-HER3 scFv) is efficacious in both ablating PI3K/Akt signaling and reducing tumor cell proliferation in the presence of

heregulin. Importantly, and of direct relevance to therapy, the bispecific antibody is a more potent inhibitor of signaling and growth than either HER2- or HER3-specific antibodies alone or a mixture of antibodies of both specificities. In a second approach, we compared the effect on tumor cell signaling and growth of a multivalent anti-HER3 antibody (Ab6tet) that is designed to enhance HER3 degradation with its bivalent counterpart, Ab6. In the presence of heregulin and lapatinib, Ab6tet has higher activity. By comparison with bivalent Ab6, this multivalent construct induces more rapid HER3 internalization into early endosomes. By contrast, the bispecific TAb6 induces less HER3 degradation than either Ab6 or Ab6tet, and yet is more effective in reducing cell signaling and proliferation. This indicates that the internalization resistance or recycling behavior of HER2[149, 150] has a dominant effect on HER3 in the forced HER2-HER3 heterodimers. Further, the internalization resistance is consistent with earlier studies in which endocytic uptake of EGFR or HER3 is reduced by dimerization with HER2[149, 150]. Importantly, our data indicate that the locking of HER3 into inactive HER2-HER3 complexes, even if they remain on the plasma membrane, is a more effective strategy for the ablation of heregulin-mediated signaling than induction of increased HER3 degradation.

The question arises as to why the anti-HER3 antibody, which competes for heregulin binding[19], is not as effective either alone or in combination with trastuzumab as the bispecific antibody, TAb6, in reducing HER3-PI3K signaling. In addition to locking HER3 into dimers, TAb6 would be expected to enhance the avidity of binding of Ab6 to HER3 through bridging of trastuzumab-HER2 complexes. The trastuzumab-

HER2 interaction is of very high affinity (100 pM)[3], and this, combined with high HER2 expression levels on the cell surface, should increase avidity effects. Further, although Ab6tet is expected to bind with increased avidity over Ab6 through increased valency, the Ab6-HER3 interaction is of lower affinity (0.8 nM)[111]. Thus, the improved efficacy of Ab6tet relative to Ab6 could be due to both increased degradation of HER3 and higher avidity binding, but the avidity enhancement resulting from multivalent binding would be lower than that for TAb6.

The use of bispecific antibodies of different formats is an active area in the development of cancer therapeutics[152]. For example, strategies to target both HER2 and HER3 using several different bispecific antibody formats or mixtures of antibodies have been described[63, 68, 118]. Of relevance to the use of bispecifics, however, we observe that in the absence of lapatinib (and heregulin), exposure of SK-BR-3, BT-474 or HCC1419 cells to bispecific antibodies comprising either trastuzumab or pertuzumab and the anti-HER3 scFv, Ab6 (TAb6 or PAb6, respectively), results in increased PI3K/Akt signaling and proliferation. The possibility that this activation is due to relief of feedback inhibition of the FoxO1/3a transcription factors, leading to upregulation of multiple receptor tyrosine kinases such as HER3 and IGF-1R[130, 147, 148], is excluded by the rapid kinetics of pAkt induction (15 min). The observation that bispecifics containing either trastuzumab (TAb6) or pertuzumab (PAb6) are both active in inducing HER3 phosphorylation and PI3K/Akt signaling suggests that proximity rather than a specific configuration of HER2 and HER3 is sufficient for HER3 transphosphorylation. This is consistent with our observation that bispecific HER2/HER3 specific antibodies can

sequester HER3 into HER2-HER3 heterodimers that, if inhibited by HER2-specific TKIs, effectively silence HER3.

We also characterized the effect of using antibodies of different designs on intracellular trafficking. The increased internalization and trafficking to lysosomes induced by using a multivalent anti-HER3 antibody (Ab6tet) suggests that this approach could be used to enhance the activity of antibody-drug conjugates for which lysosomal delivery is required[141]. By contrast, a high proportion of the bispecific, TAb6, persists on the plasma membrane where it is exposed for recognition by FcγRs or complement receptors, allowing antibody dependent cell-mediated cytotoxicity/phagocytosis (ADCC/ADCP) or complement-mediated cytotoxicity by appropriate effector cells[140].

Earlier studies have demonstrated that dual targeting of HER2 and HER3, using either bispecific scFvs or mixtures of individual antibodies specific for HER2 and HER3, reduces tumor cell growth in the presence of lapatinib[63, 118]. Significantly, we demonstrate that TAb6 is more effective than mixtures of trastuzumab and Ab6. This is consistent with the concept that TAb6 anchors HER3 into lapatinib-inactivated HER2-HER3 dimers, thereby sequestering it from interactions with other kinase competent partners and enabling Ab6 to bind to HER3 with increased avidity. By analogy with our observations, the use of a bispecific scFv-human albumin fusion (MM-111) has been shown to have anti-tumor effects in the presence of heregulin that were increased by the addition of lapatinib[63], although the efficacy of MM-111 was not directly compared with that of anti-HER2 or anti-HER3 antibodies of the same specificities as those present in MM-111. Further, and by contrast with this earlier report, we observe lower levels of

heregulin-induced proliferation and, for most conditions or cell lines, no significant anti-proliferative effects of monotherapy with lapatinib or trastuzumab in the presence of heregulin. These apparent discrepancies may be due to differences in assay conditions, such as the addition of heregulin following antibody treatment[63] rather than simultaneous addition as used in the current study.

An important difference between the activity of TAb6 and MM-111 is that, in the absence of heregulin and lapatinib, MM-111 does not induce proliferation[63]. The design of TAb6 and MM-111 differs in several respects: first, the scFvs specific for HER2 and HER3 in MM-111 are distinct from those in TAb6. Although both the anti-HER3 scFv (H3[153]) and Ab6 compete with heregulin for binding to HER3, this does not exclude the possibility that the two antibodies recognize distinct epitopes. The HER2-specific scFv, B1D2, binds to an epitope that does not overlap with trastuzumab[63, 154]. Second, TAb6 has two anti-HER2 and two anti-HER3 Fabs/Fvs per molecule, whereas MM-111 has one scFv of each specificity. Tetravalency is expected to enhance the avidity of the interaction with HER2/HER3. Third, TAb6 has an antibody Fc region whereas the scFvs in MM-111 are linked to albumin, resulting in variations in the "span" distance of the Fv components of the two constructs. One or more of these factors could contribute to the different activities of MM-111 compared with TAb6. Significantly, the presence of an Fc region in TAb6 confers effector function activities such as ADCC. The surface retention of targeting antibodies such as TAb6 is expected to enhance ADCC and other cell-mediated cytotoxicity pathways, which in turn could enhance anti-tumor activity[140].

Other multivalent antibody-based or designed ankyrin repeat proteins (DARPins) that target HER2 or HER3 have been recently described[64, 155, 156]. Specifically, a tetravalent antibody (MM-141), with a similar design to TAb6 in the current study, that targets both HER3 and IGF-1R has been shown to have anti-proliferative effects both *in vitro* and *in vivo*[64]. Analogously to our observations using TAb6 in combination with lapatinib, MM-141 is more effective in reducing tumor cell signaling and growth than mixtures of the individual antibodies of the corresponding specificities. However, MM-141 may not be as effective as TAb6 in targeting HER2-overexpressing tumors, given the importance of the HER2/HER3 signaling axis in such malignancies. In the context of targeting HER2, a divalent anti-HER2 DARPin has been optimized to "lock" HER2 into an inactive dimeric configuration on the cell surface[156]. This DARPin-based construct represents a notable expansion to the possible types of molecular approaches for targeting HER2-addicted tumors.

Future experiments will be directed toward analyzing the anti-tumor activity of a combination of lapatinib and our lead antibody, TAb6, in tumor-bearing mice. Earlier studies using lapatinib with the bispecific anti-HER2/HER3 antibody, MM-111, indicated that weekly dosing of antibody with daily lapatinib was unexpectedly more effective than MM-111 delivery every three days with daily lapatinib[63]. This indicates that the dosing regimen of lapatinib and TAb6, which has a longer *in vivo* persistence than MM-111[63], will require optimization. Collectively, we compared the effects of targeting HER2, HER3 or both receptors with several different antibody formats on the proliferation and signaling of breast cancer cell lines. These studies demonstrate that in

the presence of the TKI inhibitor, lapatinib, a bispecific anti-HER2/HER3 antibody has higher activity than individual (multivalent) antibodies specific for HER2 and HER3 in inhibiting heregulin-induced signaling through the PI3K/Akt pathway and cell proliferation. These observations suggest that the use of such bispecifics in combination therapy with lapatinib to sequester HER3 into inactive heterodimers may provide an effective pathway for the treatment of cancer.

2.4 Materials and methods

2.4.1 Cell lines and reagents

The human breast cancer cell lines BT-474 and SK-BR-3 were obtained from the American Type Culture Collection (ATCC, catalog nos. HTB-20 and HTB-30, respectively) and cultured in Hybricare Medium (ATCC, catalog no. 46-X) and McCoy 5a (Gibco, catalog no. 12330–031/Hyclone, catalog no. SH30200.01), with 1% penicillin/streptomycin and 10% FCS, respectively. The human breast cancer cell line HCC1419 (a generous gift of Drs Adi Gazdar, John Minna, and Kenneth Huffman, Hamon Center for Therapeutic Oncology Research, University of Texas Southwestern Medical Center at Dallas, Dallas, Texas) was cultured in RPMI 1640 with 1% penicillin/ streptomycin and 5% FCS. For imaging experiments, cells were cultured in phenol-red free DMEM (Gibco, catalog no. 31053–028) supplemented with 1% penicillin/streptomycin, 1% L-Glutamine, 10 mM HEPES buffer, 1 mM sodium pyruvate, 100 nM MEM non-essential amino acids, 55 nM 2-mercaptoethanol and 10% FCS. Polyclonal antibodies specific for phospho-Akt-T308 (catalog no. 9275S), Akt, phospho-Erk1,2 (catalog no. 9101S), Erk1,2 (catalog no. 9102S), phospho-HER2 Y1221/1222 (catalog no. 2249S), and monoclonal antibodies against phospho-Akt-S473 (D9E) (catalog no. 4060L), and phospho-HER3 Y1289 (D1B5) (catalog no. 2842) were obtained from Cell Signaling Technologies. Polyclonal anti-HER3 antibody (C-17) (catalog no. SC-285) was from Santa Cruz Biotechnology and monoclonal anti-c-erbB2 antibody (Ab-3 3B5) (catalog no. OP15L) was from Millipore. The monoclonal anti-actin antibody (Ab-5) (catalog no. 612656) was from BD Bioscience. Horseradish

peroxidase-labeled goat anti-rabbit and anti-mouse IgG (H+L) (catalog nos. 111-035-003 and 115-035-003, respectively) were purchased from Jackson ImmunoResearch Laboratories. Lapatinib (catalog no. L-4804) was obtained from LC Laboratories and recombinant human heregulin-β1 (HRG-β1; EGF-like domain, catalog no. 100–03) was obtained from Peprotech.

2.4.2 Recombinant antibodies

Clinical grade trastuzumab and pertuzumab were obtained from the UT Southwestern Pharmacy. For comparative purposes, trastuzumab and pertuzumab were also expressed in recombinant form using the same expression host as the other antibodies used in this study. Expression plasmids for the production of antibodies in stably transfected CHO cells were generated as follows: the genes encoding the heavy and light chain variable domains (VH and VL, respectively) of trastuzumab[3], pertuzumab[143], and Ab6 (US patent 20100266584A1; MM-121[19]) were synthesized commercially (Integrated DNA Technology, Genscript, or Thermo Fisher) and used to generate full-length human IgG1 and human kappa genes with the leader peptide (MGWSCIILFLVATATGVHS) from the anti-lysozyme antibody, Hulys10[157], using standard methods of molecular biology. The vectors pcDNA 3.3 TOPO and pOptiVECTOPO (OptiCHO Ab Express Kit, Life Technologies, catalog nos. K8300–01 and 12744017, respectively) were used for the expression of the light and heavy chain genes, respectively. To generate expression constructs for bispecific, tetravalent antibodies, a similar design to that described previously was used[158]. A linker sequence

containing a unique *Xho*I site was inserted at the 3′ end of the heavy chain genes (trastuzumab and pertuzumab) using a designed oligonucleotide and the PCR. A scFv gene encoding the Ab6 scFv with codons encoding a $(Gly_4Ser)_3$ linker peptide between the VH (JH) and VL gene was generated using standard methods of molecular biology. *Xho*I sites and Gly-Ser-Ser codons to connect the CH3 domain to the VH gene, were appended to the 5′ and 3′ ends of the scFv gene using the PCR. This scFv gene was cloned into the *Xho*I sites at the 3′ ends of the trastuzumab and pertuzumab heavy chain genes to generate full-length heavy chains linked to the Ab6 scFv. Complete sequences of all expression plasmids are available upon request.

2.4.3 Transfection and expression of recombinant antibodies

Light chain expression constructs were transfected into CD/DG44 CHO cells (Life Technologies, catalog no. A11000-01) using electroporation. Desired clones were selected in CD/DG44 CHO medium (Life Technologies, catalog no. 12610010) containing 500 µg/ml geneticin without the HT supplement. The clone expressing the highest levels of light chain was identified by screening culture supernatants with ELISAs using goat anti-human kappa light chain antibody for detection (Sigma-Aldrich, catalog no. A7164). Heavy chain expression constructs were then transfected into their respective stably transfected light chain expressing CD/DG44 CHO clones via electroporation and selected with Opti-CHO Medium (Life Technologies, catalog no. 12681-011) containing 500 µg/ml geneticin. Supernatants of clones were screened by sandwich ELISA using goat anti-human IgG (Fab-specific, Sigma-Aldrich, catalog no.

I5260) as capture antibody and goat anti-human IgG (Fc-specific) conjugated to horseradish peroxidase (Sigma-Aldrich, catalog no. A0170) as detection antibody. The clones expressing the highest levels of antibody were expanded and cultured in increasing concentrations of methotrexate (MTX, 50 nM–4 μM), to induce gene amplification. Clones were further expanded in shake flasks (130 rpm) in 8% CO_2 and antibody purified from culture supernatants using protein G-Sepharose (GE Healthcare, catalog no. 17-0618-05). Several antibodies were also scaled up and purified by BioXCell.

2.4.4 Surface plasmon resonance analyses

Surface plasmon resonance experiments were performed using a BIAcore 2000 and previously described methods[159, 160]. Recombinant Fc-HER2 (R&D Systems, catalog no. 1129-ER-050) and HER3 (Acro Biosystems, catalog no. ER3-H5223) were coupled to flow cells of CM5 sensor chips to densities of 758 and 467 RU, respectively. Antibodies at a concentration of 50 nM were injected in phosphate buffered saline (PBS) plus 0.01% Tween at a flow rate of 10 μl/min. At the end of an 800 s dissociation phase, bound antibody was stripped from the flow cells using 0.1 M glycine, 0.9 M NaCl, pH 3.8. Data were analyzed using BIAevaluation software.

2.4.5 Pharmokinetics

The *in vivo* half-lives of ^{125}I labeled Ab6tet and TAb6 were analyzed following intravenous or intraperitoneal delivery in BALB/c SCID mice (Jackson Laboratories) using previously described methods and whole body counting[161].

2.4.6 Proliferation assays

Cells were plated in 96-well plates at a density of 2,500 cells per well and incubated overnight. Cells were treated with lapatinib (1 μM), HRG-β1 (6.25 nM), anti-HER3 antibody Ab6 or the tetrameric form, Ab6tet, trastuzumab (anti-HER2), pertuzumab (anti-HER2), or the bispecific anti-HER2/ HER3 antibodies TAb6 and PAb6 as indicated in the figure legends. Antibodies were used at a concentration of 50 nM unless otherwise indicated. Dimethyl sulfoxide or PBS were used as vehicle controls for lapatinib or HRG-β1/antibodies, respectively. After 5 d of incubation in a 37 °C 5% CO_2 incubator, cell proliferation was quantitated using CellTiter 96 AQueous One Solution Proliferation Assay kit (Promega, catalog no. G3580) according to the manufacturer's instructions.

2.4.7 Immunoblotting

Cells cultured to near confluence in 6-well plates were treated with lapatinib, HRG-β1 or antibodies as for proliferation assays. Following 15 min, 1 h, or 24 h incubation, cells were lysed using RIPA buffer (50 mM Tris, 150 mM NaCl, 0.5% sodium deoxycholate, 1% Triton X-100, 0.1% sodium dodecyl sulfate, 2 μg/ml

aprotinin, 2 µg/ml leupeptin, 1 µg/ml pepstatin A, and 0.4 mg/ml pefabloc SC PLUS). Lysates were centrifuged for 20 min at 14,600 rpm at 4 °C and supernatants were collected. Protein concentrations in each lysate were determined using the BCA protein assay reagent (Pierce, catalog no. 23223). Total lysates were fractionated by SDS-PAGE and transferred onto polyvinylidene difluoride (PVDF) membranes (Millipore, catalog no. IPVH00010) or nitrocellulose membranes (Bio-Rad, catalog no. 162-0145). Membranes were incubated with 5% bovine serum albumin in Tris-buffered saline with 0.1% Tween (TBST, pH 8.0) for 1 h following transfer to block non-specific binding sites. Blocked membranes were incubated with primary antibodies overnight at 4 °C with agitation. Prior to incubation with the secondary antibodies conjugated to horseradish peroxidase, blots were washed three times (10 min per wash) with TBST. Following incubation with secondary antibodies for 1 h and washing, bound secondary antibody was detected using chemiluminescent detection regent (GE Healthcare, catalog no. RPN 2209/AF).

2.4.8 Fluorescence microscopy

SK-BR-3 cells incubated overnight at a density of 50,000 cells per dish were treated with 50 nM Ab6, Ab6tet, or TAb6 for 5 or 15 min at 37 °C and then either immediately washed and fixed or chased in medium at 37 °C for 10, 20, or 45 min prior to washing and fixation. For fixation, cells were treated with 1.7% (w/v) paraformaldehyde for 10 min at 37 °C and then permeabilized with 0.05% (v/v) saponin for 10 min at room temperature in PBS. A pre-block with 4% BSA/PBS was performed

prior to staining with 2 µg/ml of polyclonal rabbit anti-LAMP-1 antibody (Abcam, catalog no. AB24170) and 12.5 µg/ml monoclonal mouse anti-EEA-1 (clone 14) from BD Bioscience (catalog no. 610456) for 30 min at room temperature. After blocking for 30 min with goat serum (Sigma-Aldrich, catalog no. G6767), bound primary antibodies were detected by incubating cells with the following secondary antibody conjugates for 25 min at room temperature: Alexa 555-labeled goat anti-human IgG (H+L) (Life Technologies, catalog no. A21433), Alexa 647-labeled goat anti-mouse IgG (H+L) (Life Technologies, catalog no. A21236) and Alexa 488-labeled goat anti-rabbit IgG (H+L) (Life Technologies, catalog no. A11034). Cells were washed twice with PBS between each incubation step and were stored at 4 °C in 1% BSA/PBS. Images were acquired using a Zeiss Axiovert 200M inverted fluorescence microscope with a 63X Plan Apochromat objective as described previously[162, 163]. Data was processed using custom written software in MatLab (MIAtool/LABSoft; http://www.wardoberlab.com/software/miatool/).

2.4.9 Statistical analyses

Statistical significance for differences in mean values of triplicate samples (immunoblots, ELISAs) was determined by Student *t* test. *P* values < 0.05 were considered to be significant.

2.4.10 Labeling of antibodies

Antibodies were labeled with either Alexa Fluor® 647 carboxylic acid, succinimidyl ester (Life Technologies, Catalog # A-20173) or Alexa Fluor® 488 carboxylic acid, succinimidyl ester (Life Technologies, Catalog # A-10235) using methods recommended by the manufacturer. Following the labeling reaction, antibodies were extensively dialyzed against PBS to remove unincorporated Alexa dye.

2.4.11 Flow cytometry

Cells were seeded at a density of 100,000 cells per well in 24 well plates, incubated overnight, and subsequently treated with either 1 μM lapatinib or vehicle control (DMSO) for 24 hours at 37 °C in a CO_2 incubator. Treated cells were incubated with Alexa 647-labeled Ab6 and Alexa 488-labeled trastuzumab (50 nM each) for 15 minutes at 37 °C in a CO_2 incubator. Following incubation, cells were trypsinized, washed, and suspended in PBS. Stained cells were analyzed using a BD FACScalibur and data processed using FlowJo (Tree Star).

2.4.12 Size exclusion chromatography

Following protein G-Sepharose purification, antibodies were analyzed by size exclusion chromatography using HPLC and a Hiload 16/600 Superdex 200 pg column (GE Healthcare, catalog no. 28989335) or a Yarra 3U SEC-3000 (catalog no. 00H-4513-E0) column. TAb6, Ab6tet and Ab6 were also purified as homodimeric, bispecific antibodies using the Hiload 16/600 Superdex 200 pg column. We observed that the

purified, homodimeric proteins had analogous activities to that of the material purified only on protein G-Sepharose in both MTS/proliferation and immunoblotting experiments (data not shown).

2.4.13 Serum stability assays

Antibodies were diluted into mouse serum (Thermo Scientific, catalog no. 31881) to a concentration of 40 μg/ml and incubated for 3 or 6 days at 37 °C. Samples were diluted in PBS and analyzed by sandwich ELISA. 96 well plates were coated with goat species anti-human Cκ antibody (Sigma-Aldrich, catalog no. K3502), blocked with 1% BSA/PBS and dilutions of serum samples in PBS added. Bound antibodies were detected using a goat anti-human IgG (Fc-specific) antibody conjugated to horseradish peroxidase (Sigma-Aldrich, catalog no. A0170).

3. ENGINEERING ANTIBODY-RECEPTOR INTERACTIONS TO GENERATE HIGHER POTENCY ANTIBODY-DRUG CONJUGATES[†]

3.1 Introduction

Antibody-drug conjugates (ADCs) represent a rapidly expanding class of cancer therapeutics that combine the high specificity of antibodies with the potent cytotoxicity of drugs[164-166]. ADCs comprise antibodies that are chemically conjugated to highly cytotoxic drugs that include microtubule-disrupting agents (maytansinoids, auristatins) and DNA-damaging agents (calicheamicin, pyrrolobenzodiazepine dimers)[164, 165]. By targeting the drug to surface receptors on tumor cells, rather than systemic delivery of drug throughout the body, the toxicities associated with conventional chemotherapeutic treatments can be reduced. For the majority of current ADC formats, internalization and entry into acidic, degradative compartments are essential for drug delivery to the cytosol following binding of the ADC to target at the cell surface[164, 165]. Although the concept of targeting cancer with ADCs was originally proposed in the 1980s, until recently, clinical success was hampered by limitations in linkage chemistry for drug conjugation and insufficient potency of the drug[164, 165, 167, 168]. Major advances in linker technology combined with the identification of more potent drugs have led to the approval of several ADCs for use in the clinic and ~65 different ADCs in clinical trials[164, 165, 169-171]. However, despite the promise of ADCs in preclinical models, their translation into the

[†] This study has been submitted to the journal *Nature Biotechnology* (Kang JC, Sun W, Khare P, Karimi M, Wang X, Shen Y, Ober RJ, Ward ES) and is currently under review.

clinic has been hindered by dose-limiting toxicities, resulting in delivery of doses that can be suboptimal for therapeutic effects[71, 172].

To achieve the threshold payload of drug delivery to induce cell death of tumor cells using ADCs, relatively high levels of expression of the tumor target are necessary[164, 165]. For example, in clinical trials using the FDA-approved ADC comprising the HER2-specific antibody, trastuzumab, linked to the maytansinoid derivative, DM1 (trastuzumab-DM1, T-DM1[169]), breast cancer patients with lower levels of HER2 expression showed poor responses compared with those observed in patients with HER2-overexpressing tumors[165, 173, 174]. Although increased payload delivery could be achieved by delivering higher doses of ADC, this approach can lead to unacceptably high toxicities towards normal cells[71, 172]. Consequently, a major limitation of current ADC platforms is the observation of dose-limiting toxicities, that in some cases, necessitate the use of doses that are below those required for efficacy in preclinical models[172]. An additional issue with current targeting approaches is that ADC treatment can lead to resistance due to a reduction of the level of surface biomarker. For example, decreases in surface levels of targets such as HER2 have been observed in tumor cells following treatment with T-DM1[175, 176]. Such reductions in surface expression levels of the targeted cancer biomarker narrows the therapeutic window even further.

A possible pathway towards overcoming these limitations is to develop ways of generating ADCs that deliver their payload more efficiently to the desired subcellular compartment, typically late endosomes or lysosomes, within target cells. Such an approach would endow the ADC with higher anti-tumor activity without the need to

increase the dose. Consideration of the trafficking and delivery pathway of an ADC and its target suggests a possible strategy. To release their toxic payload, the majority of current ADCs are designed to internalize and enter lysosomes[164, 165]. Due to the typically high affinity of the ADC for target at endosomal, acidic pH, payload delivery is therefore usually accompanied by target downregulation in these degradative compartments. These effects provide support for the premise that engineering the ADC to confer dissociation from its target within endosomes will enable payload entry into lysosomes, combined with recycling of unliganded target and reloading with additional ADC. This approach holds the promise to result in both increased payload delivery and reduced target downregulation, leading to therapeutic efficacy of ADCs at lower doses in combination with cytotoxicity towards cells with a broader range of target expression levels. A possible strategy towards achieving this is to generate 'acid-switched' ADCs comprising engineered antibodies that bind to their target with substantially higher affinity at near neutral, extracellular pH relative to acidic pH, to result in endosomal dissociation of the ADC following internalization into cells.

In the current study we have used two distinct engineering approaches to generate acid-switched variants of the HER2-specific antibody pertuzumab[177, 178]. The acid-switched antibodies have been conjugated to monomethyl auristatin E (MMAE) to produce ADCs that, compared with their parent, wild type pertuzumab conjugates, deliver MMAE at higher levels to HER2-expressing cells and are more effective in reducing tumor growth in mouse xenograft models. Importantly, these enhanced therapeutic effects are observed for tumors that express intermediate levels of HER2.

Further, increased efficacy has been observed following the delivery of relatively low doses of acid-switched ADCs with only two drug molecules per antibody. Consequently, this approach has the potential to reduce the toxicities associated with current ADCs by increasing payload delivery within target cells. This novel platform technology for ADCs also has broad relevance to multiple tumor types and targets.

3.2 Results

3.2.1 Generation of acid-switched antibodies

We initially analyzed the interactions of two clinically-approved, HER2-specific antibodies (trastuzumab[179] and pertuzumab[177]) with recombinant HER2-ECD (extracellular domain of HER2 fused to Fc) as the pH decreases from 7.4 to 6.0. The affinity of trastuzumab for HER2 is similar across the pH range 6.0-7.4, whereas the affinity of pertuzumab is around 10-fold higher at pH 7.4 compared with pH 6.0 (Fig. 3-1). Pertuzumab was therefore chosen for further engineering to generate acid-switched variants[180-182] using two approaches. First, we mutated complementarity-determining region (CDR) residues of pertuzumab that either directly interact with, or are in proximity to, HER2 residues in the X-ray crystallographic structure of the pertuzumab-HER2 complex[177] to histidine (Fig. 3-2a). Second, we randomly mutated residues in CDRH1, CDRH2, CDRH3 and CDRL2 (Fig. 3-2b), to generate five different phage display (scFv) libraries. Recombinant phage were panned against HER2-ECD with conditions designed to isolate acid-switched variants (selection at pH 7.4; elution at pH 5.8).

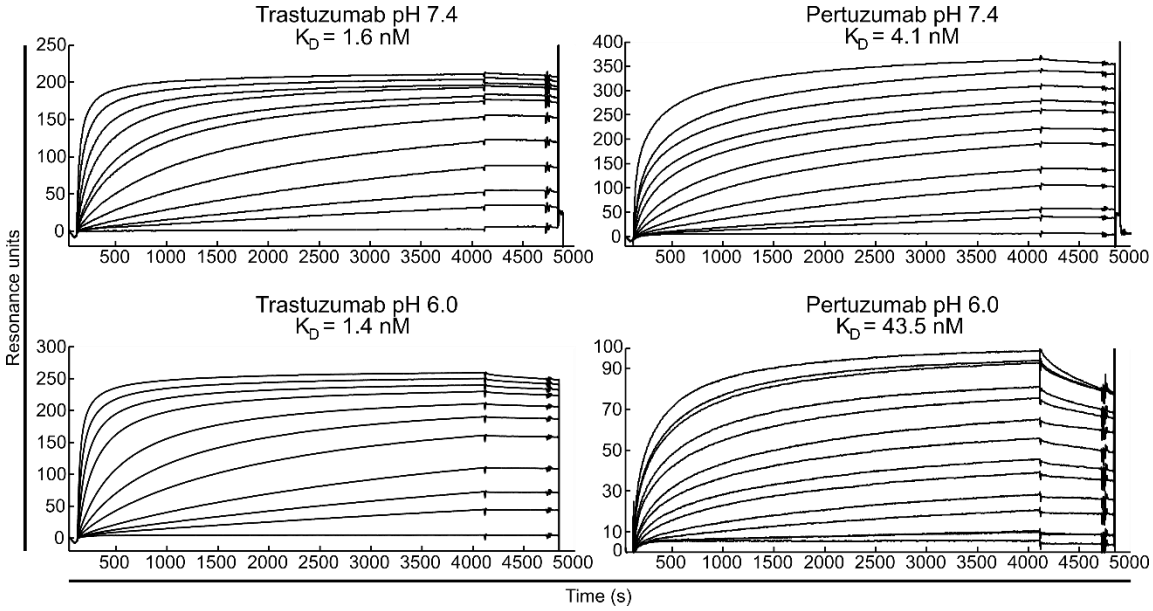

Figure 3-1. Surface plasmon resonance analyses of the interaction of clinical grade trastuzumab or clinical grade pertuzumab with immobilized recombinant human HER2 extracellular domain fused to Fc (HER2-ECD). Antibodies were injected at either pH 7.4 or pH 6.0 at concentrations ranging from 0.25-2,200 nM and equilibrium dissociation constants (K_Ds) determined. Representative traces for duplicate or triplicate injections for each analyte concentration are presented. Data shown are representative of at least two independent experiments.

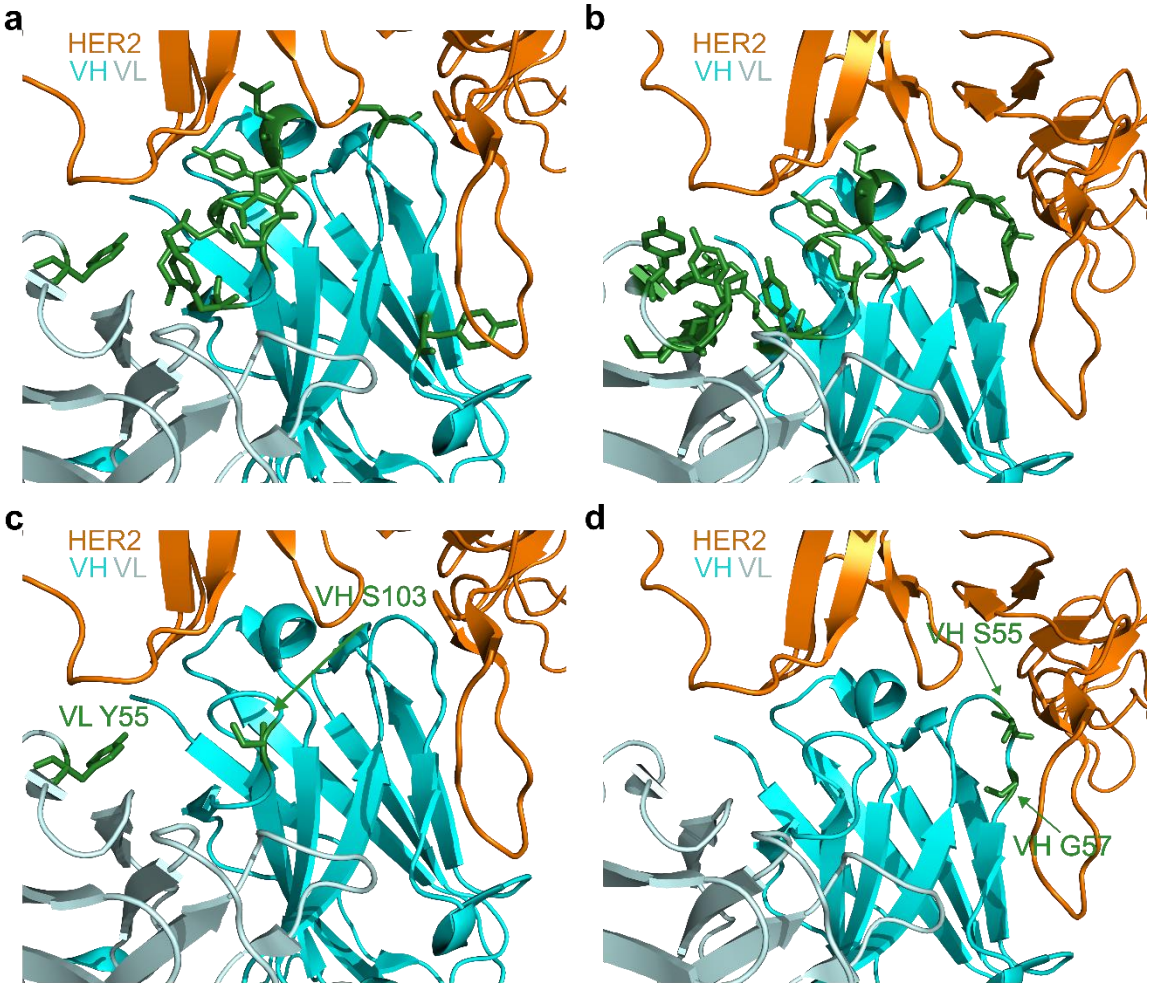

Figure 3-2. Strategy for generating acid-switched variants of pertuzumab and equilibrium dissociation constants of pertuzumab (WT or mutant) interactions with HER2. The X-ray crystallographic structure of the pertuzumab:HER2 extracellular domain complex (Protein Data Bank: 1S78) is shown, with the pertuzumab VH domain, VL domain and HER2 domain II shown in cyan, light cyan and orange, respectively. Residues targeted for mutagenesis by histidine replacement (a) or for production of phage display libraries (b) are shown in green. (c) Residues Tyr55 (CDRL2) and Ser103 (CDRH3) that were mutated to histidine to generate the YS mutant are shown in green. (d) Residues Ser55 (CDRH2) and Gly57 (CDRH2) that were mutated to His and Glu, respectively, to generate the SG mutant are displayed in green. (e) Equilibrium dissociation constants (K_Ds) for the interactions of HER2-ECD with WT pertuzumab or mutated variants, YS and SG. * estimated binding affinity from the amount bound at equilibrium (see methods). **N.D., not determined, since binding too low to estimate a dissociation constant.

e

	K_D (nM)			
	pH			
Antibodies	7.4	7.0	6.5	5.8
WT	2.9	5.9	27.2	137.6
YS	6.3	22.1	67.9	~1.6 x 10^3*
SG	4.7	46.4	172.7	N.D.**

Figure 3-2. Continued.

Using histidine replacement of CDR residues, two mutated variants of pertuzumab (Tyr55 to His in CDRL2; Ser103 to His in CDRH3; Fig. 3-2c) with moderate increases in pH-dependence were identified by analyzing the binding of the corresponding recombinant, pertuzumab-derived Fab fragments to HER2-ECD at pH 7.4 and 5.8. These two mutations were combined to generate the acid-switched variant 'YS' (**Y**55H-VL/**S**103H-VH) (Fig. 3-2c). In addition, an acid-switched variant with two mutations of centrally located residues in CDRH2, Ser55 to His, Gly57 to Glu ('SG') (Fig. 3-2d), was selected using phage display, and the pH-dependence of the corresponding phage for binding to HER2-ECD was substantially increased over that of phage bearing wild type (WT) pertuzumab (scFv; Fig. 3-3a). The equilibrium dissociation constants of the YS and SG variants, expressed as human IgG1/κ antibodies, with HER2 were determined at different pH values (Fig. 3-2e). Binding of these two mutants at pH 6.5 and 7.0 was also analyzed (Fig. 3-2e), since the pH of the tumor microenvironment can be within this range due to lactate production by cancer cells[183, 184]. The YS and SG mutants have similar affinities for HER2 at pH 7.4, whereas the binding affinities of the SG mutant for HER2 decrease more rapidly than that of the

YS mutant as the pH is lowered (Fig. 3-2e). Both YS and SG mutants showed no detectable aggregation following storage at 4 °C or 37 °C (30 or 5 days, respectively), and were stable in human serum during a 5 day incubation period at 37 °C, indicating favorable properties for further development (Fig. 3-3b,c).

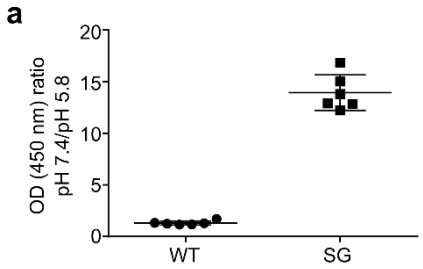

Figure 3-3. Binding behavior of phage bearing WT pertuzumab or SG mutant (as single chain Fvs, scFvs) and stability analyses of WT pertuzumab and SG, YS mutants (as full length human IgG1/κ antibodies). (a) Phage-displayed scFvs (WT or SG mutant) were analyzed for binding to HER2-ECD at pH 7.4 and 5.8 using ELISA. The ratio of signal measured at pH 7.4 to pH 5.8 was calculated. Data is representative of two individual experiments and the data show is the mean ratio (n = 6) ± SD. (b) WT pertuzumab or SG, YS mutants were stored at 4 °C for 0 days, 4 °C for 30 days, or 37 °C for 5 days and analyzed using size exclusion chromatography. (c) WT pertuzumab or SG, YS mutants were incubated in IgG-depleted, human serum for 0, 3, or 5 days at 37 °C. Antibodies were immunoprecipitated and analyzed by immunoblotting. Data shown are representative of at least two independent experiments.

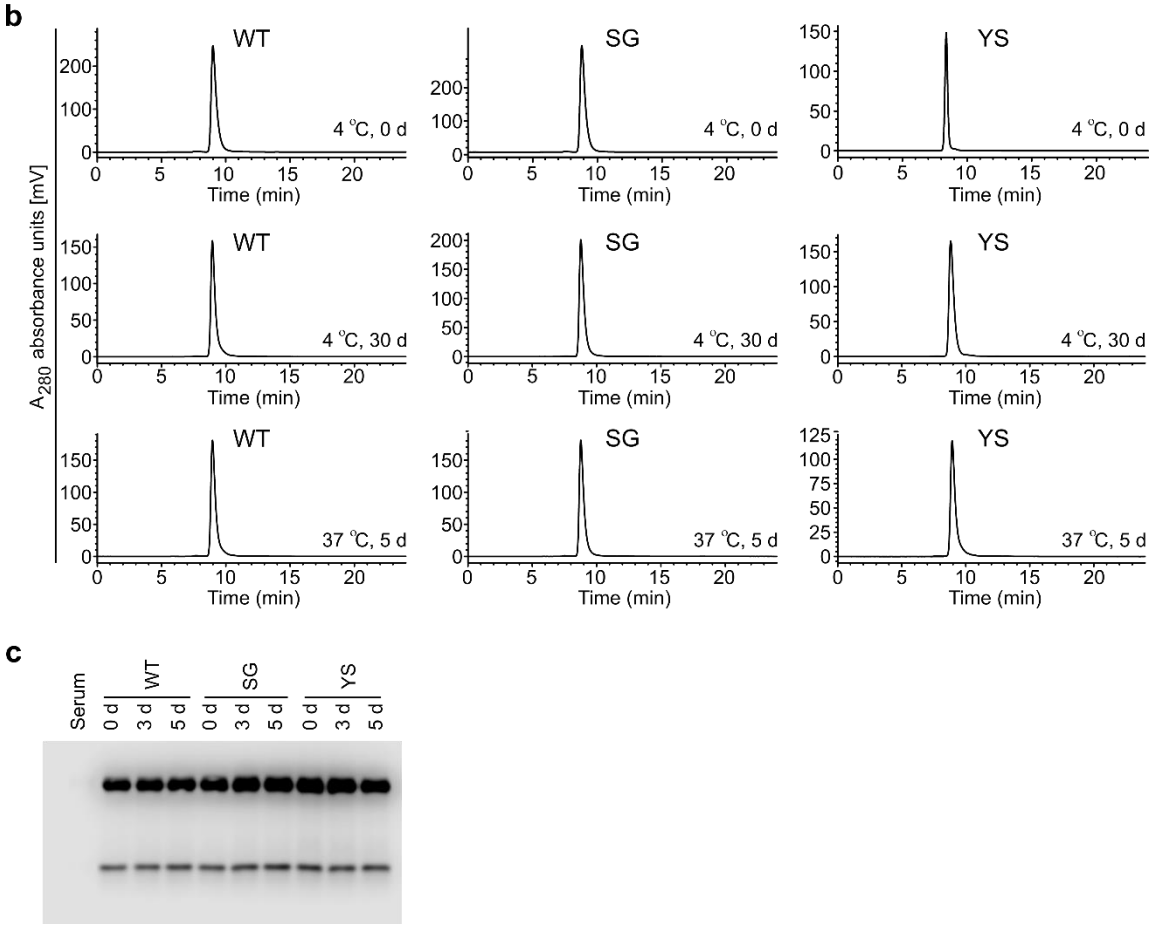

Figure 3-3. Continued

3.2.2 Acid-switched ADCs accumulate to higher levels within HER2-expressing cells

We next conjugated WT pertuzumab, the YS and SG mutants to MMAE through hinge disulfide bonds to maleimidocaproyl-valine-citrulline-p-aminobenzoyloxycarbonyl-monomethyl auristatin E (MC-VC-PAB-MMAE). The cysteines that form disulfide bonds in the hinge and between the upper hinge and Cκ domain (Cys220, Cys229 of heavy chain; Cys214 of light chain; EU numbering[185]) were mutated to serines, to result in conjugation to Cys226 with a maximum drug:antibody

ratio (DAR) of two. This lower conjugation level was used to reduce the hydrophobicity that has been reported for ADCs with higher DARs and can lead to lower *in vivo* persistence[186, 187]. HPLC analyses using hydrophobic interaction and size exclusion columns indicated that the DAR ranges from 1.7-1.9, and that conjugation did not induce aggregation (Fig. 3-4a). The ADCs were stable in human serum for up to 5 days at 37 °C (Fig. 3-4b), and analyses using ELISA demonstrated similar binding properties for HER2-ECD as their parent, unconjugated antibodies (Fig. 3-4c**)**.

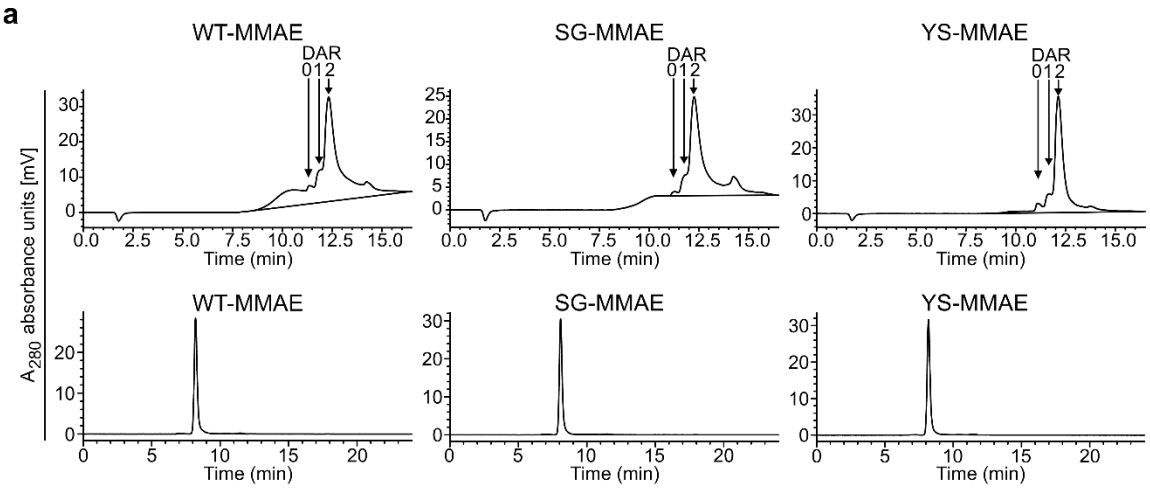

Figure 3-4. Characterization of WT pertuzumab and acid-switched mutants (SG, YS) following conjugation to MMAE. (a) MMAE-conjugated antibodies (WT-MMAE, SG-MMAE or YS-MMAE) were analyzed using a hydrophobic interaction column to determine the drug-to-antibody ratio (upper row). Analyses of MMAE-conjugated antibodies using size exclusion chromatography are also shown (lower row). (b) WT-MMAE, SG-MMAE or YS-MMAE were incubated in IgG-depleted human serum for 0, 3, or 5 days at 37 °C. Following incubation, ADCs were immunoprecipitated and analyzed by immunoblotting. (**c**) Antibodies (WT, SG and YS) and their respective MMAE-conjugated ADCs were analyzed for binding to HER2-ECD using ELISA at pH 7.0 and 5.8. Mean values for triplicate samples ± SD are shown. For panels (b) and (c), data shown is representative of two independent experiments.

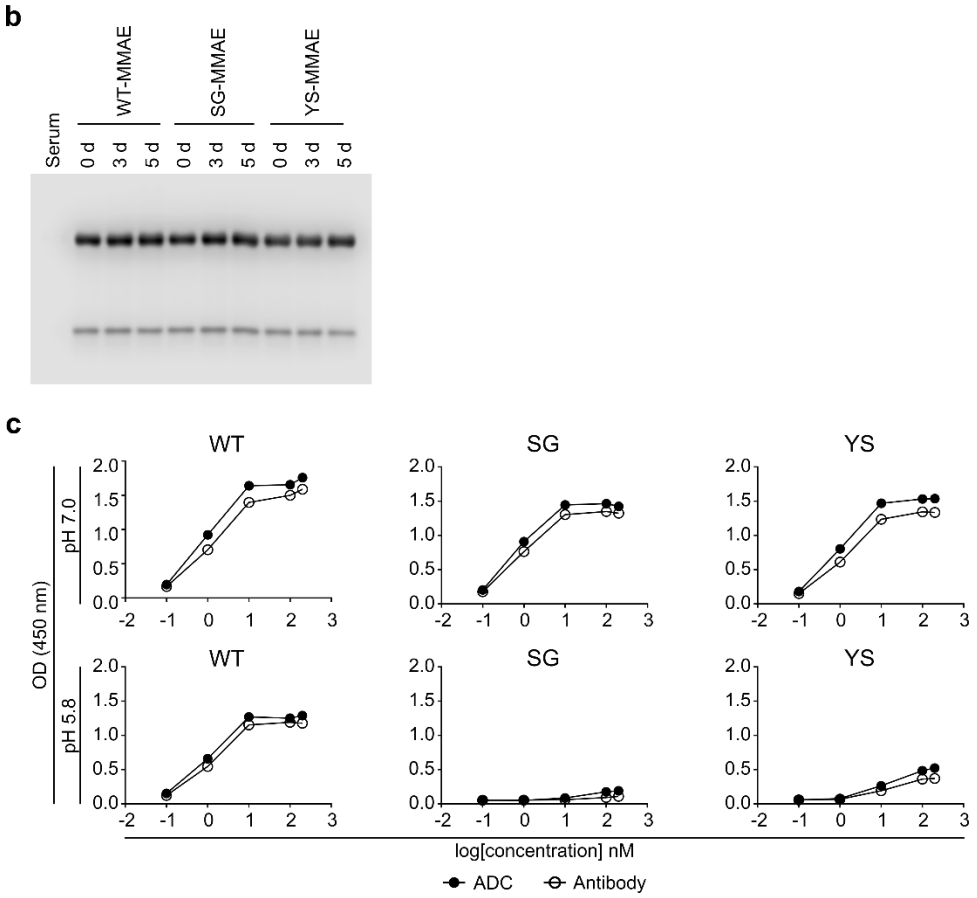

Figure 3-4. Continued.

We next investigated the effect of acid-switching on the accumulation of SG-MMAE and YS-MMAE in the HER2-expressing tumor cell lines, SK-BR-3, HCC1954, SK-OV-3, MDA-MB-453 and JIMT-1. Analyses of surface HER2 expression levels for these cell lines confirmed earlier studies[82, 188] demonstrating that SK-BR-3, HCC1954, and SK-OV-3 have high HER2 levels ($HER2^{hi}$), whereas MDA-MB-453 and JIMT-1 have intermediate levels ($HER2^{int}$) (Fig. 3-5). To quantitate the intracellular accumulation and retention of the acid-switched pertuzumab-MMAE variants, the tumor cells were treated with Alexa 488-labeled ADCs for 0.5, 4, and 20 hours. Following

these incubation times, the surface signal was quenched using an Alexa 488-specific antibody[188, 189] to quantitate internalized ADC (Fig. 3-6). Significantly higher intracellular levels of YS-MMAE and SG-MMAE were observed in all HER2^{hi} and HER2^{int} cells following incubation for 4 and 20 hours compared with WT pertuzumab conjugated to MMAE (WT-MMAE). These analyses also demonstrated that conjugated SG-MMAE accumulated to higher levels relative to YS-MMAE in the HER2-expressing cells (Fig. 3-6).

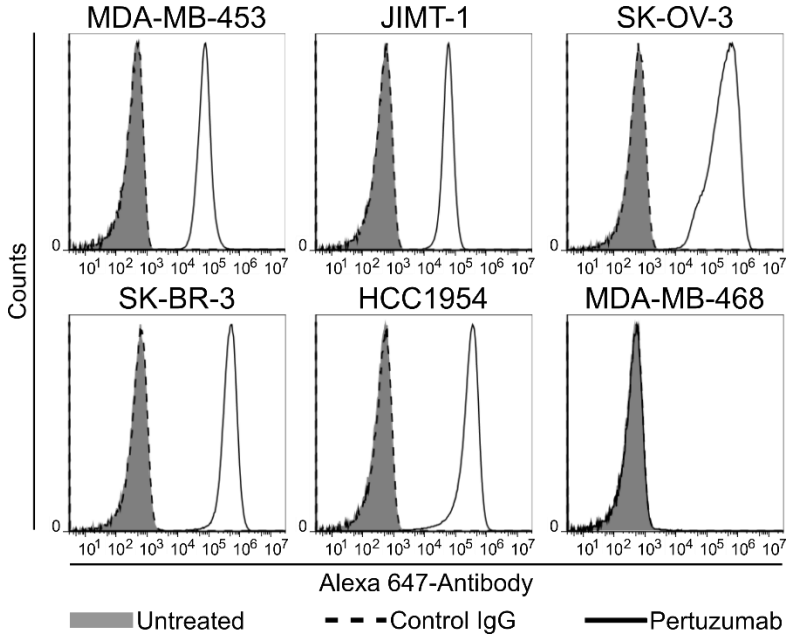

Figure 3-5. Cell surface levels of HER2 on cancer cells. Cells were incubated on ice with 33 nM Alexa 647-labeled pertuzumab (Pertuzumab), an Alexa 647-labeled isotype control (Control IgG), or media (Untreated) for 30 minutes, washed and analyzed by flow cytometry. Data shown is representative of three individual experiments.

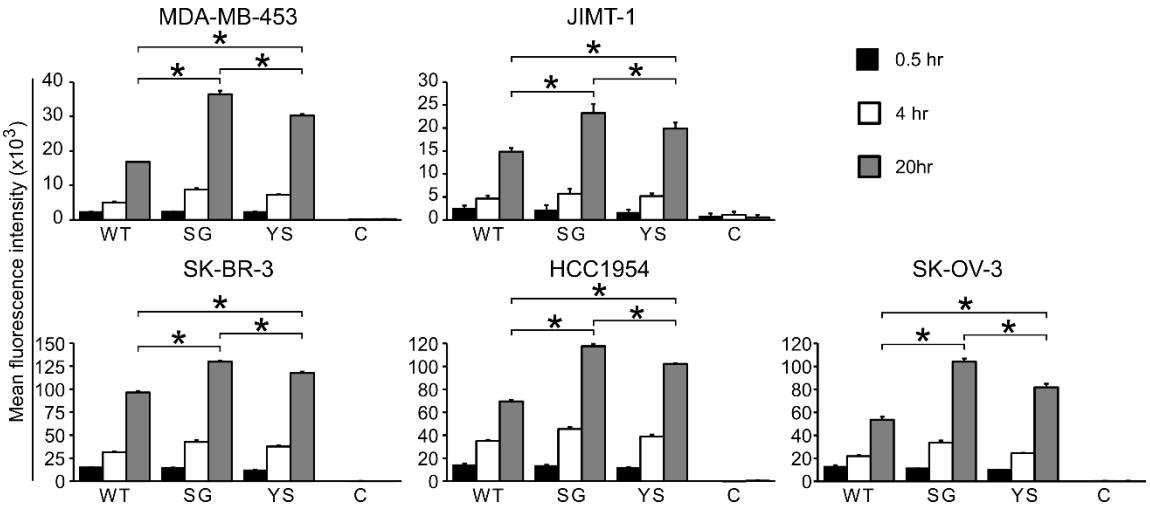

Figure 3-6. Acid-switching results in increased accumulation of ADCs in HER2-expressing tumor cells. Cells were incubated in triplicates with 10 nM Alexa 488-labeled MMAE-conjugated antibody (WT, SG, YS or control hen egg lysozyme-specific antibody, C) for the indicated times at 37 °C, washed, incubated with Alexa 488-specific quenching antibody and analyzed by flow cytometry. Mean fluorescence intensities (means of triplicate samples) showing levels of cell-associated Alexa 488-labeled ADCs at the indicated times. Error bars indicate SD. Statistically significant differences are indicated by * (unpaired two-tailed *t*-test; $p < 0.05$). Data is representative of two independent experiments.

Fluorescence microscopy was used to investigate the intracellular location of the acid-switched ADCs. Cells were pulse-chased with fluorescently labeled dextran to label lysosomes[163], and subsequently treated with ADCs for 4 or 20 hours (Fig. 3-7). Consistent with the flow cytometry analyses, both SG-MMAE and YS-MMAE accumulated to higher levels than WT-MMAE in dextran-positive lysosomes within cells following incubation for 20 hours.

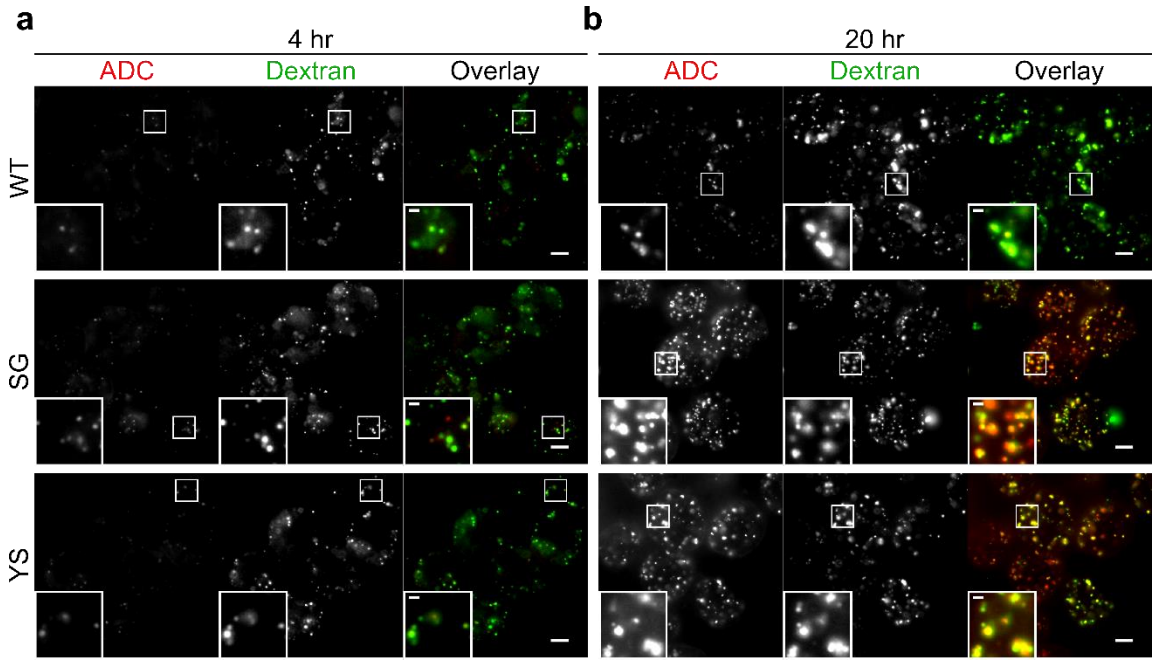

Figure 3-7. Acid-switching results in increased delivery of ADCs to dextran-positive lysosomes. MDA-MB-453 cells were incubated with 5 µM Alexa 647-labeled dextran for 2 hours followed by a 3 hour chase period to label lysosomes. Following dextran treatment, cells were incubated with 10 nM Alexa 488-labeled/MMAE-conjugated antibodies (WT, SG or YS) for 4 hours (a) or 20 hours (b). Following washing, cells were treated with Alexa 488-specific antibody for 30 minutes on ice to quench cell surface-associated signal. Samples were then fixed and imaged. Cropped regions are expanded in the lower left region of each image. Alexa 488 and Alexa 647 are pseudocolored red and green, respectively, in the overlays. Size bars = 5 µm (larger images) or 1 µm (insets). Images shown are representative cells ($n \geq 27$) from two independent experiments.

3.2.3 Acid-switched ADCs are more effective in reducing the growth of tumor cells

We next evaluated the ability of the acid-switched ADCs to reduce tumor cell viability. HER2-expressing cell lines were treated with ADCs and cell viability determined following 4 days incubation. Consistenst with the increases in accumulation of the acid-switched ADCs in $HER2^{int}$ cells, these ADCs were more effective than WT-MMAE in reducing cell viability (Fig. 3-8a). By contrast, with the exception of SKOV-3 cells, SG-MMAE, YS-MMAE, and WT-MMAE showed similar dose responses for cytotoxicity towards the $HER2^{hi}$ cell lines, SKBR-3 and HCC1954. As expected, in MDA-MB-468 cells that are $HER2^{neg}$ [82], high ADC doses were necessary to induce an inhibitory effect, and there was no difference between WT-MMAE, SG-MMAE and YS-MMAE. Collectively, our observations indicate that acid-switched ADCs are more effective than their WT parent antibody-derived ADCs in targeting HER2-expressing cells, particularly if HER2 expression is at intermediate levels.

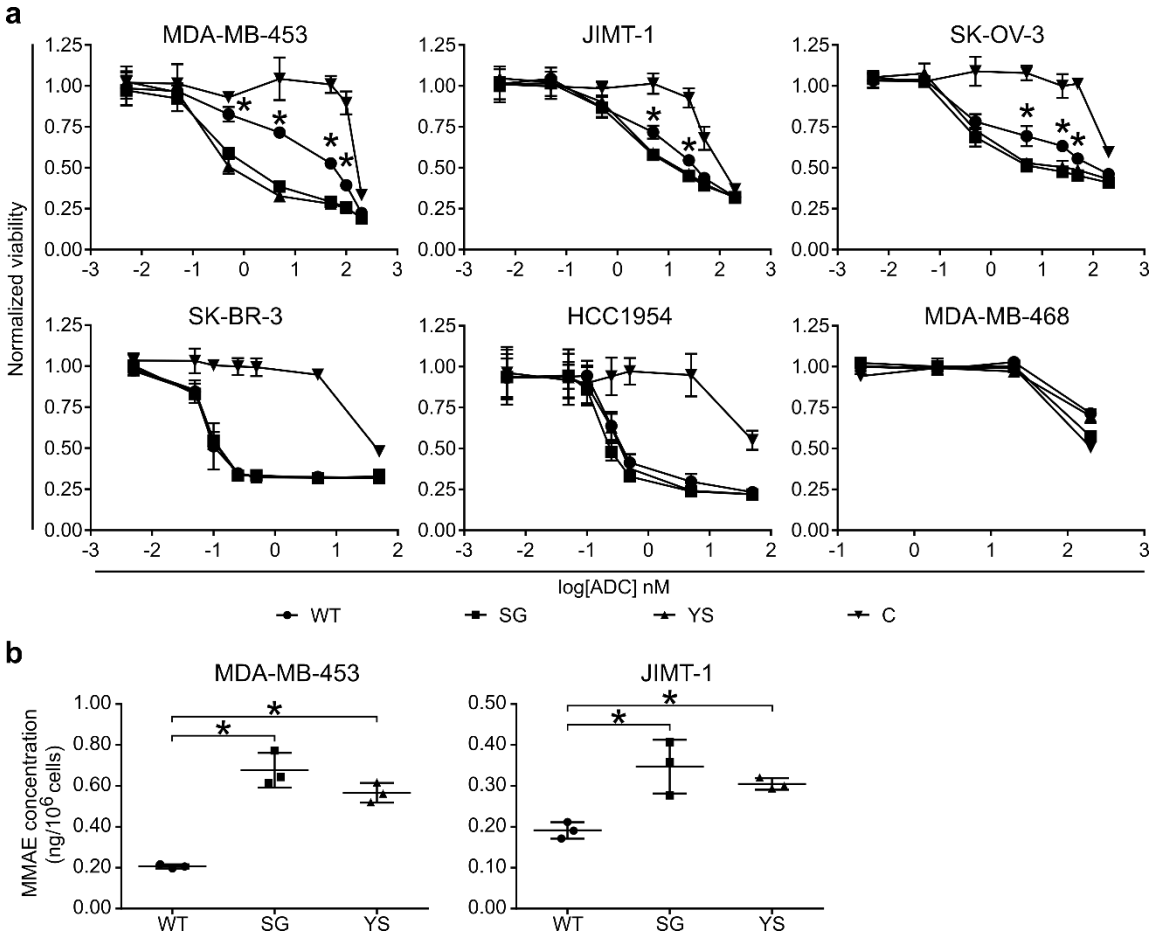

Figure 3-8. Acid-switched ADCs are more effective at reducing proliferation of HER2-expressing cells and deliver higher levels of MMAE to cells compared with WT-MMAE. (a) HER2-expressing cancer cells, or HER2-negative (MDA-MB-468) cells, were treated with the indicated concentrations of MMAE-conjugated antibodies (WT, SG, YS or control hen egg lysozyme-specific antibody, C) for 4 days and cell viability determined using the MTS reagent. (b) MDA-MB-453 and JIMT-1 cancer cells were incubated with 10 nM MMAE-conjugated antibodies (WT, SG or YS) for 20 hours. Samples were subsequently lysed in methanol and cell-associated MMAE quantitated using LC-MS/MS. Means of triplicate samples are shown, and error bars indicate SD. Statistically significant differences between YS or SG and WT are indicated by * (n = 3 independent samples per group; one-way ANOVA and Tukey's multiple comparison test; $p < 0.05$). Data is representative of at least two independent experiments.

We also used LC-MS/MS to quantitate the levels of MMAE in the HER2-expressing cell lines, MDA-MB-453 and JIMT-1, following treatment for 20 hours with 10 nM WT-MMAE, SG-MMAE or YS-MMAE (Fig. 3-8b). These analyses demonstrated that significantly higher levels of MMAE were present in these cells following treatment with SG-MMAE or YS-MMAE compared with WT-MMAE, although the difference was greater for MDA-MB-453 cells (~3-fold difference vs. ~1.5-fold for JIMT-1) (Fig. 3-8a). Consequently, the increased cytotoxicity of the acid-switched ADCs are consistent with their higher activity in delivering MMAE to target cells.

3.2.4 Acid-switching enhances therapeutic effects in mouse xenograft models

Prior to analyzing the therapeutic effects of the acid-switched ADCs, we investigated their pharmacokinetic behavior in BALB/c SCID mice. WT-MMAE, SG-MMAE and YS-MMAE have similar β-phase half-lives of 190.6 ± 4.4 hours, 184.4 ± 11.7 hours, and 195.2 ± 29.5 hours, respectively (mean ± SD, n = 5 mice/group; Fig. 3-9). The therapeutic effects of the acid-switched ADCs were next compared with WT-MMAE and the clinically approved ADC, trastuzumab-DM1 (T-DM1), in mouse xenograft models. A dose (2 mg/kg) that is suboptimal for T-DM1[82] was used to evaluate whether the acid-switched ADCs had greater anti-tumor effects. Female BALB/c SCID mice were implanted with MDA-MB-453 ($HER2^{int}$) cells and treated with ADC twice, with a three week interval (Fig. 3-10a). Treatment with SG-MMAE or YS-MMAE is more effective than WT-MMAE, T-DM1 or WT pertuzumab

(unconjugated) in inhibiting tumor growth (Fig. 3-10a). For three mice in the SG-MMAE treatment group (n = 8), tumors could not be detected at the end of the experiment (Fig. 3-11a). We also treated mice bearing JIMT-1 ($HER2^{int}$) tumors, that are relatively resistant to T-DM1[82, 190], with 2 mg/kg SG-MMAE, WT-MMAE, T-DM1 and, as controls, unconjugated WT pertuzumab or SG mutant at weekly intervals for three weeks (Fig. 3-10b). The therapeutic effect of SG-MMAE was significantly higher than that of WT-MMAE, T-DM1, and unconjugated control antibodies (Fig. 3-10b,3-11b). In all therapy experiments, ADC delivery did not result in elevated alanine aminotransferase (ALT) activity or significant weight loss, indicating that the ADCs are well tolerated (Fig. 3-11c,d).

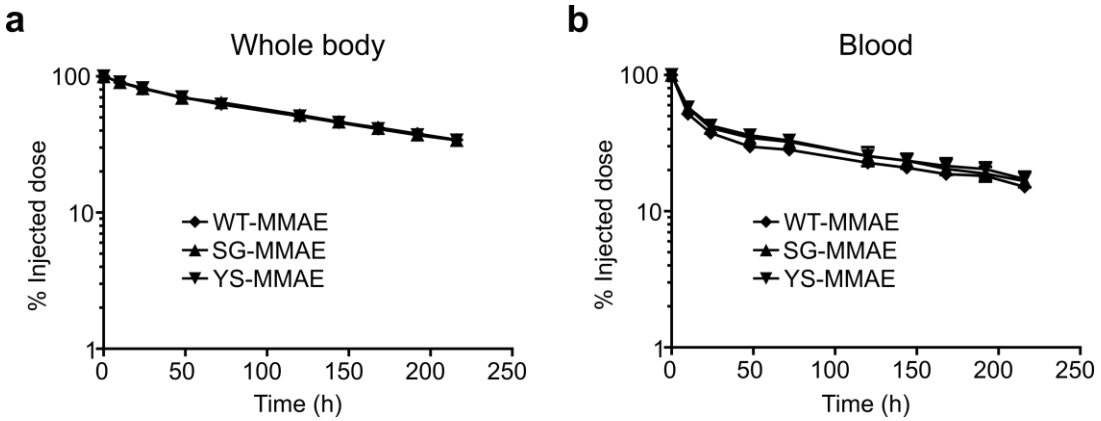

Figure 3-9. Pharmacokinetic behavior of WT-MMAE and acid-switched ADCs, SG-MMAE and YS-MMAE. Female BALB/c SCID mice (n = 5 mice/group) were injected intravenously with ^{125}I-labeled ADC and radioactivity levels in the whole body (a) or blood (b) were determined at the indicated times. Data shown represent means of normalized counts ± SE for mice within each group.

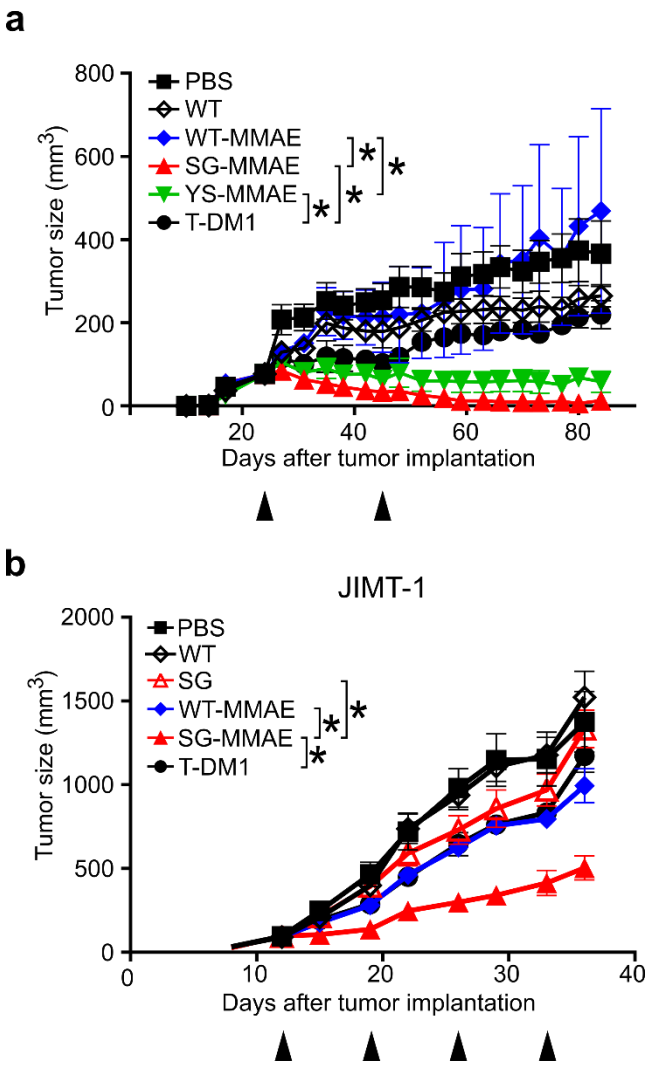

Figure 3-10. Acid-switched ADCs have higher therapeutic efficacy against tumor xenografts than WT-MMAE or T-DM1. (a) Female BALB/c SCID mice bearing HER2^{int}, MDA-MB-453 tumors were treated twice, with a 21 day interval, with 2 mg/kg ADC (WT-MMAE, SG-MMAE or YS-MMAE), T-DM1, unconjugated WT pertuzumab (WT) or vehicle (PBS) (n = 7-8 mice per group). Tumors were measured every 3-4 days. (b) Female BALB/c SCID mice bearing HER2^{int}, JIMT-1 tumors were treated weekly (four times) with 2 mg/kg ADC (WT-MMAE or SG-MMAE), T-DM1, unconjugated WT or SG mutant, or vehicle (PBS) (n = 6-7 mice per group). Measurements shown indicate mean tumor volume for mice within each treatment group. For (a) and (b), arrowheads and error bars indicate treatment day and SE, respectively. Statistically significant differences at the experimental endpoints in (a) and (b) are indicated by * (two-tailed Mann-Whitney *U* test and unpaired two-tailed *t*-test, respectively; $p < 0.05$). Data is representative of two independent experiments (n = 5-9 mice/group).

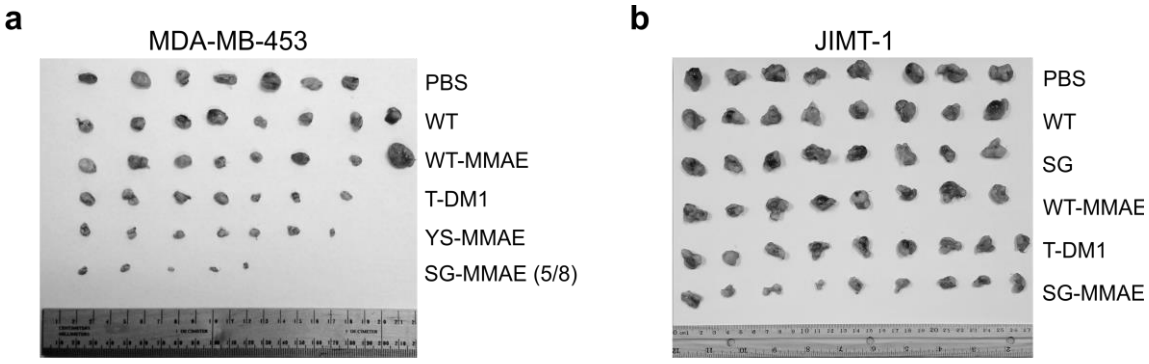

Figure 3-11. Analyses of excised tumors, serum alanine transaminase (ALT) activity, and body weight of female BALB/c SCID mice following treatment with ADCs. (a) Female BALB/c SCID mice bearing MDA-MB-453 tumors were treated twice, with a 21 day interval, with 2 mg/kg ADC (WT-MMAE, SG-MMAE or YS-MMAE), T-DM1, unconjugated WT pertuzumab (WT) or PBS (n = 7-8 mice per group). (b) JIMT-1 xenografts were treated weekly (four times) with 2 mg/kg ADC (WT-MMAE or SG-MMAE), T-DM1, WT or SG mutant, or PBS (n = 6-7 mice per group). Tumors from (a) and (b) were extracted and photographed at the end of the experiment. Note that tumors could not be detected in 3 of 8 mice treated with SG-MMAE, and 5 tumors are therefore shown in (a). (c) Blood was collected from mice 4-5 days after the second (MDA-MB-453 xenograft model, n = 7-8 mice/group) or fourth (JIMT-1 xenograft model, n = 6-7 mice/group) dose of ADCs or control and tested for ALT activity, where the units of mU are defined as nmol/min. The mean ALT activity ± SE for each group is presented. No statistical significance (n.s.) was found (one-way ANOVA with Tukey's multiple comparisons test; $p > 0.05$). (d) Body weights of BALB/c SCID mice treated as in panel (**c**) were determined at the indicated times. Arrowheads indicate treatment days, and mean weight ± SE for each group is shown. The data shown corresponds to the mice used in the treatment experiments presented in Fig. 5. Data is representative of two independent experiments (n = 5-9 mice/group).

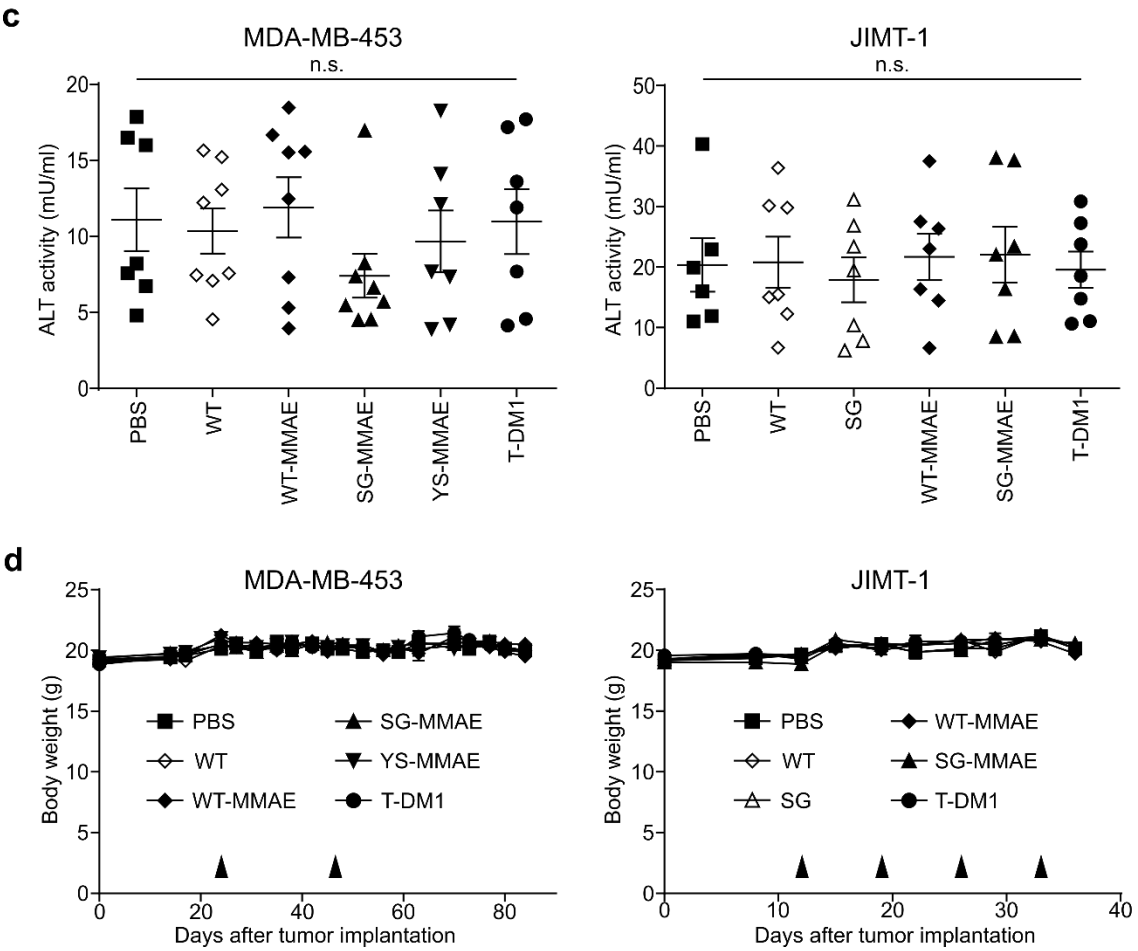

Figure 3-11. Continued.

3.2.5 Molecular modeling analyses of the interaction of the SG mutant with HER2

We carried out modeling studies to investigate the molecular basis of the loss of affinity at pH 5.8 of the lead acid-switched variant, SG, for HER2 relative to WT pertuzumab (Fig. 3-12). These analyses resulted in a model in which protonation of His55 in CDRH2, that replaces Ser55 in WT pertuzumab, at Nε of the imidazole ring predominates over that of Nδ1 at near neutral pH, whereas the protonated Nδ1 tautomer is favored at lower, acidic pH (5.8). Protonation of Nδ1 leads to an electrostatic interaction with Glu57 (E57) in CDRH2 of SG in combination with interactions with Tyr252 of HER2. By contrast with the solvent exposure of Glu57 and Tyr252 residues in the SG mutant:HER2 complex at pH 7.4, the change in protonation state of histidine at pH 5.8 results in reorientation of Glu57 and Tyr252. In the model, this reorientation results in an unfavorable desolvation penalty that is a primary contributor to the loss of affinity of the SG mutant at acidic pH.

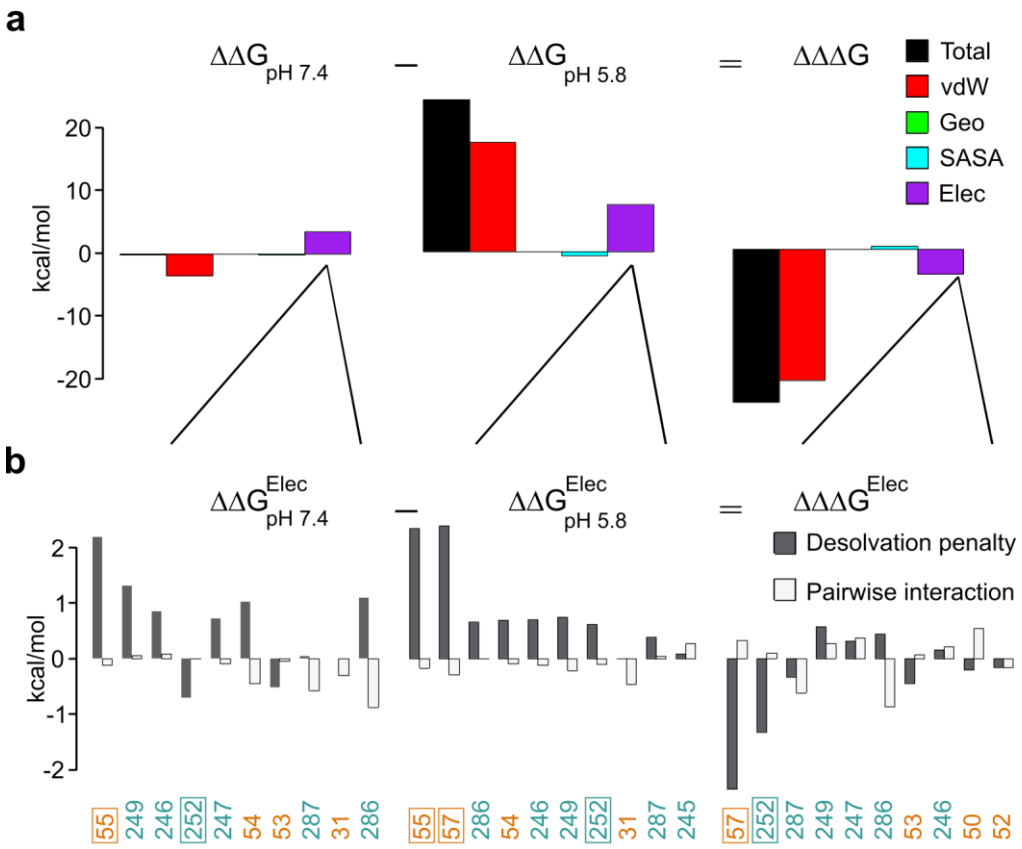

Figure 3-12. Structural modeling comparing the interaction of WT pertuzumab with the acid-switched mutant, SG, to HER2 at pH 7.4 and 5.8. (a) Analyses of the contribution of van der Waals (vdW), geometry (Geo), nonpolar hydration free energy (based on the solvent-accessible surface area, or SASA), and continuum electrostatics (Elec) to the differences in binding free energies (ΔΔG) between the SG mutant and WT pertuzumab interacting with HER2 at pH 7.4 and 5.8. (b) Energy decompositions of the Elec interactions shown in (a) for the residues that make the largest energetic contributions to the different binding behavior of WT and SG (HER2 and pertuzumab CDRH2 residues are shown in orange and cyan, respectively), with the most important contributors indicated by boxes. (c,d) The differences in the protonation states (residue His55 and Ser55 of SG and WT, respectively) and conformational states (residue Tyr252 of HER2) between WT pertuzumab and the SG mutant at pH 7.4 and 5.8. The modeled structures of the pertuzumab:HER2 extracellular domain complex are shown, with the pertuzumab VH domain, VL domain and HER2 domain II shown in cyan, light cyan, and orange, respectively. SG and WT residues are labeled in bold and parentheses, respectively.

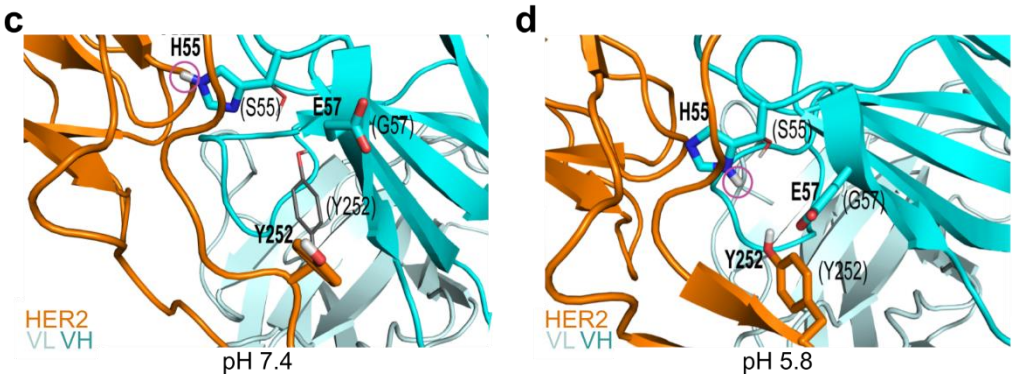

Figure 3-12. Continued.

3.3 Discussion

Despite their promise as therapeutic agents, the clinical use of ADCs can frequently provoke adverse events, leading to the delivery of doses that are suboptimal for tumor destruction[172]. To overcome these limitations, in the current study we describe a novel ADC platform that results in higher efficiency of cytotoxic drug delivery to target cells. Specifically, we have generated acid-switched ADCs specific for the tumor target, HER2, that have been engineered to bind with substantially higher affinity to this receptor at near neutral, extracellular pH, than at acidic, endosomal pH. We demonstrate that, relative to an ADC comprising the parent wild type antibody, pertuzumab, acid-switched ADCs deliver the cytotoxic drug, MMAE, more efficiently to tumor cells and have more potent therapeutic effects in mouse xenograft models. As such, this approach has broad implications for the engineering of ADCs with the goal of achieving therapeutic efficacy with lower doses.

To date, the targeting of HER2 with ADCs such as T-DM1 has met with disappointing results for HER2-positive tumors that do not overexpress this receptor[165, 173, 174]. Our demonstration that $HER2^{int}$ cells can be effectively targeted with acid-switched ADCs suggests that tumors with lower target expression levels, that lead to narrow therapeutic windows with conventional ADCs, could be successfully treated with engineered ADCs of this class. By contrast with the improved activity of acid-switched ADCs against $HER2^{int}$ tumor cells, however, we do not see significant differences for the HER2-overexpressing cells, SK-BR-3 and HCC1954. A possible reason for these observations is that for cytotoxicity, internalization of a relatively low proportion of

surface HER2 molecules is necessary on HER2-overexpressing cells, resulting in less dependence on endosomal HER2:ADC dissociation and ADC reloading compared with $HER2^{int}$ cells. It is also conceivable that acid-switching could be combined with strategies to enhance ADC internalization, such as the co-opting of HER2 into higher order aggregates with antibody mixtures[82, 191], biparatopic antibodies[82], or into cross-linked complexes with the internalizing receptor, CD63, using bispecific antibodies[192], to further improve therapeutic efficacy.

The engineering of antibodies to generate acid-switched variants has been described as a strategy to enhance the clearance of soluble target antigens[180-182, 193, 194]. Based on these studies, the relatively high affinity of (wild type) pertuzumab for HER2 at endosomal pH would be expected to limit endosomal dissociation, consistent with the current study. Nevertheless, the intrinsic pH-dependence with ~10 fold higher affinity binding at pH 7.4 relative to pH 6.0, suggested that this antibody is a suitable candidate for further engineering to generate acid-switched variants with negligible binding at acidic, endosomal pH. Combined with the use of the X-ray crystallographic structure of the pertuzumab:HER2 complex[177] as a guide, we have generated acid-switched variants of pertuzumab using two approaches: first, we have substituted 'likely' candidate residues in the CDRs with histidine. This approach resulted in two mutated variants (Y55H in CDRL2, S103H in CDRH3) with increased pH-dependence that were subsequently combined to generate the YS mutant. Second, CDR residues proximal to the interaction site were randomly mutated and pH-dependent variants selected using phage display to isolate the SG mutant. Modeling has been used to investigate the

molecular basis for the increased pH-dependence of the lead SG mutant, and indicates that pH-dependent changes in the protonation of the imidazole side chain of His55, that replaces Ser55 in WT pertuzumab, results in a relatively large desolvation penalty for proximal HER2 residues at lower, acidic pH.

Although the expression of the IgG-recycling receptor, FcRn, would be expected to mitigate the effect of endosomal dissociation of acid-switched ADCs from their target[195], this receptor is expressed at low to undetectable levels in the majority of breast, prostate and lung tumor cells[196, 197]. This low expression enables the accumulation of increased levels of albumin, a second ligand for FcRn[198], within the cells due to reduced recycling following fluid phase internalization. Following lysosomal delivery of albumin, its degradation to amino acids represents an important supply of nutrients to meet the extraordinarily high metabolic needs of cancer cells[196, 199, 200]. Consequently, we expect that for many tumor types, acid-switched ADCs will not be efficiently recycled following endosomal dissociation, by contrast with FcRn-mediated recycling in normal cells, the majority of which express this receptor[201, 202].

In summary, we have described a novel ADC platform that, based on improved intracellular trafficking, results in increased delivery of cytotoxic payload to target cells. We show that acid-switched ADCs have higher therapeutic efficacy in HER2^{int} tumor cells compared with ADCs containing the parent, WT antibody or T-DM1. This approach not only has potential to treat patients with tumors expressing a broad range of HER2 levels, but also promises to have general applicability in overcoming the current limitations of dose-limiting toxicities for other tumor targets.

3.4 Materials and methods

3.4.1 Cell lines and reagents

The following cancer cell lines were obtained from the American Type Culture Collection (Manassas, VA, USA): SK-BR-3, SK-OV-3, MDA-MB-453, and MDA-MB-468. SK-BR-3 and SK-OV-3 cells were cultured in McCoy's 5a medium, whereas MDA-MB-453 and MDA-MB-468 cells were cultured in RPMI1640 medium. The breast cancer cell line JIMT-1 was obtained from AddexBio and cultured in DMEM medium. The HCC1954 cell line was a generous gift from Drs. Adi Gazdar, John Minna, and Kenneth Huffman (Hamon Center for Therapeutic Oncology Research, University of Texas Southwestern Medical Center at Dallas) and was cultured in RPMI1640 medium. All media were supplemented with 1% penicillin/streptomycin, 1% GlutaMAX (Thermo Fisher Scientific, Waltham, MA, USA), 1% sodium pyruvate and 10% fetal calf serum. The cell lines were tested monthly for mycoplasma contamination and were authenticated annually at the University of Arizona Genetics Core through DNA fingerprint analysis.

3.4.2 Histidine scanning of pertuzumab

The sequences encoding the pertuzumab variable heavy (VH) and variable light (VL) chain domains[177] were synthesized by GenScript (Piscataway, NJ, USA) and used to generate an expression vector to produce pertuzumab Fab fragments (human CH1, Cκ) using standard methods of molecular biology. Residues in the complementarity-determining regions (CDRs) of the VH and VL domain genes of pertuzumab were

selected for histidine scanning using the crystal structure of pertuzumab in complex with HER2 (Protein Data Bank accession code 1N8Z)[177] in PyMOL (Schrödinger, New York, NY, USA) as a guide. The following residues, that are in proximity to or contact HER2, were targeted: Asp31, Tyr32, Asn54, Tyr60, Leu100, Gly101, Pro102, Ser103, Tyr105, Asp107 in the VH domain and Tyr55 in the VL domain. These residues were mutated to histidine using splicing by overlap extension[203], and the corresponding Fab fragments were expressed as periplasmically secreted proteins using *E. coli* as an expression host[204]. Fab fragments were purified using Ni^{2+}-NTA-agarose[204].

3.4.3 Generation of phage display libraries

To express pertuzumab as a single chain Fv fragment (scFv) using the phagemid, pHEN1[205], the expression vector for the pertuzumab Fab fragment was modified using standard methods of molecular biology to insert a linker peptide [$(Gly_4Ser)_3$ linker] between the pertuzumab VH and VL domain genes, followed by cloning into pHEN1 as a *Not*I-*Sfi*I fragment. Libraries were generated with random mutations in CDR1, 2 and 3 of the VH domain (targeting Asp31, Tyr32 and Thr33; Asn75, Ser76, Gly77 and Gly78; Gly101, Ser103, Tyr105 and Tyr108) and CDR2 of the VL domain (targeting Ile48, Tyr49 and Ser50 or Ala51, Tyr53, and Tyr55). The following oligonucleotides were used, combined with splicing by overlap extension, to generate five libraries: Library 1: CDRH1Back, 5’ GCT TCT GGA TTC ACA TTC ACA NNB NNB NNB ATG GAT TGG GTG AGA CAG GCT 3’ and CDRH1For, 5’ TGT GAA TGT GAA TCC AGA AG C 3’; Library 2: CDRH2Back, 5’ TGG GTG GCT GAT GTG AAT CCT NNB NNB

NNB NNB TCT ATC TAC AAT CAG AGA TTC 3' and CDRH2For, 5' AGG ATT CAC ATC AGC CAC CCA 3'; Library 3: CDRH3Back, 5' TAC TAC TGT GCT AGA AAT CTG NNB CCT NNB TTC NNB TTC GAT NNB TGG GGA CAG GGA ACA CTG 3' and CDRH3For, 5' CAG ATT TCT AGC ACA GTA GTA 3'; Library 4: CDRL2-1Back, 5' CCT AAG CTG CTG ATC TAC TCT NNB TCT NNB AGA NNB ACA GGA GTG CCT TCT AGA 3' and CDRL2-1For, 5' AGA GTA GAT CAG CAG CTT AGG 3'; Library 5: CDRL2-2Back, 5' GGA AAG GCT CCT AAG CTG CTG NNB NNB NNB GCT TCT TAC AGA TAC ACA GGA 3' and CDRL2-2For5, 5' CAG CAG CTT AGG AGC CTT TCC 3' (N = A, C, T or G; B = C, T, or G. The resulting gene libraries were transfected into *E. coli* TG1 (Lucigen, Middleton, WI, USA) to generate libraries of 2.6 $x10^6$-1.7 x 10^8 clones. Each library was pooled and grown overnight at 30 °C in 4XTY broth supplemented with M13KO7 helper phage (New England Biolabs, Ipswich, MA, USA), 100 µg/ml ampicillin, and 50 µg/ml kanamycin. Phage were precipitated with a solution of PEG-8000 and NaCl to a concentration of 4% PEG-8000/0.5 M NaCl followed by centrifugation at 10,000 RCF. The phage were washed with 4% (w/v) PEG-8000/0.5 M NaCl prior to suspension in 1% (w/v) bovine serum albumin (BSA)/phosphate buffered saline (PBS). To select phage that display pertuzumab-derived scFvs that bind to HER2 with increased pH-dependence, recombinant phage were first pre-panned in Nunc 96-well flat-bottom immuno plates (Thermo Fisher Scientific) coated with 4% (w/v) milk powder/PBS (pH 7.4), and subsequently transferred to 96-well Nunc plates that had been coated with 2 µg/ml recombinant HER2-ECD (R&D Research, Minneapolis, MN, USA) and blocked with

4% (w/v) milk powder/PBS (pH 7.4). Following a 2 hour incubation, the plates were washed 5 times with PBS plus 0.1% Tween 20 (PBST) pH 7.4 followed by 5 washes with PBS pH 7.4. Bound phage were then eluted by the addition of 20 mM 2-(N-morpholino)ethanesulfonic acid (MES) pH 5.8 for 10 minutes. The eluted phage were amplified by re-infection of *E. coli* TG1, followed by two additional rounds of selection using 10 washes with PBST pH 7.4 and 10 washes with PBS pH 7.4. Eluted phage (pH 5.8) from the third round of panning were used to re-infect *E. coli* TG1, single clones expanded in 96 deep well plates and treated with helper phage using previously described methods[206]. Culture supernatants containing phage were used in ELISAs with plates coated with recombinant HER2-ECD, followed by washing with PBST pH 7.3 or pH 5.8. Bound phage were detected using anti-M13 antibody conjugated to horse radish peroxidase (HRP) (GE Healthcare, Chicago, IL, USA) at a 1:5,000 dilution in 4% milk powder in PBS, pH 7.3 or 5.8, followed by detection with 3'3'5,5' tetramethylbenzidine substrate. For ELISAs using purified phage, phage suspensions were added to each well and binding at pH 5.8 and 7.4 was detected using the same protocol.

3.4.4 Recombinant antibodies

VH and VL domain genes encoding acid-switched pertuzumab variants that were obtained by histidine scanning or phage display were used to generate constructs for the expression of full length human IgG1, Cκ antibodies using standard methods of molecular biology and the vector, pcDNA3.4 (Life Technologies). The hinge disulfide bonds that link the Cκ domain to the hinge region and one hinge disulfide that links the

two heavy chains to each another were removed by mutating the light chain cysteine (Cys214; EU numbering[185]) and two heavy chain cysteines (Cys220, Cys229; EU numbering[185]) to serine.

For use as a control antibody, the VH and VL domains of the hen-egg lysozyme antibody, HuLys10[207], were reformatted as heavy and light chain constructs to generate a full length human IgG1/κ antibody with one hinge disulfide (as above) using pcDNA3.4.

Recombinant antibodies were produced in Expi293F cells (Life Technology, Carlsbad, CA, USA) following transient transfection with the Expi293 expression system kit (Life Technology) as previously described[208]. Antibodies were purified from culture supernatants using protein G-Sepharose (GE Healthcare) and dialyzed against PBS. Purified antibodies were loaded onto a Hiload 16/600 Superdex 200 gel filtration column (GE Healthcare) to remove aggregates, followed by analyses of the 'monomeric' antibodies using a Yarra 3000 column (Phenomenex, Torrance, CA, USA).

Clinical grade trastuzumab and pertuzumab were acquired from the University of Texas Southwestern Medical Center Pharmacy.

3.4.5 Surface plasmon resonance analyses

Binding analyses were carried out using a Biacore 2000 or T200 (GE Healthcare). Flow cells of CM5 sensor chips were coupled using amine coupling chemistry with recombinant HER2-ECD (R&D Research) or coupling buffer only (10 mM sodium acetate pH 4.8) as a reference. Fab fragments or antibodies were injected over immobilized HER2-ECD (coupled to densities ranging from 426-956 relative units

on flow cells of CM5 sensor chips) at a flow rate of 5 or 10 µl/min at 25 °C in PBS plus 0.01% (v/v) Tween and 0.05% (w/v) sodium azide (pH 7.4, 7.0, 6.5, 5.8). Flow cells were regenerated following each injection using 0.15 M NaCl/0.1 M glycine (pH 2.8) buffer. For full length antibodies, equilibrium dissociation constants were determined using custom written software[209] to yield apparent dissociation constants (due to bivalent binding of the antibodies to immobilized HER2). The K_D of the YS mutant at pH 5.8 was too high to accurately determine (i.e. levels of binding close to saturation could not be reached), and was therefore estimated using the following equation: $R_{eq}(C_k) = \frac{C_k R_{max}}{K_D + C_k}$, where K_D is the calculated equilibrium dissociation constant (nM), C_K is the concentration of analyte flowed over the chip (nM), R_{max} is the maximum analyte binding capacity (RU), and $R_{eq}(C_k)$ is the equilibrium signal for concentration C_K (RU)[209].

3.4.6 Conjugation and labeling of antibodies

Antibodies (10 µM) in PBS were reduced by addition of 80 µM of tris(2-carboxyethyl)phosphine (TCEP) and 1 mM ethylenediaminetetraacetic acid (EDTA) for 2 hours at 37 °C. Reduced antibodies were cooled on ice and 40 µM maleimidocaproyl-valine-citrulline-p-aminobenzoylcarbonyl-monomethyl auristatin E (MMAE; Concortis, San Diego, CA, USA) was added. Following 4 hours incubation on ice, unconjugated MMAE was removed by extensive dialysis against PBS. Conjugated antibodies were analyzed using size exclusion chromatography (Yarra 3000) and hydrophobic interaction chromatography (HIC; TSKgel Butyl-NPR; Tosoh, Tokyo, Japan) to determine drug-to-

antibody ratios (DARs). For HIC, solvent A was 10 mM potassium phosphate with 1.5 M ammonium sulfate at pH 7.0 and solvent B was 10 mM potassium phosphate at pH 7.0 with 20% (v/v) isopropanol. The gradient method used was 0-5 min (0% B), 5-15 min (0% to 100% B), and 15-20 min (100% B) at a flow rate of 0.5 ml/min.

ADCs were labeled with Alexa 488 Fluor (Thermo Fisher Scientific) or radiolabeled with ^{125}I-Iodogen [Perkin Elmer or MP Biomedical (Solon, OH, USA)] as described previously[210, 211], except that a 1:1 molar ratio of Alexa 488:ADC was used during the labeling reaction.

3.4.7 Enzyme-linked immunosorbent assays

ADCs and antibodies were analyzed by ELISA for their binding to HER2-ECD (R&D Research). 96-well Nunc plates were coated with HER2-ECD at a concentration of 2 µg/ml overnight at 4 °C. ADCs and antibodies were diluted in 4% (w/v) milk powder/PBS (pH 5.8 or pH 7.0) and added to coated plates at concentrations ranging from 0.1 nM to 200 nM. Plate wells were washed 4 times with PBST (pH 5.8 or 7.0, as indicated). Antibodies and ADCs were detected with goat anti-human IgG (Fab-specific) conjugated with HRP (Sigma-Aldrich).

3.4.8 Serum stability analyses of antibodies and ADCs

Human serum (Sigma-Aldrich, St. Louis, MO, USA) was depleted of endogenous IgG by passage through a protein G-Sepharose column. Antibodies and ADCs were incubated at 40 µg/ml in IgG-depleted serum for 0, 3, or 5 days at 37 °C followed by immunoprecipitation using agarose beads coupled to goat anti-human Fc-

specific antibody (Sigma-Aldrich). Immunoprecipitated antibodies and ADCs were run on SDS-polyacrylamide gels and transferred onto nitrocellulose membranes (0.45 µm pore size; Genesee Scientific, San Diego, CA, USA). Immunoblotting was carried out using standard methods with goat anti-human IgG (H + L) antibodies conjugated with HRP (Jackson Immunoresearch, West Grove, PA, USA). HRP was detected using SuperSignal West Pico Chemiluminescent Substrate (Thermo Fisher Scientific) followed by scanning with a C-DiGit blot scanner (LI-COR Biosciences, Lincoln, NE, USA).

3.4.9 ADC accumulation assay

Cancer cells were plated in 48-well plates and incubated overnight in a 37 °C incubator with 5% CO_2, followed by treatment with 10 nM Alexa 488-labeled ADC in medium (pH 7.0) for 0.5, 4, and 20 hours. Treated cells were cooled on ice and surface fluorescence of Alexa 488-labeled ADC quenched with 5 µg/ml rabbit anti-Alexa 488 antibody (Thermo Fisher Scientific) for 30 minutes at 4 °C. The quenching efficiency was determined using separate cell samples which had been incubated with Alexa 488-labeled ADC on ice (to prevent internalization) followed by treatment with anti-Alexa 488 antibody or vehicle control. Samples were washed, harvested by trypsinization, resuspended in PBS, analyzed using a BD Accuri C6 flow cytometer (BD Biosciences, San Jose, CA, USA) and data processed with FlowJo (FlowJo, Ashland, OR, USA).

3.4.10 Fluorescence microscopy

MDA-MB-453 cells were plated in coverglass-bottomed Mattek dishes and allowed to adhere overnight in a 37 °C, 5% CO_2 incubator. Cells were pre-treated with

Alexa 647-labeled dextran (5 μM pulse for 2 hours and chase for 3 hours) followed by a treatment of 10 nM Alexa 488-labeled WT-MMAE, SG-MMAE, or YS-MMAE for 4 or 20 hours. Samples were treated with 5 μg/ml rabbit anti-Alexa 488 antibody for 30 minutes on ice to quench surface Alexa 488 fluorescence, and subsequently fixed at room temperature with 3.4% (w/v) paraformaldehyde plus 0.025% (v/v) glutaraldehyde. Fixed cell samples were imaged with an Axio Observer Z1 inverted epifluorescent microscope (Zeiss, Oberkochen, Germany) equipped with a 63 X, 1.4 NA Plan-Apochromat objective (Zeiss), and a Zeiss 1.6 X internal optovar. A broadband LED lamp (X-cite 110LED, Excelitas Technologies, Waltham, MA, USA) was employed as the excitation source, and a digital CCD camera (Hamamatsu Orca-ER; Hamamatsu Photonics, Japan) as the detector. Standard fluorescent filter sets for Alexa 488 (FITC-3540C) and Alexa 647 (Cy5-4040C) were purchased from Semrock (Rochester, NY, USA). Images were acquired at room temperature using custom software written in Java and the C programming language. Acquired images were analyzed using the custom written software MIATool[212]. Acquired images for Alexa 488 were linearly adjusted with the same intensity adjustment settings. Independent linear adjustments were made for the Alexa 647 signal for each time point.

3.4.11 Cell viability assays

Cells were plated in 96-well plates at a density of 5,000 cells per well and treated with different concentrations of ADCs. Cells were treated for 4 days in a 37 °C, 5% CO_2 incubator, followed by the use of CellTiter 96 AQueous One Solution Proliferation

Assay kit (Promega, Madison, WI, USA) to determine cell viability using the manufacturer's protocol.

3.4.12 Quantitation of MMAE using LC-MS/MS

Cancer cells were plated in 6 well plates and incubated overnight in a 37 °C, 5% CO_2 incubator. Cells were treated with 10 nM ADC for 20 hours, followed by washing with PBS and harvesting by trypsinization. Trypsinized cells were counted and resuspended in 100% methanol containing 1.67 ng/ml deuterium-labeled MMAE (D8-MMAE; MedchemExpress, Monmouth Junction, NJ, USA) at a density of 8.3 x 10^5 cells per ml. Samples were lysed for 16 hours at -20 °C and then centrifuged at 21,100 RCF for 15 mins at 4 °C. The supernatants were transferred to 12 x 75 mm borosilicate glass tubes (Kimble Chase, Rockwood, TN, USA) and dried under a stream of nitrogen gas. The residue was resuspended in 20% methanol with 0.1% (v/v) formic acid (10% of original volume). To generate a standard curve, different concentrations of MMAE ranging from 0.017-3.33 ng/ml were mixed with 1.67 ng/ml D8-MMAE in lysates of untreated tumor cells and treated as above.

Targeted liquid chromatography mass spectrometry (LC-MS/MS) analysis was performed using a Quantiva triple quadrupole mass spectrometer (Thermo Fisher Scientific) coupled to a binary pump HPLC (Ultimate 3000; Thermo Fisher Scientific). Chromatographic separation was achieved on a Hypersil Gold 5 µm, 50 mm x 3 mm column (Thermo Fisher Scientific) maintained at 30 °C using a solvent gradient method. Solvent A was H_2O containing 0.1% (v/v) formic acid. Solvent B was acetonitrile

containing 0.1% (v/v) formic acid. The gradient method used was 0-1 min (20% B to 60% B), 1-1.5 min (60% B to 95% B), 1.5-3 min (95% B), 3-4.1 min (95% B to 20% B), 4.1-5 min (20% B) with a flow rate of 0.5 ml/min. The sheath, auxiliary, and sweeping gasses were set at 50, 15, and 1 arbitrary units, respectively. The spray voltage was set to 3.5 kV and the vaporizer and capillary temperatures were maintained at 375 °C and 350 °C, respectively. Transitions of 718.8 m/z -134.1 m/z and 727.6 m/z – 134.1 m/z were used for the quantitation of MMAE and D8-MMAE, respectively. Sample acquisition and data analysis were performed using TraceFinder (Thermo Fisher Scientific).

3.4.13 Pharmacokinetic analyses

Pharmacokinetic experiments were carried out in 7-10-week old female BALB/c SCID mice using protocols approved by the Texas A&M University IACUC. Lugol solution (Sigma-Aldrich) was added to drinking water 48-72 hours prior to starting the experiment, and maintained throughout the experiment. Mice were injected intravenously with 15 µg ^{125}I-labeled ADC in 200 µl PBS with 0.1% (w/v) BSA. Whole body counts were measured using an Atom Lab 100 dose calibrator (Biodex, Shirley, NY, USA). Mice were retroorbitally bled with 10 µl capillary tubes (Drummond Scientific, Broomall, PA, USA) and radioactive counts measured by gamma counting (Perkin Elmer, Waltham, MA, USA). Radioactivity counts were normalized to the values obtained immediately following injection.

3.4.14 Therapy experiments

Therapy experiments were carried out using protocols approved by the Texas A&M University IACUC. BALB/c SCID mice were purchased from Jackson Laboratories, bred and maintained in specific pathogen-free housing. 6-8-week old female mice were implanted with 3-5 x 106 MDA-MB-453 cells or 4-5 x 106 JIMT-1 cells suspended in 100 µl 50% RPMI1640 media and 50% Matrigel (Corning, Corning, NY, USA) in the mammary fat pad. When the tumor size reached a volume of 50-100 mm^3, mice were randomized into groups and dosed intravenously with 2 mg/kg antibody, ADC, or vehicle twice with a three week interval (MDA-MB-453) or four times with one week intervals (JIMT-1). Tumor size was determined using the formula: $tumor\ size = \frac{tumor\ length \times tumor\ width^2}{2}$, where the tumor length and tumor width were measured with digital calipers every 3-4 days for the duration of the experiment. Mice with tumor volumes exceeding 2000 mm^3 were euthanized. Alanine aminotransferase activity in serum samples from mice were analyzed using Alanine Aminotransferase Activity Assay Kits (Sigma-Aldrich) and the manufacturer's protocol.

3.4.15 Modeling analyses

The X-ray crystallographic structure of the HER2-pertuzumab complex[177] (PDB accession code: 1S78) was minimized using the molecular modeling software CHARMM v36[213] in a CHARMM22 force field, and all missing residues and atoms were added. PROPKA v. 3.1[214, 215] was used for empirical pKa prediction and protonation state determination for the minimized structure at pH 7.4 and 5.8,

respectively. The resulting structure at either pH value was minimized for 5,000 steps with explicit solvent molecules and then subjected to a 10 ns molecular dynamics (MD) simulation using the computer program NAMD2 v. 2.10[216]. MD protocols followed similar details as described previously[217]. Snapshots were retained at the 0^{th} ns (the beginning) and every ns from the 6^{th} to the 10^{th} ns to represent a conformational ensemble of the HER2-pertuzumab complex at either pH.

Structures of HER2 in complex with the SG mutant were modeled using iCFN[218], an exact algorithm for multi-state protein design with substate ensembles, which was customized here for pH-dependence. First, the positive and negative substates were defined as conformational ensembles of the complex at pH 7.4 and 5.8, respectively. Substate energies were folding stabilities of the complex that include Coulomb electrostatics, van der Waals, calculated internal energies, and a nonpolar contribution to the hydration free energy based on solvent accessible surface area (SASA)[218]. A positive-substate stability cutoff was set at 10 kcal/mol and positive-versus-negative substate specificity was essentially not mandated with a cutoff of 1000 kcal/mol. Second, pertuzumab VH residues 55 and 57 were allowed to change to any amino acid, including histidines in δ-, ε-, and doubly protonated states. Residues within 5 Å from the mutated amino acids were allowed to be flexible. In addition, His245 of HER2 was allowed to be in any of the 3 possible protonation states and Asp50 of pertuzumab VH was allowed to be deprotonated or singly protonated at either oxygen atom on the side chain. Top conformations of each sequence-protonation combination in each substate (backbone conformation here) generated from iCFN for either pH were geometrically

grouped into representatives and then screened by PROPKA for protonation states. Later, complex folding stabilities (G) and binding affinities (ΔG) of the top sequence-conformation ensembles retained for either pH were re-evaluated and re-ordered with a higher-resolution energy model where continuum electrostatics replaced Coulombic electrostatics[218]. Lastly, the representative conformation/protonation at either pH was chosen based on the best binding affinity (lowest ΔG) amongst those whose folding energies were within 1 kcal/mol of the most stable complex.

Each calculated binding energy relative to WT, ΔΔG, was further decomposed into contributions of van der Waals (vdW), continuum electrostatics, SASA-dependent nonpolar solvation interactions, and internal energy. vdW and electrostatics were found to be the most important contributors to pH-dependent binding. The calculated vdW contribution was largely due to the modeled clashes between the bulkier pertuzumab His55 and a HER2 loop at pH 5.8 whereas the clashes could be largely ameliorated by the flexible HER2 loop. Therefore, long-range electrostatic binding affinity, being less sensitive to conformational details, was further analyzed as an origin of the pH-dependent binding. Specifically, continuum electrostatics for binding were first decomposed into the contributions of the lost desolvation penalties and the gained solvent-screened intermolecular interactions. Desolvations were then decomposed into contributions of all residues and screened intermolecular electrostatic interactions into those of all residue pairs. To sum up screened intermolecular electrostatic interactions and avoid double counting for each residue, half of the pairwise interactions for each residue with all other residues were considered. Those residues with insignificant

contributions (desolvation plus the half of the summed pairwise interactions) to electrostatic binding specificity ΔΔΔG (ΔΔΔG = $\Delta\Delta G_{pH\ 7.4}$ - $\Delta\Delta G_{pH\ 5.8}$) were not considered further. Since desolvation penalties dominated over screened electrostatic interactions in contributions to electrostatic binding specificity ΔΔΔG, the top 10 remaining residues with the highest desolvation contributions were reported for $\Delta\Delta G_{pH\ 7.4}$, $\Delta\Delta G_{pH\ 5.8}$, and ΔΔΔG, respectively.

3.4.16 Statistical analyses

Statistical significance was analyzed using two-tailed *t*-test, two-tailed Mann-Whitney *U* test or one-way ANOVA with Tukey's multiple comparison test as indicated in the figure legends. P values less than 0.05 were considered to be statistically significant.

4. SUMMARY

The use of antibodies for the treatment of HER2-expressing cancers has had an enormous impact on the clinical use of this class of therapeutics. Initially, antibody therapies targeting HER2-expressing cancers were used exclusively to treat breast cancer, but have recently been found to have potential uses for the therapy of other malignancies such as gastric cancers[219]. Bladder, gallbladder, cervical, and uterine cancers, have also been shown to have subpopulations expressing HER2 and are being considered for HER2-targeted therapy[220-222]. However, despite the initial promise of trastuzumab, a high percentage of patients suffer from tumor relapse[223]. Consequently there is a need for improvement of these therapeutic approaches.

One pathway through which HER2-expressing tumors escape following treatment with HER2-specific antibodies is through the intratumoral production of ligands for HER3 which drive the formation of HER2/HER3 heterodimers. These dimers are known to potently signal through the PI3K/Akt axis. In Section 2 of the thesis, this problem has been addressed by engineering a bsAb comprising the binding sites of a HER2-specific antibody, trastuzumab, and of a HER3-specific antibody. This bsAb has been used to target HER2 and HER3 simultaneously on tumor cells. In Section 3, we have investigated how to improve the delivery of a cytotoxic drug to HER2-expressing target cells by engineering the interactions of a HER2-specific antibody with HER2 to modulate the subcellular delivery properties of the corresponding ADC. Combined,

these studies demonstrate how antibody engineering can be used to produce therapeutic antibodies/ADCs with significantly improved efficacy.

The study in Section 2 describes the effects of a bsAb that targets both HER2 and HER3 in the presence of HER3 ligand, heregulin. Co-treatment of HER2-expressing cells with the inhibitor of HER2 phosphorylation, lapatinib, and the HER2/HER3 bsAb results in potent inhibition of downstream PI3K/Akt signaling and inhibition of cell proliferation. By contrast, the combination of parent antibodies with lapatinib does not inhibit signaling in the presence of heregulin, leading to the activation of the PI3K/Akt pathway and ultimately cell survival and proliferation. In comparison with the parent monoclonal antibodies, the bsAb likely has a higher avidity for HER3 due to bridging effects of the trastuzumab portion of the bsAb binding to the excess of HER2, relative to HER3 level, on the cell surface (Figure 4-1), thereby locking the targeted receptors into dimers that cannot signal due to the presence of lapatinib. This approach represents a novel method for silencing a major signaling pathway that drives tumor cell proliferation.

Despite the promise of ADCs as therapeutics, their efficacy in the clinic has been limited by dose-limiting toxicities that result in doses being used that can be insufficient to kill the tumor cells[73]. This problem is exacerbated when the target antigen expression is not high, such as in HER2-expressing cells that express intermediate levels of surface HER2 receptors. This issue is addressed in Section 3 by generating an ADC that is more effective in delivering its cytotoxic payload to lysosomes in target cells. In this study, an acid-switched ADC has been generated that comprises engineered pertuzumab variants

that bind to HER2 in a highly pH-dependent manner, with substantially lower affinity at endosomal (acidic) pH than at extracellular (near neutral) pH. Acid-switched ADCs result in increased payload delivery to late endosomal or lysosomal compartments and increased cytotoxicity. These effects are observed with tumor cells that express ~20 fold lower level of HER2 ($HER2^{int}$). Significantly, treatment of tumor-bearing mice demonstrated that the acid-switched ADCs have higher therapeutic efficacy against $HER2^{int}$ tumor cells than an ADC comprising their parent wild type antibody and the clinically approved ADC, T-DM1. These results demonstrate the potential of using acid-switched ADCs for increasing payload delivery to target cells and have broad applications to other tumor types and targets.

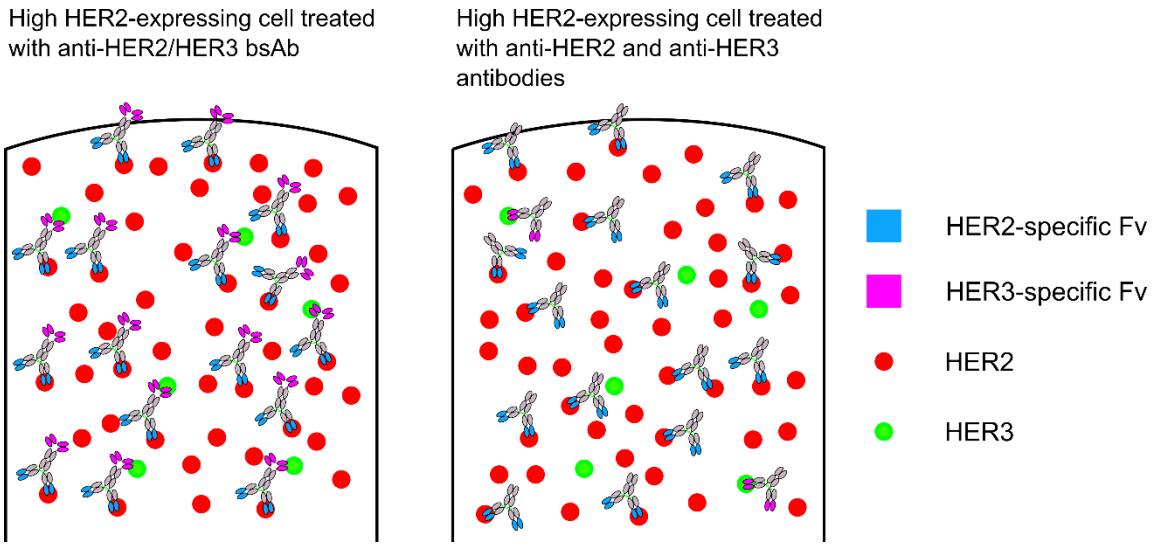

Figure 4-1. HER2/HER3-specific bsAbs have higher avidity for HER3 due to the high expression of HER2 on the cell surface. BsAbs (left) bind tightly to HER2 on the cell surface which increases avidity for HER3. In comparison, parent HER3-specific antibodies (right) do not benefit from HER2-specific antibody binding to surface HER2.

REFERENCES

1. Schroeder, H.W., Jr. & Cavacini, L. Structure and function of immunoglobulins. *J Allergy Clin Immunol* **125**, S41-52 (2010).
2. Irani, V. *et al.* Molecular properties of human IgG subclasses and their implications for designing therapeutic monoclonal antibodies against infectious diseases. *Mol Immunol* **67**, 171-182 (2015).
3. Carter, P. *et al.* Humanization of an anti-p185HER2 antibody for human cancer therapy. *Proc Natl Acad Sci U S A* **89**, 4285-4289 (1992).
4. Adams, C.W. *et al.* Humanization of a recombinant monoclonal antibody to produce a therapeutic HER dimerization inhibitor, pertuzumab. *Cancer Immunol Immunother* **55**, 717-727 (2006).
5. Alt, F.W. *et al.* VDJ recombination. *Immunol Today* **13**, 306-314 (1992).
6. Duncan, A.R. & Winter, G. The binding site for C1q on IgG. *Nature* **332**, 738-740 (1988).
7. Wines, B.D., Powell, M.S., Parren, P.W., Barnes, N. & Hogarth, P.M. The IgG Fc contains distinct Fc receptor (FcR) binding sites: the leukocyte receptors Fc gamma RI and Fc gamma RIIa bind to a region in the Fc distinct from that recognized by neonatal FcR and protein A. *J Immunol* **164**, 5313-5318 (2000).
8. Shields, R.L. *et al.* High resolution mapping of the binding site on human IgG1 for Fc gamma RI, Fc gamma RII, Fc gamma RIII, and FcRn and design of IgG1 variants with improved binding to the Fc gamma R. *J Biol Chem* **276**, 6591-6604 (2001).
9. Kohler, G. & Milstein, C. Continuous cultures of fused cells secreting antibody of predefined specificity. *Nature* **256**, 495-497 (1975).

10. Vigeral, P. *et al.* Prophylactic use of OKT3 monoclonal antibody in cadaver kidney recipients. Utilization of OKT3 as the sole immunosuppressive agent. *Transplantation* **41**, 730-733 (1986).

11. Kimball, J.A. *et al.* The OKT3 antibody response study: a multicentre study of human anti-mouse antibody (HAMA) production following OKT3 use in solid organ transplantation. *Transpl Immunol* **3**, 212-221 (1995).

12. Ober, R.J., Radu, C.G., Ghetie, V. & Ward, E.S. Differences in promiscuity for antibody-FcRn interactions across species: implications for therapeutic antibodies. *Int Immunol* **13**, 1551-1559 (2001).

13. Reff, M.E. *et al.* Depletion of B cells in vivo by a chimeric mouse human monoclonal antibody to CD20. *Blood* **83**, 435-445 (1994).

14. Osterborg, A. *et al.* Humanized CD52 monoclonal antibody Campath-1H as first-line treatment in chronic lymphocytic leukaemia. *Br J Haematol* **93**, 151-153 (1996).

15. Jones, P.T., Dear, P.H., Foote, J., Neuberger, M.S. & Winter, G. Replacing the complementarity-determining regions in a human antibody with those from a mouse. *Nature* **321**, 522-525 (1986).

16. Riechmann, L., Clark, M., Waldmann, H. & Winter, G. Reshaping human antibodies for therapy. *Nature* **332**, 323-327 (1988).

17. Jespers, L.S., Roberts, A., Mahler, S.M., Winter, G. & Hoogenboom, H.R. Guiding the selection of human antibodies from phage display repertoires to a single epitope of an antigen. *Biotechnology (N Y)* **12**, 899-903 (1994).

18. Ritchie, M., Tchistiakova, L. & Scott, N. Implications of receptor-mediated endocytosis and intracellular trafficking dynamics in the development of antibody drug conjugates. *MAbs* **5**, 13-21 (2013).

19. Schoeberl, B. *et al.* An ErbB3 antibody, MM-121, is active in cancers with ligand-dependent activation. *Cancer Res* **70**, 2485-2494 (2010).

20. Baselga, J. & Swain, S.M. Novel anticancer targets: revisiting ERBB2 and discovering ERBB3. *Nat Rev Cancer* **9**, 463-475 (2009).

21. Weiner, G.J. Rituximab: mechanism of action. *Semin Hematol* **47**, 115-123 (2010).

22. Gelderman, K.A., Kuppen, P.J., Okada, N., Fleuren, G.J. & Gorter, A. Tumor-specific inhibition of membrane-bound complement regulatory protein Crry with bispecific monoclonal antibodies prevents tumor outgrowth in a rat colorectal cancer lung metastases model. *Cancer Res* **64**, 4366-4372 (2004).

23. Uggla, C.K., Geisberg, M., Jondal, M. & Knowles, R.W. Agonistic effects of anti-CD2 and anti-CD16 antibodies on human natural killer killing. *Scand J Immunol* **29**, 507-515 (1989).

24. Kawase, I. *et al.* Murine tumor cell lysis by antibody-dependent macrophage-mediated cytotoxicity using syngeneic monoclonal antibodies. *Cancer Res* **45**, 1663-1668 (1985).

25. Trinchieri, G. & Valiante, N. Receptors for the Fc fragment of IgG on natural killer cells. *Nat Immun* **12**, 218-234 (1993).

26. Junttila, T.T. *et al.* Superior in vivo efficacy of afucosylated trastuzumab in the treatment of HER2-amplified breast cancer. *Cancer Res* **70**, 4481-4489 (2010).

27. Indik, Z.K., Park, J.G., Hunter, S. & Schreiber, A.D. Structure/function relationships of Fc gamma receptors in phagocytosis. *Semin Immunol* **7**, 45-54 (1995).

28. Overdijk, M.B. *et al.* Antibody-mediated phagocytosis contributes to the anti-tumor activity of the therapeutic antibody daratumumab in lymphoma and multiple myeloma. *MAbs* **7**, 311-321 (2015).

29. Taylor, R.P. & Lindorfer, M.A. Fcgamma-receptor-mediated trogocytosis impacts mAb-based therapies: historical precedence and recent developments. *Blood* **125**, 762-766 (2015).

30. Boross, P., Jansen, J.H., Pastula, A., van der Poel, C.E. & Leusen, J.H. Both activating and inhibitory Fc gamma receptors mediate rituximab-induced trogocytosis of CD20 in mice. *Immunol Lett* **143**, 44-52 (2012).

31. Joly, E. & Hudrisier, D. What is trogocytosis and what is its purpose? *Nat Immunol* **4**, 815 (2003).

32. Velmurugan, R., Challa, D.K., Ram, S., Ober, R.J. & Ward, E.S. Macrophage-mediated trogocytosis leads to death of antibody-opsonized tumor cells. *Mol Cancer Ther* **15**, 1879-1889 (2016).

33. Genovese, M.C. *et al.* Combination therapy with etanercept and anakinra in the treatment of patients with rheumatoid arthritis who have been treated unsuccessfully with methotrexate. *Arthritis Rheum* **50**, 1412-1419 (2004).

34. Malm, M., Frejd, F.Y., Stahl, S. & Lofblom, J. Targeting HER3 using mono- and bispecific antibodies or alternative scaffolds. *MAbs* **8**, 1195-1209 (2016).

35. Mazor, Y. *et al.* Improving target cell specificity using a novel monovalent bispecific IgG design. *MAbs* **7**, 377-389 (2015).

36. Kontermann, R.E. Dual targeting strategies with bispecific antibodies. *MAbs* **4**, 182-197 (2012).

37. Linke, R., Klein, A. & Seimetz, D. Catumaxomab: clinical development and future directions. *MAbs* **2**, 129-136 (2010).

38. Wolf, E., Hofmeister, R., Kufer, P., Schlereth, B. & Baeuerle, P.A. BiTEs: bispecific antibody constructs with unique anti-tumor activity. *Drug Discov Today* **10**, 1237-1244 (2005).

39. Turner, J. & Schneider, S.M. Blinatumomab: A new treatment for adults with relapsed acute lymphocytic leukemia. *Clin J Oncol Nurs* **20**, 165-168 (2016).

40. Holmes, D. Buy buy bispecific antibodies. *Nat Rev Drug Discov* **10**, 798-800 (2011).

41. Nosenko, M.A. *et al.* VHH-based bispecific antibodies targeting cytokine production. *Front Immunol* **8**, 1073 (2017).

42. Bargou, R. *et al.* Tumor regression in cancer patients by very low doses of a T cell-engaging antibody. *Science* **321**, 974-977 (2008).

43. Nisonoff, A. & Rivers, M.M. Recombination of a mixture of univalent antibody fragments of different specificity. *Arch Biochem Biophys* **93**, 460-462 (1961).

44. Staerz, U.D., Kanagawa, O. & Bevan, M.J. Hybrid antibodies can target sites for attack by T cells. *Nature* **314**, 628-631 (1985).

45. Karpovsky, B., Titus, J.A., Stephany, D.A. & Segal, D.M. Production of target-specific effector cells using hetero-cross-linked aggregates containing anti-target cell and anti-Fc gamma receptor antibodies. *J Exp Med* **160**, 1686-1701 (1984).

46. Perez, P., Hoffman, R.W., Shaw, S., Bluestone, J.A. & Segal, D.M. Specific targeting of cytotoxic T cells by anti-T3 linked to anti-target cell antibody. *Nature* **316**, 354-356 (1985).

47. Milstein, C. & Cuello, A.C. Hybrid hybridomas and their use in immunohistochemistry. *Nature* **305**, 537-540 (1983).

48. Shatz, W. *et al.* An efficient route to bispecific antibody production using single-reactor mammalian co-culture. *MAbs* **8**, 1487-1497 (2016).

49. Ridgway, J.B., Presta, L.G. & Carter, P. 'Knobs-into-holes' engineering of antibody CH3 domains for heavy chain heterodimerization. *Protein Eng* **9**, 617-621 (1996).

50. Carter, P. Bispecific human IgG by design. *J Immunol Methods* **248**, 7-15 (2001).

51. Klein, C., Schaefer, W. & Regula, J.T. The use of CrossMAb technology for the generation of bi- and multispecific antibodies. *MAbs* **8**, 1010-1020 (2016).

52. Gunasekaran, K. *et al.* Enhancing antibody Fc heterodimer formation through electrostatic steering effects: applications to bispecific molecules and monovalent IgG. *J Biol Chem* **285**, 19637-19646 (2010).

53. Choi, H.J., Kim, Y.J., Lee, S. & Kim, Y.S. A heterodimeric Fc-based bispecific antibody simultaneously targeting VEGFR-2 and Met exhibits potent antitumor activity. *Mol Cancer Ther* **12**, 2748-2759 (2013).

54. James, N.D. *et al.* A phase II study of the bispecific antibody MDX-H210 (anti-HER2 x CD64) with GM-CSF in HER2+ advanced prostate cancer. *Br J Cancer* **85**, 152-156 (2001).

55. Burges, A. *et al.* Effective relief of malignant ascites in patients with advanced ovarian cancer by a trifunctional anti-EpCAM x anti-CD3 antibody: a phase I/II study. *Clin Cancer Res* **13**, 3899-3905 (2007).

56. Hubalek, M., Brantner, C. & Marth, C. Role of pertuzumab in the treatment of HER2-positive breast cancer. *Breast Cancer (Dove Med Press)* **4**, 65-73 (2012).

57. Li, B. *et al.* Bispecific antibody to ErbB2 overcomes trastuzumab resistance through comprehensive blockade of ErbB2 heterodimerization. *Cancer Res* **73**, 6471-6483 (2013).

58. Cheng, H. *et al.* EGFR expression is associated with decreased benefit from trastuzumab in the NCCTG N9831 (Alliance) trial. *Br J Cancer* **111**, 1065-1071 (2014).

59. Gala, K. & Chandarlapaty, S. Molecular pathways: HER3 targeted therapy. *Clin Cancer Res* **20**, 1410-1416 (2014).

60. Nahta, R., Yuan, L.X., Zhang, B., Kobayashi, R. & Esteva, F.J. Insulin-like growth factor-I receptor/human epidermal growth factor receptor 2 heterodimerization contributes to trastuzumab resistance of breast cancer cells. *Cancer Res* **65**, 11118-11128 (2005).

61. Shattuck, D.L., Miller, J.K., Carraway, K.L., 3rd & Sweeney, C. Met receptor contributes to trastuzumab resistance of Her2-overexpressing breast cancer cells. *Cancer Res* **68**, 1471-1477 (2008).

62. Zhuang, G. *et al.* Elevation of receptor tyrosine kinase EphA2 mediates resistance to trastuzumab therapy. *Cancer Res* **70**, 299-308 (2010).

63. McDonagh, C.F. *et al.* Antitumor activity of a novel bispecific antibody that targets the ErbB2/ErbB3 oncogenic unit and inhibits heregulin-induced activation of ErbB3. *Mol Cancer Ther* **11**, 582-593 (2012).

64. Fitzgerald, J.B. *et al.* MM-141, an IGF-IR- and ErbB3-directed bispecific antibody, overcomes network adaptations that limit activity of IGF-IR inhibitors. *Mol Cancer Ther* **13**, 410-425 (2014).

65. Campbell, M.R., Amin, D. & Moasser, M.M. HER3 comes of age: new insights into its functions and role in signaling, tumor biology, and cancer therapy. *Clin Cancer Res* **16**, 1373-1383 (2010).

66. Kang, J.C. & Poovassery, J.S. *et al.* Engineering multivalent antibodies to target heregulin-induced HER3 signaling in breast cancer cells. *MAbs* **6**, 340-353 (2014).

67. Brack, S. *et al.* A bispecific HER2-targeting FynomAb with superior antitumor activity and novel mode of action. *Mol Cancer Ther* **13**, 2030-2039 (2014).

68. Robinson, M.K. *et al.* Targeting ErbB2 and ErbB3 with a bispecific single-chain Fv enhances targeting selectivity and induces a therapeutic effect in vitro. *Br J Cancer* **99**, 1415-1425 (2008).

69. Vogel, C.L. *et al.* Efficacy and safety of trastuzumab as a single agent in first-line treatment of HER2-overexpressing metastatic breast cancer. *J Clin Oncol* **20**, 719-726 (2002).

70. Chung, A., Cui, X., Audeh, W. & Giuliano, A. Current status of anti-human epidermal growth factor receptor 2 therapies: predicting and overcoming herceptin resistance. *Clin Breast Cancer* **13**, 223-232 (2013).

71. Hinrichs, M.J. & Dixit, R. Antibody drug conjugates: nonclinical safety considerations. *AAPS J* **17**, 1055-1064 (2015).

72. Saber, H. & Leighton, J.K. An FDA oncology analysis of antibody-drug conjugates. *Regul Toxicol Pharmacol* **71**, 444-452 (2015).

73. de Goeij, B.E. & Lambert, J.M. New developments for antibody-drug conjugate-based therapeutic approaches. *Curr Opin Immunol* **40**, 14-23 (2016).

74. Lambert, J.M. & Morris, C.Q. Antibody-drug conjugates (ADCs) for personalized treatment of solid tumors: a review. *Adv Ther* **34**, 1015-1035 (2017).

75. Lyon, R.P. *et al.* Reducing hydrophobicity of homogeneous antibody-drug conjugates improves pharmacokinetics and therapeutic index. *Nat Biotechnol* **33**, 733-735 (2015).

76. Tian, F. *et al.* A general approach to site-specific antibody drug conjugates. *Proc Natl Acad Sci U S A* **111**, 1766-1771 (2014).

77. Ogitani, Y. *et al.* DS-8201a, A novel HER2-targeting ADC with a novel DNA topoisomerase I inhibitor, demonstrates a promising antitumor efficacy with differentiation from T-DM1. *Clin Cancer Res* **22**, 5097-5108 (2016).

78. Ogitani, Y., Hagihara, K., Oitate, M., Naito, H. & Agatsuma, T. Bystander killing effect of DS-8201a, a novel anti-human epidermal growth factor receptor 2 antibody-drug conjugate, in tumors with human epidermal growth factor receptor 2 heterogeneity. *Cancer Sci* **107**, 1039-1046 (2016).

79. Tiberghien, A.C. *et al.* Design and synthesis of tesirine, a clinical antibody-drug conjugate pyrrolobenzodiazepine dimer payload. *ACS Med Chem Lett* **7**, 983-987 (2016).

80. Wang, Y., Fan, S., Zhong, W., Zhou, X. & Li, S. Development and properties of valine-alanine based antibody-drug conjugates with monomethyl auristatin E as the potent payload. *Int J Mol Sci* **18** (2017).

81. Elgersma, R.C. *et al.* Design, synthesis, and evaluation of linker-duocarmycin payloads: toward selection of HER2-targeting antibody-drug conjugate SYD985. *Mol Pharm* **12**, 1813-1835 (2015).

82. Li, J.Y. *et al.* A biparatopic HER2-targeting antibody-drug conjugate induces tumor regression in primary models refractory to or ineligible for HER2-targeted therapy. *Cancer Cell* **29**, 117-129 (2016).

83. Diamantis, N. & Banerji, U. Antibody-drug conjugates--an emerging class of cancer treatment. *Br J Cancer* **114**, 362-367 (2016).

84. Elias, D.J. *et al.* Monoclonal antibody KS1/4-methotrexate immunoconjugate studies in non-small cell lung carcinoma. *Am J Respir Crit Care Med* **150**, 1114-1122 (1994).

85. Tolcher, A.W. *et al.* Randomized phase II study of BR96-doxorubicin conjugate in patients with metastatic breast cancer. *J Clin Oncol* **17**, 478-484 (1999).

86. Liang, H. *et al.* A collagen-binding EGFR single-chain Fv antibody fragment for the targeted cancer therapy. *J Control Release* **209**, 101-109 (2015).

87. M, M.R. *et al.* Nectin-4: a new prognostic biomarker for efficient therapeutic targeting of primary and metastatic triple-negative breast cancer. *Ann Oncol* **28**, 769-776 (2017).

88. Perrino, E. *et al.* Curative properties of noninternalizing antibody-drug conjugates based on maytansinoids. *Cancer Res* **74**, 2569-2578 (2014).

89. Gebleux, R., Stringhini, M., Casanova, R., Soltermann, A. & Neri, D. Non-internalizing antibody-drug conjugates display potent anti-cancer activity upon proteolytic release of monomethyl auristatin E in the subendothelial extracellular matrix. *Int J Cancer* **140**, 1670-1679 (2017).

90. Chalouni, C. & Doll, S. Fate of Antibody-Drug Conjugates in Cancer Cells. *J Exp Clin Cancer Res* **37**, 20 (2018).

91. Bouchard, H., Viskov, C. & Garcia-Echeverria, C. Antibody-drug conjugates-a new wave of cancer drugs. *Bioorg Med Chem Lett* **24**, 5357-5363 (2014).

92. Boghaert, E.R. *et al.* Determination of pharmacokinetic values of calicheamicin-antibody conjugates in mice by plasmon resonance analysis of small (5 microl) blood samples. *Cancer Chemother Pharmacol* **61**, 1027-1035 (2008).

93. Kato, Y. *et al.* Acidic extracellular microenvironment and cancer. *Cancer Cell Int* **13**, 89 (2013).

94. Balendiran, G.K., Dabur, R. & Fraser, D. The role of glutathione in cancer. *Cell Biochem Funct* **22**, 343-352 (2004).

95. Ikebuchi, M. *et al.* Effect of medium pH on glutathione redox cycle in cultured human umbilical vein endothelial cells. *Metabolism* **42**, 1121-1126 (1993).

96. Wu, A.M. & Senter, P.D. Arming antibodies: prospects and challenges for immunoconjugates. *Nat Biotechnol* **23**, 1137-1146 (2005).

97. McCombs, J.R. & Owen, S.C. Antibody drug conjugates: design and selection of linker, payload and conjugation chemistry. *AAPS J* **17**, 339-351 (2015).

98. Lewis Phillips, G.D. *et al.* Targeting HER2-positive breast cancer with trastuzumab-DM1, an antibody-cytotoxic drug conjugate. *Cancer Res* **68**, 9280-9290 (2008).

99. Panowski, S., Bhakta, S., Raab, H., Polakis, P. & Junutula, J.R. Site-specific antibody drug conjugates for cancer therapy. *MAbs* **6**, 34-45 (2014).

100. Doronina, S.O. *et al.* Development of potent monoclonal antibody auristatin conjugates for cancer therapy. *Nat Biotechnol* **21**, 778-784 (2003).

101. Burns, K.E., Robinson, M.K. & Thevenin, D. Inhibition of cancer cell proliferation and breast tumor targeting of pHLIP-monomethyl auristatin E conjugates. *Mol Pharm* **12**, 1250-1258 (2015).

102. Sun, X. *et al.* Effects of drug-antibody ratio on pharmacokinetics, biodistribution, efficacy, and tolerability of antibody-maytansinoid conjugates. *Bioconjug Chem* **28**, 1371-1381 (2017).

103. Yurkovetskiy, A.V. *et al.* A polymer-based antibody-vinca drug conjugate platform: characterization and preclinical efficacy. *Cancer Res* **75**, 3365-3372 (2015).

104. Takegawa, N. *et al.* DS-8201a, a new HER2-targeting antibody-drug conjugate incorporating a novel DNA topoisomerase I inhibitor, overcomes HER2-positive gastric cancer T-DM1 resistance. *Int J Cancer* **141**, 1682-1689 (2017).

105. Pettit, G.R. The dolastatins. *Fortschr Chem Org Naturst* **70**, 1-79 (1997).

106. Oroudjev, E. *et al.* Maytansinoid-antibody conjugates induce mitotic arrest by suppressing microtubule dynamic instability. *Mol Cancer Ther* **9**, 2700-2713 (2010).

107. Khalil, M.W., Sasse, F., Lunsdorf, H., Elnakady, Y.A. & Reichenbach, H. Mechanism of action of tubulysin, an antimitotic peptide from myxobacteria. *Chembiochem* **7**, 678-683 (2006).

108. Zein, N., Sinha, A.M., McGahren, W.J. & Ellestad, G.A. Calicheamicin gamma 1I: an antitumor antibiotic that cleaves double-stranded DNA site specifically. *Science* **240**, 1198-1201 (1988).

109. Holbro, T. *et al.* The ErbB2/ErbB3 heterodimer functions as an oncogenic unit: ErbB2 requires ErbB3 to drive breast tumor cell proliferation. *Proc Natl Acad Sci U S A* **100**, 8933-8938 (2003).

110. Lee-Hoeflich, S.T. *et al.* A central role for HER3 in HER2-amplified breast cancer: implications for targeted therapy. *Cancer Res* **68**, 5878-5887 (2008).

111. Schoeberl, B. *et al.* Therapeutically targeting ErbB3: a key node in ligand-induced activation of the ErbB receptor-PI3K axis. *Sci Signal* **2**, ra31 (2009).

112. Tzahar, E. *et al.* A hierarchical network of interreceptor interactions determines signal transduction by Neu differentiation factor/neuregulin and epidermal growth factor. *Mol Cell Biol* **16**, 5276-5287 (1996).

113. Yarden, Y. & Sliwkowski, M.X. Untangling the ErbB signalling network. *Nat Rev Mol Cell Biol* **2**, 127-137 (2001).

114. Hellyer, N.J., Kim, M.S. & Koland, J.G. Heregulin-dependent activation of phosphoinositide 3-kinase and Akt via the ErbB2/ErbB3 co-receptor. *J Biol Chem* **276**, 42153-42161 (2001).

115. Murphy, C.G. & Modi, S. HER2 breast cancer therapies: a review. *Biologics* **3**, 289-301 (2009).

116. Nahta, R., Yu, D., Hung, M.C., Hortobagyi, G.N. & Esteva, F.J. Mechanisms of disease: understanding resistance to HER2-targeted therapy in human breast cancer. *Nat Clin Pract Oncol* **3**, 269-280 (2006).

117. Hurvitz, S.A., Hu, Y., O'Brien, N. & Finn, R.S. Current approaches and future directions in the treatment of HER2-positive breast cancer. *Cancer Treat Rev* **39**, 219-229 (2013).

118. Garrett, J.T., Sutton, C.R., Kuba, M.G., Cook, R.S. & Arteaga, C.L. Dual blockade of HER2 in HER2-overexpressing tumor cells does not completely eliminate HER3 function. *Clin Cancer Res* **19**, 610-619 (2013).

119. Li, Q., Ahmed, S. & Loeb, J.A. Development of an autocrine neuregulin signaling loop with malignant transformation of human breast epithelial cells. *Cancer Res* **64**, 7078-7085 (2004).

120. Montero, J.C. *et al.* Neuregulins and cancer. *Clin Cancer Res* **14**, 3237-3241 (2008).

121. Dunn, M. *et al.* Co-expression of neuregulins 1, 2, 3 and 4 in human breast cancer. *J Pathol* **203**, 672-680 (2004).

122. Kaufman, B. *et al.* Lapatinib monotherapy in patients with HER2-overexpressing relapsed or refractory inflammatory breast cancer: final results and survival of the expanded HER2+ cohort in EGF103009, a phase II study. *Lancet Oncol* **10**, 581-588 (2009).

123. Gomez, H.L. *et al.* Efficacy and safety of lapatinib as first-line therapy for ErbB2-amplified locally advanced or metastatic breast cancer. *J Clin Oncol* **26**, 2999-3005 (2008).

124. Burstein, H.J. *et al.* Neratinib, an irreversible ErbB receptor tyrosine kinase inhibitor, in patients with advanced ErbB2-positive breast cancer. *J Clin Oncol* **28**, 1301-1307 (2010).

125. Gradishar, W.J. Emerging approaches for treating HER2-positive metastatic breast cancer beyond trastuzumab. *Ann Oncol* **24**, 2492-2500 (2013).

126. Baselga, J. *et al.* Phase II and tumor pharmacodynamic study of gefitinib in patients with advanced breast cancer. *J Clin Oncol* **23**, 5323-5333 (2005).

127. Folkes, A.J. *et al.* The identification of 2-(1H-indazol-4-yl)-6-(4-methanesulfonyl-piperazin-1-ylmethyl)-4-morpholin-4-yl-t hieno[3,2-d]pyrimidine (GDC-0941) as a potent, selective, orally bioavailable inhibitor of class I PI3 kinase for the treatment of cancer. *J Med Chem* **51**, 5522-5532 (2008).

128. Brachmann, S.M. *et al.* Specific apoptosis induction by the dual PI3K/mTor inhibitor NVP-BEZ235 in HER2 amplified and PIK3CA mutant breast cancer cells. *Proc Natl Acad Sci U S A* **106**, 22299-22304 (2009).

129. Sergina, N.V. *et al.* Escape from HER-family tyrosine kinase inhibitor therapy by the kinase-inactive HER3. *Nature* **445**, 437-441 (2007).

130. Chakrabarty, A., Sanchez, V., Kuba, M.G., Rinehart, C. & Arteaga, C.L. Feedback upregulation of HER3 (ErbB3) expression and activity attenuates antitumor effect of PI3K inhibitors. *Proc Natl Acad Sci U S A* **109**, 2718-2723 (2012).

131. Scaltriti, M. *et al.* Lapatinib, a HER2 tyrosine kinase inhibitor, induces stabilization and accumulation of HER2 and potentiates trastuzumab-dependent cell cytotoxicity. *Oncogene* **28**, 803-814 (2009).

132. Amin, D.N. *et al.* Resiliency and vulnerability in the HER2-HER3 tumorigenic driver. *Sci Transl Med* **2**, 16ra17 (2010).

133. Eichhorn, P.J. *et al.* Phosphatidylinositol 3-kinase hyperactivation results in lapatinib resistance that is reversed by the mTOR/phosphatidylinositol 3-kinase inhibitor NVP-BEZ235. *Cancer Res* **68**, 9221-9230 (2008).

134. Wilson, T.R. *et al.* Widespread potential for growth-factor-driven resistance to anticancer kinase inhibitors. *Nature* **487**, 505-509 (2012).

135. Xia, W. *et al.* An heregulin-EGFR-HER3 autocrine signaling axis can mediate acquired lapatinib resistance in HER2+ breast cancer models. *Breast Cancer Res* **15**, R85 (2013).

136. Sato, Y., Yashiro, M. & Takakura, N. Heregulin induces resistance to lapatinib-mediated growth inhibition of HER2-amplified cancer cells. *Cancer Sci* **104**, 1618-1625 (2013).

137. Engelman, J.A. *et al.* MET amplification leads to gefitinib resistance in lung cancer by activating ERBB3 signaling. *Science* **316**, 1039-1043 (2007).

138. Knowlden, J.M. *et al.* erbB3 recruitment of insulin receptor substrate 1 modulates insulin-like growth factor receptor signalling in oestrogen receptor-positive breast cancer cell lines. *Breast Cancer Res* **13**, R93 (2011).

139. Sak, M.M. *et al.* The oncoprotein ErbB3 is endocytosed in the absence of added ligand in a clathrin-dependent manner. *Carcinogenesis* **33**, 1031-1039 (2012).

140. Chan, A.C. & Carter, P.J. Therapeutic antibodies for autoimmunity and inflammation. *Nat Rev Immunol* **10**, 301-316 (2010).

141. Sievers, E.L. & Senter, P.D. Antibody-drug conjugates in cancer therapy. *Annu Rev Med* **64**, 15-29 (2013).

142. Cho, H.S. *et al.* Structure of the extracellular region of HER2 alone and in complex with the Herceptin Fab. *Nature* **421**, 756-760 (2003).

143. Franklin, M.C. *et al.* Insights into ErbB signaling from the structure of the ErbB2-pertuzumab complex. *Cancer Cell* **5**, 317-328 (2004).

144. Gymnopoulos, M., Elsliger, M.A. & Vogt, P.K. Rare cancer-specific mutations in PIK3CA show gain of function. *Proc Natl Acad Sci U S A* **104**, 5569-5574 (2007).

145. Weigelt, B., Warne, P.H. & Downward, J. PIK3CA mutation, but not PTEN loss of function, determines the sensitivity of breast cancer cells to mTOR inhibitory drugs. *Oncogene* **30**, 3222-3233 (2011).

146. Junttila, T.T. *et al.* Ligand-independent HER2/HER3/PI3K complex is disrupted by trastuzumab and is effectively inhibited by the PI3K inhibitor GDC-0941. *Cancer Cell* **15**, 429-440 (2009).

147. Chandarlapaty, S. *et al.* AKT inhibition relieves feedback suppression of receptor tyrosine kinase expression and activity. *Cancer Cell* **19**, 58-71 (2011).

148. Serra, V. *et al.* PI3K inhibition results in enhanced HER signaling and acquired ERK dependency in HER2-overexpressing breast cancer. *Oncogene* **30**, 2547-2557 (2011).

149. Haslekas, C. *et al.* The inhibitory effect of ErbB2 on epidermal growth factor-induced formation of clathrin-coated pits correlates with retention of epidermal growth factor receptor-ErbB2 oligomeric complexes at the plasma membrane. *Mol Biol Cell* **16**, 5832-5842 (2005).

150. Sak, M.M. *et al.* Pertuzumab counteracts the inhibitory effect of ErbB2 on degradation of ErbB3. *Carcinogenesis* **34**, 2031-2038 (2013).

151. Le, X.F. *et al.* Anti-HER2 antibody and heregulin suppress growth of HER2-overexpressing human breast cancer cells through different mechanisms. *Clin Cancer Res* **6**, 260-270 (2000).

152. Reichert, J.M. & Dhimolea, E. The future of antibodies as cancer drugs. *Drug Discov Today* **17**, 954-963 (2012).

153. Horak, E. *et al.* Isolation of scFvs to in vitro produced extracellular domains of EGFR family members. *Cancer Biother Radiopharm* **20**, 603-613 (2005).

154. Schier, R. *et al.* In vitro and in vivo characterization of a human anti-c-erbB-2 single-chain Fv isolated from a filamentous phage antibody library. *Immunotechnology* **1**, 73-81 (1995).

155. Xu, L. *et al.* Rapid optimization and prototyping for therapeutic antibody-like molecules. *MAbs* **5**, 237-254 (2013).

156. Jost, C. *et al.* Structural basis for eliciting a cytotoxic effect in HER2-overexpressing cancer cells via binding to the extracellular domain of HER2. *Structure* **21**, 1979-1991 (2013).

157. Foote, J. & Winter, G. Antibody framework residues affecting the conformation of the hypervariable loops. *J Mol Biol* **224**, 487-499 (1992).

158. Coloma, M.J. & Morrison, S.L. Design and production of novel tetravalent bispecific antibodies. *Nat Biotechnol* **15**, 159-163 (1997).

159. Zhou, J., Mateos, F., Ober, R.J. & Ward, E.S. Conferring the binding properties of the mouse MHC class I-related receptor, FcRn, onto the human ortholog by sequential rounds of site-directed mutagenesis. *J Mol Biol* **345**, 1071-1081 (2005).

160. Vaccaro, C., Zhou, J., Ober, R.J. & Ward, E.S. Engineering the Fc region of immunoglobulin G to modulate in vivo antibody levels. *Nat Biotechnol* **23**, 1283-1288 (2005).

161. Vaccaro, C., Bawdon, R., Wanjie, S., Ober, R.J. & Ward, E.S. Divergent activities of an engineered antibody in murine and human systems have implications for therapeutic antibodies. *Proc Natl Acad Sci U S A* **103**, 18709-18714 (2006).

162. Ober, R.J., Martinez, C., Vaccaro, C., Zhou, J. & Ward, E.S. Visualizing the site and dynamics of IgG salvage by the MHC class I-related receptor, FcRn. *J Immunol* **172**, 2021-2029 (2004).

163. Gan, Z., Ram, S., Vaccaro, C., Ober, R.J. & Ward, E.S. Analyses of the recycling receptor, FcRn, in live cells reveal novel pathways for lysosomal delivery. *Traffic* **10**, 600-614 (2009).

164. Sievers, E.L. & Senter, P.D. Antibody-drug conjugates in cancer therapy. *Annu Rev Med* **64**, 15-29 (2013).

165. Lambert, J.M. & Berkenblit, A. Antibody-drug conjugates for cancer treatment. *Annu Rev Med* **69**, 191-207 (2018).

166. Chari, R.V. Expanding the reach of antibody-drug conjugates. *ACS Med Chem Lett* **7**, 974-976 (2016).

167. Beck, A., Goetsch, L., Dumontet, C. & Corvaia, N. Strategies and challenges for the next generation of antibody-drug conjugates. *Nat Rev Drug Discov* **16**, 315-337 (2017).

168. Teicher, B.A. & Chari, R.V. Antibody conjugate therapeutics: challenges and potential. *Clin. Cancer Res* **17**, 6389-6397 (2011).

169. Lewis Phillips, G.D. *et al.* Targeting HER2-positive breast cancer with trastuzumab-DM1, an antibody-cytotoxic drug conjugate. *Cancer Res* **68**, 9280-9290 (2008).

170. Shen, B.Q. *et al.* Conjugation site modulates the in vivo stability and therapeutic activity of antibody-drug conjugates. *Nat Biotechnol* **30**, 184-189 (2012).

171. Doronina, S.O. *et al.* Development of potent monoclonal antibody auristatin conjugates for cancer therapy. *Nat Biotechnol* **21**, 778-784 (2003).

172. de Goeij, B.E. & Lambert, J.M. New developments for antibody-drug conjugate-based therapeutic approaches. *Curr Opin Immunol* **40**, 14-23 (2016).

173. Burris, H.A., 3rd *et al.* Phase II study of the antibody drug conjugate trastuzumab-DM1 for the treatment of human epidermal growth factor receptor 2 (HER2)-positive breast cancer after prior HER2-directed therapy. *J Clin Oncol* **29**, 398-405 (2011).

174. Barok, M., Joensuu, H. & Isola, J. Trastuzumab emtansine: mechanisms of action and drug resistance. *Breast Cancer Res* **16**, 209 (2014).

175. Loganzo, F. *et al.* Tumor cells chronically treated with a trastuzumab-maytansinoid antibody-drug conjugate develop varied resistance mechanisms but respond to alternate treatments. *Mol Cancer Ther* **14**, 952-963 (2015).

176. Li, G. *et al.* Mechanisms of acquired resistance to trastuzumab emtansine in breast cancer cells. *Mol Cancer Ther* **17**, 1441-1453 (2018).

177. Franklin, M.C. *et al.* Insights into ErbB signaling from the structure of the ErbB2-pertuzumab complex. *Cancer Cell* **5**, 317-328 (2004).

178. Nahta, R., Hung, M.C. & Esteva, F.J. The HER-2-targeting antibodies trastuzumab and pertuzumab synergistically inhibit the survival of breast cancer cells. *Cancer Res* **64**, 2343-2346 (2004).

179. Carter, P. *et al.* Humanization of an anti-p185HER2 antibody for human cancer therapy. *Proc Natl Acad Sci U S A* **89**, 4285-4289 (1992).

180. Igawa, T. *et al.* Antibody recycling by engineered pH-dependent antigen binding improves the duration of antigen neutralization. *Nat Biotechnol* **28**, 1203-1207 (2010).

181. Chaparro-Riggers, J. *et al.* Increasing serum half-life and extending cholesterol lowering in vivo by engineering antibody with pH-sensitive binding to PCSK9. *J Biol Chem* **287**, 11090-11097 (2012).

182. Devanaboyina, S.C. *et al.* The effect of pH dependence of antibody-antigen interactions on subcellular trafficking dynamics. *MAbs* **5**, 851-859 (2013).

183. Stubbs, M., McSheehy, P.M., Griffiths, J.R. & Bashford, C.L. Causes and consequences of tumour acidity and implications for treatment. *Mol Med Today* **6**, 15-19 (2000).

184. Schornack, P.A. & Gillies, R.J. Contributions of cell metabolism and H+ diffusion to the acidic pH of tumors. *Neoplasia* **5**, 135-145 (2003).

185. Kabat, E.A., Wu, T.T., Perry, H.M., Gottesman, K.S. & Foeller, C. *Sequences of proteins of immunological interest.* 5th edition, NIH publication 91-3242 (1991).

186. Lyon, R.P. *et al.* Reducing hydrophobicity of homogeneous antibody-drug conjugates improves pharmacokinetics and therapeutic index. *Nat Biotechnol* **33**, 733-735 (2015).

187. Hamblett, K.J. *et al.* Effects of drug loading on the antitumor activity of a monoclonal antibody drug conjugate. *Clin Cancer Res* **10**, 7063-7070 (2004).

188. Ram, S., Kim, D., Ober, R.J. & Ward, E.S. The level of HER2 expression is a predictor of antibody-HER2 trafficking behavior in cancer cells. *MAbs* **6**, 1211-1219 (2014).

189. Austin, C.D. *et al.* Endocytosis and sorting of ErbB2 and the site of action of cancer therapeutics trastuzumab and geldanamycin. *Mol Biol Cell* **15**, 5268-5282 (2004).

190. Barok, M., Tanner, M., Koninki, K. & Isola, J. Trastuzumab-DM1 causes tumour growth inhibition by mitotic catastrophe in trastuzumab-resistant breast cancer cells in vivo. *Breast Cancer Res* **13**, R46 (2011).

191. Friedman, L.M. *et al.* Synergistic down-regulation of receptor tyrosine kinases by combinations of mAbs: implications for cancer immunotherapy. *Proc Natl Acad Sci U S A* **102**, 1915-1920 (2005).

192. de Goeij, B.E. *et al.* Efficient payload delivery by a bispecific antibody-drug conjugate targeting HER2 and CD63. *Mol Cancer Ther* **15**, 2688-2697 (2016).

193. Yang, D. *et al.* Maximizing in vivo target clearance by design of pH-dependent target binding antibodies with altered affinity to FcRn. *MAbs* **9**, 1105-1117 (2017).

194. Henne, K.R. *et al.* Anti-PCSK9 antibody pharmacokinetics and low-density lipoprotein-cholesterol pharmacodynamics in nonhuman primates are antigen affinity-dependent and

exhibit limited sensitivity to neonatal Fc receptor-binding enhancement. *J Pharmacol Exp Ther* **353**, 119-131 (2015).

195. Engler, F.A. *et al.* "Catch-and-Release" anti-carcinoembryonic antigen monoclonal antibody leads to greater plasma and tumor exposure in a mouse model of colorectal cancer. *J Pharmacol Exp Ther* **366**, 205-219 (2018).

196. Swiercz, R. *et al.* Loss of expression of the recycling receptor, FcRn, promotes tumor cell growth by increasing albumin consumption. *Oncotarget* **8**, 3528-3541 (2017).

197. Dalloneau, E. *et al.* Downregulation of the neonatal Fc receptor expression in non-small cell lung cancer tissue is associated with a poor prognosis. *Oncotarget* **7**, 14 (2016).

198. Chaudhury, C. *et al.* The major histocompatibility complex-related Fc receptor for IgG (FcRn) binds albumin and prolongs its lifespan. *J Exp Med* **197**, 315-322 (2003).

199. Commisso, C. *et al.* Macropinocytosis of protein is an amino acid supply route in Ras-transformed cells. *Nature* **497**, 633-637 (2013).

200. Kamphorst, J.J. *et al.* Human pancreatic cancer tumors are nutrient poor and tumor cells actively scavenge extracellular protein. *Cancer Res* **75**, 544-553 (2015).

201. Challa, D.K., Velmurugan, R., Ober, R.J. & Ward, E.S. FcRn: from molecular interactions to regulation of IgG pharmacokinetics and functions. *Curr Top Microbiol Immunol* **382**, 249-272 (2014).

202. Baker, K., Rath, T., Pyzik, M. & Blumberg, R.S. The role of FcRn in antigen presentation. *Front Immunol* **5**, 408 (2014).

203. Horton, R.M., Hunt, H.D., Ho, S.N., Pullen, J.K. & Pease, L.R. Engineering hybrid genes without the use of restriction enzymes: gene splicing by overlap extension. *Gene* **77**, 61-68 (1989).

204. Ward, E.S. Secretion of T cell receptor fragments from recombinant Escherichia coli cells. *J Mol Biol* **224**, 885-890 (1992).

205. Hoogenboom, H.R. *et al.* Multi-subunit proteins on the surface of filamentous phage: methodologies for displaying antibody (Fab) heavy and light chains. *Nucleic Acids Res* **19**, 4133-4137 (1991).

206. Ghetie, V. *et al.* Increasing the serum persistence of an IgG fragment by random mutagenesis. *Nat Biotechnol* **15**, 637-640 (1997).

207. Foote, J. & Winter, G. Antibody framework residues affecting the conformation of the hypervariable loops. *J Mol Biol* **224**, 487-499 (1992).

208. Li, R. *et al.* Targeting phosphatidylserine with calcium-dependent protein-drug conjugates for the treatment of cancer. *Mol Cancer Ther* **17**, 169-182 (2018).

209. Ober, R.J. & Ward, E.S. Compensation for loss of ligand activity in surface plasmon resonance experiments. *Anal Biochem* **306**, 228-236 (2002).

210. Vaccaro, C., Zhou, J., Ober, R.J. & Ward, E.S. Engineering the Fc region of immunoglobulin G to modulate in vivo antibody levels. *Nat Biotechnol* **23**, 1283-1288 (2005).

211. Ober, R.J., Martinez, C., Vaccaro, C., Zhou, J. & Ward, E.S. Visualizing the site and dynamics of IgG salvage by the MHC class I-related receptor, FcRn. *J Immunol* **172**, 2021-2029 (2004).

212. Chao, J., Ward, E.S. & Ober, R.J. A software framework for the analysis of complex microscopy image data. *IEEE Trans Inf Technol Biomed* **14**, 1075-1087 (2010).

213. Brooks, B.R. *et al.* CHARMM: A program for macromolecular energy, minimization, and dynamics calculations. *J Comput Chem* **4**, 187-217 (1983).

214. Sondergaard, C.R., Olsson, M.H., Rostkowski, M. & Jensen, J.H. Improved treatment of ligands and coupling effects in empirical calculation and rationalization of pKa values. *J Chem Theory Comput* **7**, 2284-2295 (2011).

215. Olsson, M.H., Sondergaard, C.R., Rostkowski, M. & Jensen, J.H. PROPKA3: Consistent treatment of internal and surface residues in empirical pKa predictions. *J Chem Theory Comput* **7**, 525-537 (2011).

216. Phillips, J.C. *et al.* Scalable molecular dynamics with NAMD. *J Comput Chem* **26**, 1781-1802 (2005).

217. Humphrey, W., Dalke, A. & Schulten, K. VMD: visual molecular dynamics. *J Mol Graph* **14**, 33-38, 27-38 (1996).

218. Karimi, M. & Shen, Y. iCFN: an efficient exact algorithm for multistate protein design. *Bioinformatics*, in press (2018).

219. Javle, M. *et al.* HER2/neu-directed therapy for biliary tract cancer. *J Hematol Oncol* **8**, 58 (2015).

220. English, D.P., Roque, D.M. & Santin, A.D. HER2 expression beyond breast cancer: therapeutic implications for gynecologic malignancies. *Mol Diagn Ther* **17**, 85-99 (2013).

221. Chavez-Blanco, A. *et al.* HER2 expression in cervical cancer as a potential therapeutic target. *BMC Cancer* **4**, 59 (2004).

222. Pectasides, E. & Bass, A.J. ERBB2 emerges as a new target for colorectal cancer. *Cancer Discov* **5**, 799-801 (2015).

223. Hamy-Petit, A.S. *et al.* Pathological complete response and prognosis after neoadjuvant chemotherapy for HER2-positive breast cancers before and after trastuzumab era: results from a real-life cohort. *Br J Cancer* **114**, 44-52 (2016).

APPENDIX

A1: Determination of drug-to-antibody ratios

ADCs were analyzed using a hydrophobic interaction column (described in Section 3) and the following equation was used to determine the molar ratio of drug to antibody (DAR).

$$\frac{D0 * 0 + D1 * 1 + D2 * 2}{D0 + D1 + D2}$$

Where,

D0 = area under the curve (AUC) for the ADC population representing unconjugated antibody molecules.

D1 = AUC for the ADC population with a DAR of 1.

D2 = AUC for the ADC population with a DAR of 2.

The ADCs used for the mass spectrometry data shown in Fig. 3-8b were calculated to have DARs of 1.85, 1.72, and 1.85 (for WT-MMAE, SG-MMAE, and YS-MMAE, respectively).

A2: Generation of standard curves for mass spectrometry

Representative standard curves used to determine the amount of MMAE in each tumor cell line are shown in Fig. A-1 and A-2 (see section 3.4.12 for tumor cell lysate preparation and processing). D8-MMAE was added to both standard and test samples at a concentration of 1.67 ng/ml (all samples were adjusted to 830,000 cells per ml in methanol) to account for losses during sample preparation. For the generation of standard curves, MMAE (0.017-3.33 ng/ml) was added to lysates of untreated tumor cells. During processing, the samples were concentrated 30-fold to result in standard concentrations ranging from 0.5-100 ng/ml. Mass spectrometry analyses of a defined volume of each standard sample resulted in an AUC value that was subsequently normalized relative to the AUC value for the internal D8-MMAE standard and plotted against the MMAE concentration. These plots were used to determine the concentrations of MMAE in the cell lines shown in Fig. 3-8b.

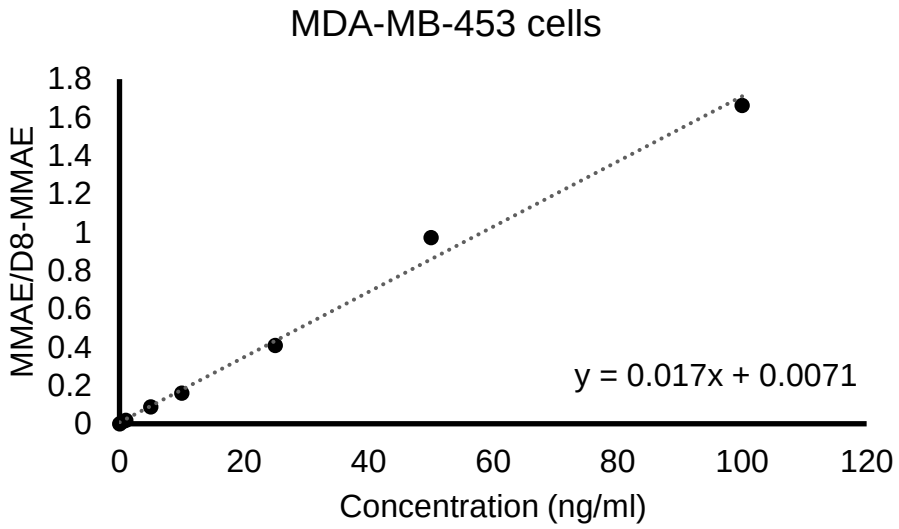

Figure A-1. Representative standard curve for the determination of MMAE concentrations in MDA-MB-453 cells.

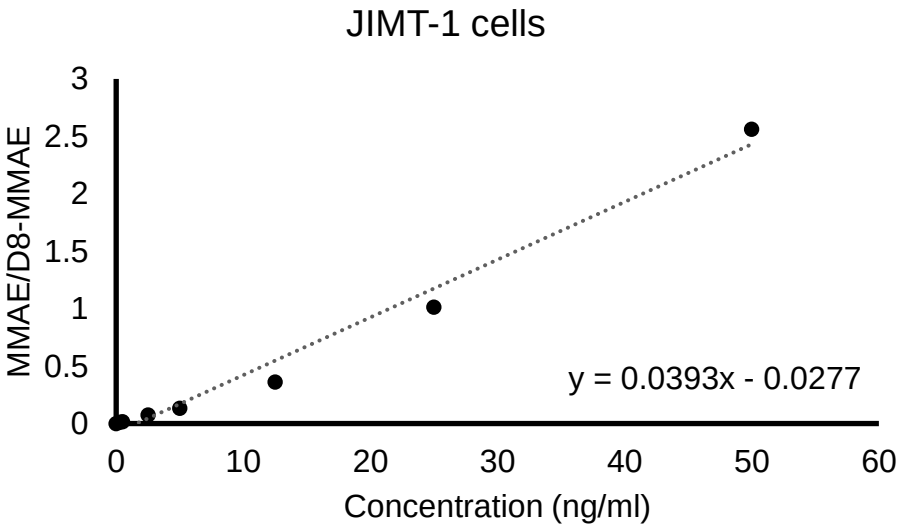

Figure A-2. Representative standard curve for the determination of MMAE concentrations in JIMT-1 cells.